Progressive Transmission of Medical Images

Thesis submitted to Cardiff University in candidature for the degree of Doctor of Philosophy.

Jen-Lung Lo

Centre of Digital Signal Processing
Cardiff University
2010

ProQuest LLC
789 East Eisenhower Parkway
P.O. Box 1346
Ann Arbor, MI 48106-1346

ABSTRACT

Real-time and bandwidth problems prevail whenever medical images are transmitted through internet or wireless network, especially in a low speed connection environment. These problems can not be solved simply by using lossy compression algorithms, because medical images typically contain a huge amount of important diagnostic information and therefore, distortion can not be allowed. A novel adaptive source-channel coding scheme for progressive transmission of medical images with a feedback system is therefore proposed in this dissertation. The overall design includes Discrete Wavelet Transform (DWT), Embedded Zerotree Wavelet (EZW) coding, Joint Source-Channel Coding (JSCC), prioterization of region of interest (RoI), variability of parity length based on feedback, and the corresponding hardware design utilizing Simulink. The DWT and EZW are appropriate embedded codings selected for progressive transmission and compression, due to their efficiency and ease of implementation in hardware design. The JSCC can achieve an efficient transmission by incorporating unequal error protection(UEP) and rate allocation. The radius of the RoI and its location within the image can be selected by the user through a user friendly interaction interface designed to enable users to see the area of particular interest in an error-free state in an early stage of transmission. An algorithm is also developed to estimate the number of erroneous data in the receiver. This number represents the practical transmission channel situation in terms of

noise. The algorithm detects the address in which the number of symbols for each subblock is indicated, and reassigns an estimated correct data according to a decision making criterion, if error data is detected. The evaluated error message will be sent back to the transmitter through the feedback system and the parity length will be adjusted automatically to provide adequate protection for the next transmission of data. The proposed system has been designed based on Simulink which can be used to generate netlist for portable devices. A new compression method called Compressive Sensing (CS) is also revisited in this work. CS exhibits many advantages in comparison with EZW based on our experimental results. In industry, one standard that is currently used is the Digital Imaging and Communications in Medicine (DICOM) standard which comprises a file format definition and a network communications protocol. DICOM JPEG2000 is an efficient coding standard for lossy or lossless multi-component image coding. However, it does not provide any mechanism for automatic RoI definition, and is more complex compared to our proposed scheme. The proposed system significantly reduces the transmission time, lowers computation cost, and maintains an error-free state in the RoI with regards to the above provided features. A Matlab-based TCP/IP connection is established to demonstrate the efficacy of the proposed interactive and adaptive progressive transmission system. The proposed system is simulated for both binary symmetric channel (BSC) and Rayleigh channel. The experimental results confirm the effectiveness of the design.

ACKNOWLEDGEMENTS

First, I would like to thank my supervisors Dr. Saeid Sanei and Prof. Jonathon Chambers for their support during these past years. Especially, I would like to express my deepest gratitude to my first Supervisor, Dr. Sanei, for his invaluable support, guidance and encourage me throughout this PhD. I have not only benefited from his research expertise but also from his enthusiasm for his students.

I am grateful to my colleagues in the Centre of Digital Signal Processing for their help and support. I will always have a nice memory of Cardiff University. Furthermore, I would like to thank to all my friends for their help and support to me and my family.

Finally, I am indebted to my beloved wife, Jui-Ling Kuo and two lovely boys, Shih-Jie and Shih-Chen, accompanied me for three years in Cardiff. I am grateful to my parents, Ha-Yi and Sue-Jane for their endless support and encouragement.

STATEMENT OF ORIGINALITY

I hereby declare that the work described in this thesis was carried out entirely by the author in the Center of Digital Signal Processing, Cardiff School of Engineering, Cardiff University. The thesis does not incorporate, without acknowledgement, any material previously submitted for a degree or diploma in any university. And that to the best of my knowledge, it does not contain any materials previously published or written by any other individual, except where due reference is made in the text.

CONTENTS

PUBLICATIONS

Conference publications:

- Jen-Lung Lo and Saeid Sanei, "A New Interactive Progressive Transmission of Medical Images," *World Congress on Medical Physics and Biomedical Engineering (WC 2006)*, Seoul, Korea, 2006.

- Jen-Lung Lo, Saeid Sanei, and Kianoush Nazarpour, "Interactive and Adaptive Progressive Transmission of Medical Images," *29th Annual International Conference of the IEEE Engineering in Medicine and Biology Society (EMBS 2007)*, p.p. 5670-5673, France, Aug. 2007.

- Jen-Lung Lo and Saeid Sanei, "An Adaptive Channel Coding Technique for Progressive Transmission of Images," *International Conference on Computer and Communication Engineering 2008 (ICCCE08)*, Malaysia, May 2008.

- Saeid Sanei, Anh Huy Phan, Jen-Lung Lo, Vahid Abolghasemi and Andrezj Cichocki, "A Compressive Sensing Approach for Progressive Transmission of Images," *16th International Conference on Digital Signal Processing (DSP2009)*, Greece, July 2009.

Journal publications:

- Jen-Lung Lo, Saeid Sanei, and Kianoush Nazarpour,"An Adaptive Source-Channel Coding with Feedback for Progressive Transmission of Medical Images," *International Journal of Telemedicine and Applications*, vol.2009, Article ID 519417, 12 pages, doi:10.1155/2009/519417.

List of Figures

List of Tables

LIST OF ACRONYMS

ASIC	Application-Specific Integrated Circuit
AWGN	Additive White Gaussian Noise
BER	Bit Error Rate
BSC	Binary Symmetric Channel
CPLD	Complex Programmable Logic Device
CRC	Cyclic Redundancy Check
CS	Compressive Sensing
CT	Computerized Tomography
CWT	Complex Wavelet Transform
dB	Decibel
DCT	Discrete Cosine Transform
DICOM	Digital Imaging and Communication in Medicine
DTCWT	Dual Tree Complex Wavelet Transform
DWT	Discrete Wavelet Transform
EBCOT	Embedded Block Coding with Optimization Truncation
EEP	Equal Error Protection
EIT	Electrical Impedance Tomography
EPS	Error Protection Strategy
EZW	Embedded Zerotree Wavelet
FEC	Forward Error Coding
FPGA	Field-Programmable Gate Array

fMRI	Functional Magnetic Resonance Imaging
FSMC	Finite-State Markov Channel
GEC	Gilbert-Elliott Channel
HALS	Hierarchical Alternative Least Squares
HARQ	Hybrid Automatic Repeat ReQuest
HDL	Hardware Description Language
HWT	Haar Wavelet Transform
IEZW	Inverse Embedded Zerotree Wavelet
IHWT	Inverse Haar Wavelet Transform
JSCC	Joint Source-Channel Coding
LDPC	Low-Density Parity-Check
MRI	Magnetic Resonance Imaging
OCT	Optical Coherence Tomography
PET	Positron Emission Tomography
PACS	Picture Archiving and Communication System
PIT	Progressive Image Transmission
PSNR	Peak Signal to Noise Ratio
RCPC	Rate-Compatible Punctured Convolutional
RLE	Run-Length Encoding
RoI	Region of Interest
RS	Reed-Solomon
RTL	Register Transfer Level
SPET	Single Positron Emission Tomography
SPIHT	Set Partitioning Hierarchical Trees
STFT	Short-Term Fourier Transform
UEP	Unequal Error Protection
US	Ultrasound

UUP Uniform Uncertainly Principle

VHDL Very High Speed Integrated Circuit Hardware Description Language

WT Wavelet Transform

LIST OF SYMBOLS

$(\cdot)^*$	Complex conjugation
$\|.\|_2$	Euclidean norm
$(.)^T$	Transpose operator
$\otimes$	Binary multiply operation
$\oplus$	Binary addition operation
$\psi(\cdot)$	Mother wavelet
ε	Error
Φ	Measurement matrix
τ	Translation factor
$\sigma(t)$	Error-location polynomial
max$(\cdot)$	Maximum coefficient
A	Known projection matrix
a_i	Approximation coefficient
C	Channel capacity
C_{opt}	Optimum parity length

d_i	Detail coefficient
$\mathbf{e}(x)$	Error pattern for signal x
$\boldsymbol{g}_1$	Half-band highpass filter in analysis stage
$\boldsymbol{g}_2$	Half-band highpass filter in synthesis stage
$\boldsymbol{g}(x)$	Generator polynomial for signal x
$\mathbf{h}$	Vector
h_1	Half-band lowpass filter in analysis stage
h_2	Half-band lowpass filter in synthesis stage
$I(x, y)$	Transmitted image
$\hat{I}(x, y)$	Received (reconstructed) image
M_i	Bitstream length
N_i	Header information
$p(x)$	Primitive polynomial with respect to x
p_i	Progressive transmission at stage i
r_a	Radius of the RoI
r_b	Radius of R1
$r(x)$	Received transmitted polynomial
S_i	Syndrome
s	Dilation factor
t_0	Initial threshold

T	Result of wavelet transform
$v(x)$	RS code polynomial output
$\mathbf{x}$	Input data
$\hat{x}$	Reconstructed signal
$\mathbf{X}$	Source image
$\mathbf{Y}$	Compressed image
$\mathbf{y}$	Output data
y_{high}	Highpass filter output
y_{low}	Lowpass filter output
$Z_0(x)$	Error-value evaluator
$\mathbf{z}$	Additive White Gaussian noise

Chapter 1

INTRODUCTION

Telemedicine is a rapidly developing tool for transferring clinical information through phone, Internet or other networks for the purpose of consulting or facilitating medical procedures or examinations. This requires an efficient means of signal, image, and data communications. A simple scenario would be a two health professionals discussing a case over the telephone, whereas a complex case would be the use of satellite technology and video-conferencing equipment to conduct a real-time consultation between medical specialists in different countries [6]. Telemedicine is particularly beneficial for populations living in isolated communities and remote regions of the world. It is currently being applied in virtually all medical domains [6].

Real-time telemedicine can be as simple as a telephone call or as complex as robotic surgery. It requires the simultaneous presence of two individuals and a communications link between them that allows a real-time interaction to take place. Video-conferencing equipment is one of the common forms of technology used in synchronous telemedicine. There are also peripheral devices which can be connected to computers or the video-conferencing equipment in order to assist an interactive examination. For instance, a tele-otoscope allows a remote physician to see inside a patient's ear; a tele-stethoscope allows hearing the patient's heartbeat remotely. Medical specialties beneficent to this kind of consultation include psychiatry,

family practice, internal medicine, rehabilitation, cardiology, pediatrics, obstetrics, gynecology, neurology, speech-language pathology and pharmacy [7].

Store-and-forward telemedicine involves acquiring medical data (such as medical images, biosignals) and then delivering this data to a doctor or medical specialist at a convenient time for an offline assessment. It does not require the presence of both parties at the same time. Dermatology, radiology, and pathology are specialties conducive to asynchronous telemedicine. A properly structured Medical Record, preferably in electronic form, should be a component of this transfer [7].

Generally, occupying a space or bed in a hospital by a patient is not favorable unless for urgent or continuous medical care. Home care telemedicine allows remote observation and care of a patient and thereby circumvents the inconveniences to both patients and medical departments. These require newer systems with higher frequency bandwidth capabilities. Such systems can also be employed for disease management, post-hospital care, and assisted living [6].

As a result of progress in biomedical electronics, various medical imaging methods, such as Ultrasound (US), Magnetic Resonance Imaging (MRI), Functional Magnetic Resonance Imaging (fMRI), Computerized Tomography (CT), Positron Emission Tomography (PET), Single Photon Emission Computed Tomography (SPECT or SPET), and digital X-ray image are now utilised to assist physicians. However, such medical imaging methods give rise to management, storage, and delivery problems, owing to the huge amount of transmitted medical images. To this end, the development of a highly reliable, high speed, and efficient transmission system for medical image is necessary. As medical images typically contain large amounts

of crucial clinical data, no error generated over the transmission channel can be tolerated. Advanced methodologies for gaining distortionless reconstructed images, in fairly acceptable transmission courses, make it possible to transmit a medical image over a noisy channel. However, even by utilizing current high-speed broadband connections, transmission of medical images is not entirely free of noise or artifacts. Although using more parity bits for channel coding enables greater data error detection and correction, the transmission time and the complexity of the channel coding considerably increase. Given the requirements for distortionless reconstructed images, shorter transmission time and low complexity, an appropriate compressor, channel coder and variable length parity code against channel noise can meet this aim.

1.1 Medical Images

Medical imaging refers to noninvasive techniques and processes used to produce images of the human body for clinical purposes or medical science. Generally, scanners capture Ultrasound, X-ray or magnetic field signals and then convert those data into images through reconstruction algorithms to generate various medical image modalities. The DICOM standard was created by the National Electrical Manufacturers Association (NEMA). Its aim is to allow the distribution and viewing of medical images from various medical modalities. A DICOM file contains a header and the image data. The DICOM image data can be compressed by either lossless or lossy algorithms to make best use of disk space and channel bandwidth and is a common standard. Several popular medical image modalities are briefly introduced in the following sub-sections.

1.1.1 Digital Radiography

X-rays are the oldest, most basic form of medical images, and the most frequently used. X-ray equipment is relatively inexpensive, easy to use and widely available in hospitals. Digital imaging techniques were applied to X-rays in the 1980s. Since then, digital X-ray sensors have been used instead of traditional photographic film. Digital X-ray technique has many advantages over traditional film-based X-ray, such as time efficiency due to bypassing of the chemical processing, the ability to digitally transfer and enhance images, and radiation reduction.

1.1.2 Ultrasound

Ultrasound imaging is based on principles of sonar and has been used for medical diagnosis since the 1960's. Ultrasound imaging in medicine is used to detect changes in the appearance of organs, tissues, and vessels or detect abnormal masses. Ultrasound scan can be repeated as often as necessary because of no known harmful effects on humans. Ultrasound is the preferred imaging modality for the diagnosis and monitoring of pregnant women and their unborn babies. In the ultrasound system, a small device called a transducer generates a stream of inaudible, high frequency sound waves into the body. Different tissues reflect these sound waves differently, therefore, the transducer receives varying sound waves back from tissues. These waves can be turned into real-time pictures with the use of computers and reconstruction software. Ultrasound imaging is a relatively inexpensive, faster and easier to use than other imaging methods, and is also excellent for non-invasive imaging.

1.1.3 Computerized Tomography

Computerized tomography (CT) is a medical imaging method which employs tomography. CT scan is a painless, noninvasive diagnostic procedure that uses X-ray equipment to take a large number of scans from the body from different angles. The images are basically the results of X-ray absorbtion by the body and the image reconstruction algorithms embedded with the imaging systems. CT scans can provide far more detailed images than ordinary X-rays since a series of X-rays are taken of the body tissues at different angles. With the aid of a computer, each cross-sectional image of the body is added together to create a tomogram. Such scans provide good pictures of soft tissues which do not show on ordinary X-ray diagraph. CT scans are performed to analyze the internal structures of various parts of the body.

1.1.4 Positron Emission Tomography

Positron Emission Tomography (PET) is a nuclear medicine imaging technique used to generate a three-dimensional image. It is noninvasive and helps physicians to examine the heart, brain, breast, lung and other internal organ. The system detects pairs of gamma rays emitted indirectly by a positron-emitting radionuclide (tracer), which is introduced into the body on a biologically active molecule. A camera generates images which show the human body's biological functions and reveal the mysteries of health and disease. All the body's organ systems can be captured within only one image. Before imaging, a radiotracer is injected into the organ or area of the patient's body which is being examined. The PET scanner works together with a computer to record the amount of radiotracer absorbed by the body and to reconstruct the signals from the gamma rays (given off by the

radiotracer) into images. These images provide details with regard to both the structure and function of organs and tissues. Today, most PET scanners consist of both a PET and CT scanner, since such combination provides more accurate diagnoses than when these scanners are used separately.

1.1.5 Single Photon Emission Computed Tomography

Single Photon Emission Computed Tomography (SPECT, or SPET) is another nuclear medicine tomographic imaging technique which uses gamma rays. A SPECT scan is a type of nuclear imaging test that shows how blood flows to tissues and organs. SPECT is similar to PET in its use of radioactive tracer material and detection of gamma rays. However, it is able to provide true 3D information, typically presented as cross-sectional slices through the patient, but which can be freely reformatted or manipulated as required.

The basic SPECT technique requires the injection of a gamma-emitting radioisotope into the patient's blood vessels. SPECT imaging is performed by using a gamma camera to acquire multiple 2-D images from multiple angles and then generate three-dimensional data by a tomographic reconstruction algorithm. This data may then be manipulated to show thin slices along any chosen axis of the body, similar to those obtained from other tomographic techniques, such as MRI, CT, and PET. SPECT scans, however, are significantly less expensive than PET scans, in part because they are able to use longer-lived more easily-obtained radioisotopes than PET. A SPECT scan is primarily used to view how blood flows through arteries and veins in the brain. Tests have shown that it might be more sensitive to brain injury than either MRI or CT scanning, because it can detect reduced blood flow at the injured sites.

1.1.6 Magnetic Resonance Imaging

Magnetic resonance imaging (MRI) has been in use since the beginning of the 1980s. An MRI scanner uses a strong magnetic field and radio waves instead of X-ray radiation to create detailed digital images. The radio waves are 10,000 to 30,000 times stronger than the magnetic field of the earth and are sent through the body. The radio waves knock the protons from their position. When the burst of radio waves stops, the protons realign back into place and emit radio signals. The protons in different tissues of the body realign at different speeds. The scanner picks up the radio signals and a reconstruction algorithm converts them into images. These images are based on the location and strength of the incoming signals and are displayed on a computer screen as two-dimensional or three-dimensional images. Before scanning, as with other medical imaging techniques, a special dye is injected into the blood vessels to make the scans clearer. The drawbacks are that the scans are very noisy and can be affected by movement. Using the MRI scan, it is possible to take image slices from various angles, whereas the CT scan only shows horizontal slices. Moreover, since CT and MRI scans are sensitive to different properties of the tissue being scanned, the appearance of the images obtained by the two techniques differs significantly. In CT, X-rays must be blocked by some form of dense tissue to create an image. Therefore, the image quality when looking at soft tissues is poor. MRI on the other hand, has much higher detail in the soft tissues. But, in the examination of bone, CT provides more detailed pathological information.

1.1.7 Functional Magnetic Resonance Imaging

Functional Magnetic Resonance Imaging (fMRI) is sequentially taking MRI scans of the same subject. It measures the hemodynamic response related

to neural activity in the brain or spinal cord of humans. fMRI is based on the increase in blood flow to the local vasculature that accompanies neural activity in the brain. It is one of the most recently developed forms of neuroimaging. Since the early 1990s, fMRI has come to dominate the brain mapping field due to its relatively low invasiveness, absence of radiation exposure, and relatively wide availability. fMRI as a technique to image brain activity has several advantages over PET, for example, the signal does not require injections of radioactive isotopes, and the total scan time required is shorter. However, the expected resolution of PET images is much larger than the usual fMRI pixel size.

1.1.8 Other imaging modalities

Electrical Impedance Tomography (EIT) is a noninvasive and inexpensive method which injects currents with different waveforms, frequencies and spatial patterns through electrodes on a object's surface, and measuring the resultant potentials developed on the same or other electrodes. The measured electrode voltages are used to calculate an image of the electrical admittance distribution within the object [8].

Optical coherence tomography (OCT) is a noninvasive cross-sectional imaging technique in biological systems that is similar in principle to ultrasound, but with superior resolution. It relies on exposing a sample to a burst of light and then measuring the reflective response from different depths and is therefore capable of scanning non-invasively beneath the surface. The ability to detect the positional delay of light reflecting from a tissue sample is at the heart of OCT [9].

There are a number of other medical imaging modalities used for various applications such as angiography, oximetry, intravascular imaging, and bone

dosimetry (radio-isotope imaging).

1.2 Research Approach

In the Picture Archiving and Communication System (PACS), various medical images based on DICOM standard are archived together and delivered for the purpose of sharing image information. However, the images are large and have different information contents. Moreover, archiving and transmission of information of no interest within these images present a computational challenge. In addition, the transmission channels (mainly wireless), introduce nonstationary noise and multi-path interferences to the reconstructed data in the receiver. Therefore, designing an efficient system for transmission of such images is a big challenge for researchers and engineers. In this research, the DWT, EZW, and Reed-Solomon (RS) coder have been adopted for JSCC. A blind technique was used to evaluate the status of the channel noise in the receiver part. A feedback scheme was also developed. Such scheme sends the noise-level over practical transmission channel back to the transmitter in order to appropriately adjust the parity length for the next transmission. An efficient communication system adopts a channel coding scheme which not only emphasizes the RoI through a progressive transmission strategy, but also compensates for the effect of channel noise through an efficient feedback system. The source compression rate is influenced by the proximity of surrounding subblocks from the RoI centre, which includes significant diagnostic information. Also, the channel coding scalability is affected by both the RoI and the channel characteristics. Accordingly, both the source compression rate and the parity code length are jointly adapted to the RoI, channel characteristics, and the required bitrate or channel capacity. The experimental results verify the effectiveness

of the design. Using the proposed system an effective transmission of large medical images through narrowband mobile communication channels can be achieved.

During the course of this research, I attended several courses, conferences, workshops in order to acquire the background knowledge needed to carry out my research. I also consulted design engineers involved in Mathworks regarding how to use the embedded Matlab function and Simulink HDL coder in order to convert the developed algorithm in Matlab codes into HDL codes. The main objectives of my research were therefore to

- understand the principles of JSCC, channel models, efficient image transmission system, and favorably implementing in telemedicine.
- review the current research on the progressive transmission of medical images.
- develop an effective source-channel coding technique, a blind technique for evaluating the level of noise in the channel, and a feedback scheme to form an interactive and adaptive transmission system in order to progressively transmit the images.
- understand the embedded Matlab function and Simulink HDL coder and Altera FPGA in order to implement a real-time progressive system.

1.3 Structure of the Thesis

Chapter 2 provides a comprehensive review of the literature on the progressive transmission of images, and focuses on the principles of JSCC, and progressive transmission. To implement the necessary hardware, the Haar

Wavelet Transform (HWT) and EZW were adopted for source coding because those methods are suitable for implementing hardware into a portable device and FPGA chip. The RS codes utilized here are block-based error correcting codes and are widely used for current communication systems. The RS(n,k) codes correct the symbol error, not the bit error, and are particularly useful in combating of random and burst errors. The JSCC and UEP scheme in this approach tries to optimize the rate-distortion function to achieve an efficient transmission.

The compression part of the proposed scheme is similar to that of JPEG2000's. However, unlike JPEG2000's scheme, our scheme provides variable parity length for an adaptive channel coding, which replaces EBCOT with EZW for compression and progressive image transmission.

Chapter 3 presents the idea developed to form an interactive and adaptive progressive transmission system. In most cases, the physician desires to inspect only one part of the transmitted image, therefore, the emphasis on the RoI is to transmit the desired image part as distortionless as possible and to speed up the transmission. The practical transmission channels are complex and therefore the conditions should be examined before the development of the transmission system. Generally, errors are detected in the receiver end. A feature called Hybrid Automatic Repeat reQuest (HARQ) ask for retransmission of erroneously received data and tradeoff bit-allocation between the source and channel codes according to a rate-distortion optimization policy. However, many studies on tradeoff for bit-allocation between source codes and channel codes assume that the noise-level in the channel is known in advance. Therefore, the feedback signal is determined based on the known noise levels and the constraints set by the user. A blind technique is introduced in this chapter to evaluate the actual channel noise and generate a

feedback to the transmitter. Accordingly, the appropriate parity length is a function of data location and feedback message.

Chapter 4 briefly introduces a new source coding called Compressive Sensing (CS). A Hierarchical Alternative Least Squares (HALS) based CS is used effectively for adaptive selection of the wavelet coefficients and non-linearly thresholding the transform coefficients. HALS based CS provides a sparse signal $x \in \Re^J$ with a few significant samples ($m << J$ nonzero coefficients) which can be recovered almost perfectly using a lower dimensional signal. The performance of CS and EZW are also compared in this chapter.

The overall system design, experimental results, analysis and comparison are presented in Chapter 5. The system block diagram consists of HWT/IHWT, EZW/IEZW, RS encoder/decoder, and the feedback strategy. Several figures and tables are provided to demonstrate the performance of the developed algorithm. The first transmitted image is the blur background image. The physicians use the computer mouse to point to the centre of RoI, and then the values of coordinate are sent back to the transmitter by the receiver. The RoI size is expanded gradually in the next stages. The variability in parity length significantly improve performance of the system.

The hardware implementation is described in Chapter 6. The design technique is proved to speed up the IC design process. Conventionally, there are three steps in the IC design process:

- Algorithm Development: Matlab, Simulink, C or C++ language,$\cdots$
- Design and Simulation: VHDL, Verilog, Modelsim, Synopsys VCS, Cadence,$\cdots$
- Prototyping and Implementation: ASIC, FPGA, CPLD.

However, the design process above has a drawback; the developed algorithm

needs to be designed by an algorithm developer and a separate hardware description language (HDL) is required. We therefore adopt the embedded Matlab function and Simulink HDL coder to achieve the overall system design. The advantage of this design method is that only Matlab language is used. The new system design process can reduce the design cost and shorten the time to market.

The conclusions drawn from the research and future research directions are presented in Chapter 7.

Chapter 2

PROGRESSIVE TRANSMISSION OF IMAGES: LITERATURE REVIEW

Transmission of medical images for medical consultation, diagnosis, treatment, or training purposes requires highly reliable high-speed communication systems. Development of an efficient and reliable system for image archival and transmission poses a serious challenge for researchers due to the enormous amount of medical image data, limitation in bandwidth, and the need to display the desired images as rapidly as possible. To achieve efficiency, source coding techniques are adopted. Such techniques can be lossless or lossy. In lossless data compression, the source coding theorem [10] states that the entropy H(x) of a source x is the minimum rate at which a source can be encoded without information loss. The definition of entropy of **X** is the following:

$$\mathbf{H(X)} = \sum_{i=1}^{n} p(x_i)\boldsymbol{I}(x_i) = -\sum_{i=1}^{n} p(x_i)\log_b p(x_i)$$

where n is number of symbols in **X**, b is the base of the logarithm used, p denotes the probability mass function of **X**. If $p(x_i)=0$, the value of the

corresponding summand $0 \log_b 0$ is taken to be 0, which is consistent with the limit:

$$\lim_{p \to 0^+} p(x_i) \log p(x_i) = 0$$

In lossy data compression however, the reconstructed data is not exactly the same as the original data. In other words, some amount of distortion D is tolerated. There are many methods for error-free coding such as run-length encoding (RLE) [11], Huffman coding [12], and arithmetic coding [13]. Techniques such as those based on discrete cosine transform (DCT) [14], fractal transform [15], wavelet transform (WT), EZW [16], set partitioning in hierarchical trees (SPIHT) [17], and JPEG [18] are lossy algorithms. The JPEG2000 [19] includes both lossy and lossless schemes. For reliable transmission, error correction techniques are used. Although the channel coding theorem states [20] that for error-free transmission over a channel with capacity C_{ch} the transmission rate needs to be smaller or equal to C_{ch}. The definition of C_{ch} is the following:

$$C_{ch} = B \log_2(1 + \frac{S}{N})$$

where B is the bandwidth of the transmission channel in hertz, S and N are power of signal and noise, respectively.

In practice, channels always attain an arbitrarily small probability of error. Channel coding techniques are used to reduce the probability of error below any predetermined level.

The transmission of images over noisy channels is of fundamental importance in many applications and is still an unsolved problem for many types of channels. The channel code (referring mostly to the forward error correction code) is used to detect and correct the corrupted signals caused by

noisy channels. The Hamming [21], cyclic redundancy check (CRC) [22], Reed-Solomon (RS) [23], BCH [23], rate-compatible punctured convolutional (RCPC) [24], low-density parity-check (LDPC) [25] and turbo codes [26] are widely used for channel coding. To achieve an efficient and reliable transmission system, separately designed source and channel coders are not suitable in practical applications, due to several drawbacks such as catering for infinite complexity and delay, and the invalidity for nonergodic and multi-user channels. Joint source-channel coding (JSCC) is therefore used instead of the current applications [27–34]. The aim of a JSCC approach is to optimally allocate bits to both source and channel coders to minimize total distortion while satisfying a constraint on the total rate [35].

The Digital Imaging and Communications in Medicine (DICOM) technique has been developed as a standard for the distribution and viewing of medical images from different modalities. The JPEG 2000 has been adopted as a standard compression component in the DICOM standard and is the ultimate state of the art image compression algorithm which includes both lossy and lossless schemes. The DWT, exploitation of RoI, quantization, and EBCOT (Embedded Block Coding with Optimization Truncation of the embedded bitstream) [36], rate-allocation, and progressive transmission algorithms are important technologies used in the JPEG 2000. EBCOT is the compression engine of JPEG2000 and includes context model arithmetic coding and post-compression rate allocation. These algorithms make the JPEG 2000 more robust against communication error compared to other existing compression algorithms. In [37], the authors describe each feature in detail and provide many experimental results to show the advantages of the JPEG2000.

Progressive image transmission (PIT) is an image transmission tech-

nique based on embedded source codes that allows the image to be transmitted in several successive stages, and is particularly useful for low rate channels. PIT can be achieved by first transmitting a low-resolution approximation of the image, then sending further information to progressively improve the quality of the reconstructed image. PIT also allows the receiver to interrupt the communication as soon as the necessary information is recognized, or the necessary quality is attained. However, even by having one error bit at the entropy decoder, the reconstructed image will be profoundly affected [38].

Many researchers have therefore proposed various methods such as JSCC, rate-distortion (R-D), unequal error protection (UEP), and the RoI-based technique in combination with PIT to achieve a reliable and efficient image transmission. In [39], the authors adopted EZW, bit-rate constraint, and RoI-based techniques to achieve a PIT scheme for medical image transmission. They showed several successive reconstructed images with/without variable compression rates. Also, according to experimental results and a comparison of EZW and JPEG2000 algorithms, the JPEG2000 achieved better PSNR in the lower compression ratio (CR) than EZW, whereas EZW had better performance in the higher CR. The proposed scheme also provides similar data protection for all transmission data. Generally, the data in the RoI has to receive higher data protection because any error is not tolerated in the data protection strategy based on the RoI. Similar work was carried out by [40]. In [41], although the authors provide a UEP scheme in the proposed PIT system, the decoding was stopped and the image was reconstructed from the correctly decoded packets if the decoder detected an error.

Generally, any error in the reconstructed medical image can not be toler-

ated, because medical images require a large amount of precise information, which can be difficult to achieve under low rate channel condition. Therefore, an image transmission system which is suitable for medical purposes should include lossless or lossy, rate variability, progressive scheme, and efficient rate-allocation features.

The goal of our proposed system is to develop a progressive medical image transmission system for portable devices. In developing the proposed scheme, we not only attempt to incorporate all the features previously implemented, but also aim to develop a less complex and more flexible system. Although EBCOT is a state-of-the-art image compression algorithm, it is very complex and occupies over half of the computation time in the coding process and is therefore memory intensive [42]. For ease of implementation in portable devices and to take into account lower hardware circuit complexity, we adopt the Haar transform and EZW as the source compression instead of EBCOT in order to reduce the memory size and hardware cost, while keeping all features similar to the JPEG2000. The schemes for both source and channel codings mentioned above are combined together as described in the following steps to achieve the proposed system.

- The DWT and EZW are used to compress images and allow gradual streaming and reconstruction of images as for progressive transmission. They are easy to implement and are therefore suitable for portable devices.

- Conventional RS channel coding adds sufficient redundancy to the data to protect it during transmission and to effectively detect and correct the corrupted messages.

- The UEP, RoI, feedback and JSCC scheme are combined together to

make an efficient progressive image transmission system possible.

- The selectivity of the RoI is totally interactive and can be defined by the user in the receiver. This makes the method favorable to clinicians who require fast access to particular information embedded in the RoI.
- An algorithm is proposed for estimating and providing the information about the noise-level in the transmission channel. Based on the feedback, an appropriate data protection can be provided for the next transmission.

The overall proposed JSCC system is shown in the block diagram in Fig. 2.1.

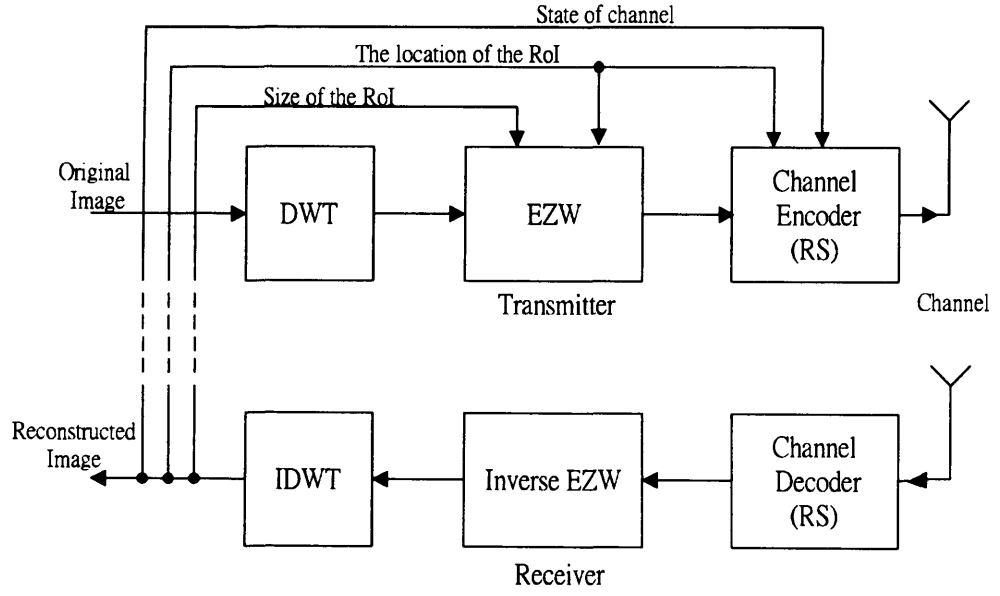

Figure 2.1. Block diagram of the proposed JSCC system.

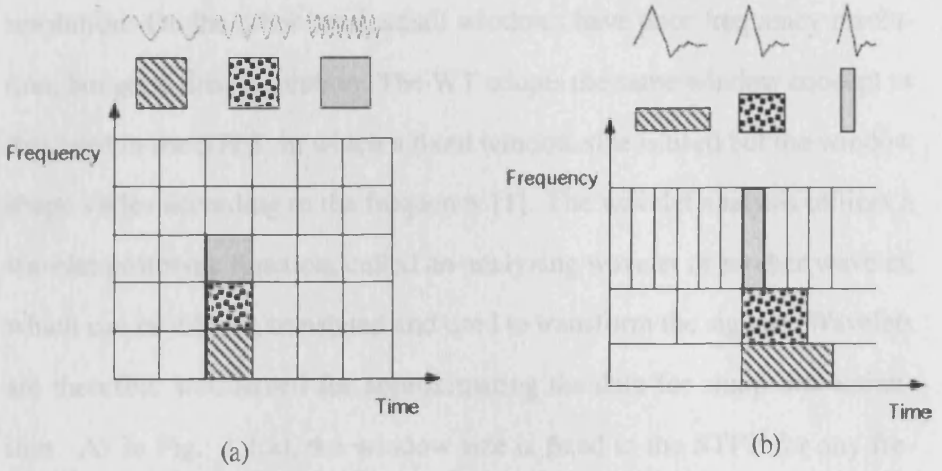

Figure 2.2. (a) Fourier basis functions, time-frequency tiles, and coverage of the time-frequency plane, (b) Daubechies wavelet basis function, time-frequency tiles, and coverage of the time-frequency plane [1].

2.1 Wavelet Transform and its Application in Image Compression

Windowed Fourier Transform or Short-Term Fourier Transform (STFT) is proposed to overcome the drawbacks of the frequency domain approaches. The STFT can be used to give information about signals in both time and frequency domains simultaneously. It is a time-frequency localization technique with a fixed size and shape window. The STFT expresses the time-frequency representation of the signal $f(t)$ as:

$$F(\tau, f) = \int_{-\infty}^{\infty} f(t)g(t-\tau)e^{-j2\pi f(t-\tau)}dt \qquad (2.1.1)$$

where $g(t)$ is the basis function of the window and τ is the shift location in the signal.

Although, according to the Uncertainty Principle [43], it is impossible to know the exact frequency and time of occurrence of this frequency in a signal, the STFT is not a perfect solution for non-stationary signals, since when using large windows it gives good frequency resolution but poor time

resolution. On the other hand, small windows have poor frequency resolution, but good time resolution. The WT adopts the same window concept as that used in the STFT, in which a fixed window size is used but the window shape varies according to the frequency [1]. The wavelet analysis utilizes a wavelet prototype function, called an analyzing wavelet or mother wavelet, which can be dilated, translated and used to transform the signals. Wavelets are therefore well-suited for approximating the data for sharp discontinuities. As in Fig. 2.2(a), the window size is fixed in the STFT for any frequency. In (b), the window size is fixed, and the window shape varies in frequency.

2.1.1 Continuous wavelet transform

A WT involves convolving the signal with particular instances of the wavelet at various time scales and positions. The mother wavelet, $\psi(t)$, is a continuous function which has two properties [1,44]:

1. The function integrates to zero:

$$\int_{-\infty}^{\infty} \psi(t)dt = 0 \tag{2.1.2}$$

2. It is square integrable or, equivalently, has finite energy:

$$\int_{-\infty}^{\infty} |\psi(t)|^2 dt < \infty \tag{2.1.3}$$

Other wavelets are dilations and translations of the mother wavelet:

$$\psi_{(s,\tau)}(t) = \frac{1}{\sqrt{|s|}}\psi(\frac{t-\tau}{s}) \tag{2.1.4}$$

where parameters s and τ show that the $\psi(s,\tau)$ is dilated by a factor s, $s < 1$ for high frequency (narrow width) and $s > 1$ for low frequency (wider width), and translated by factor τ, which is a position on the time axis. The basic idea of the wavelet transform is to represent any arbitrary function $f(t)$ as a superposition of mother wavelets.

$$\gamma(s,\tau) = \int_{-\infty}^{\infty} f(t)\psi_(s,\tau)^* dt \tag{2.1.5}$$

where $(\cdot)^*$ denotes complex conjugation.

In practical situations where the data is discrete, a discrete form namely DWT is used. The WT coefficients are used to reconstruct the data by the weighted sum of the orthogonal wavelet basis functions. To reconstruct the data from its wavelet coefficients, we have [40]:

$$f(t) = \sum_{s,\tau} \gamma(s,\tau)\psi_{s,\tau}(t) \tag{2.1.6}$$

2.1.2 Discrete wavelet transform and its applications

The DWT provides a fast, local, sparse, multiresolution analysis of real-world signals and images. The DWT may be performed using as a series of filter banks, as used in subband coding. Each digital filterbank is made up of a series of lowpass and highpass filters (see Fig. 2.3). In Fig. 2.3, $x[n]$ is the discrete input signal, $g_1[n]$ and $h_1[n]$ represent the half-band highpass and half-band lowpass filters in analysis stage, $g_2[n]$ and $h_2[n]$ represent the half-band highpass and half-band lowpass filters in synthesis stage respectively. In this figure $\downarrow 2$ represents decimation by 2 and $\uparrow 2$ represents upsampling by 2. The DWT of a signal is then presented as filtering the signal by a filter bank where the outputs of different filter stages are the transform co-

efficients. The decomposition can be mathematically expressed as:

$$y_{high}[k] = \sum_n x[n] \cdot g_1[2k - n] \tag{2.1.7}$$

$$y_{low}[k] = \sum_n x[n] \cdot h_1[2k - n] \tag{2.1.8}$$

The reconstruction of the signal is expressed as:

$$\hat{x}[n] = \sum_{k=-\infty}^{\infty} (y_{high}[k] \cdot g_2[-n + 2k]) + (y_{low}[k] \cdot h_2[-n + 2k]) \tag{2.1.9}$$

where $y_{high}[k]$ and $y_{low}[k]$ are the outputs of highpass and lowpass synthesis filters respectively, after decimation by two. To achieve perfect reconstruction, the analysis and synthesis filters have to satisfy conditions as [45]:

$$g_2(n) = (-1)^{n+1} h_1(n)$$

$$g_1(n) = (-1)^n h_2(n)$$

$$g_1(-n)g_2(n) + h_1(-z)h_2(n) = 0 \tag{2.1.10}$$

$$g_1(n)g_2(n) + h_1(n)h_2(n) = 2 \tag{2.1.11}$$

Equation (2.1.10) implies that the reconstruction is aliasing-free and (2.1.11) is to reconstruct signal, $\hat{\mathbf{x}}$.

An example of a filterbank output is shown as Fig. 2.4(a). In this transform, the approximated data in LL_N contains the most important part of the information. Wavelet coefficients in a low subband can be thought of as having four descendants in the next higher subband and each of the four descendants has four other descendants in the next higher subband. The corresponding quadtree structure of an 8×8 block is shown in Fig. 2.4(b).

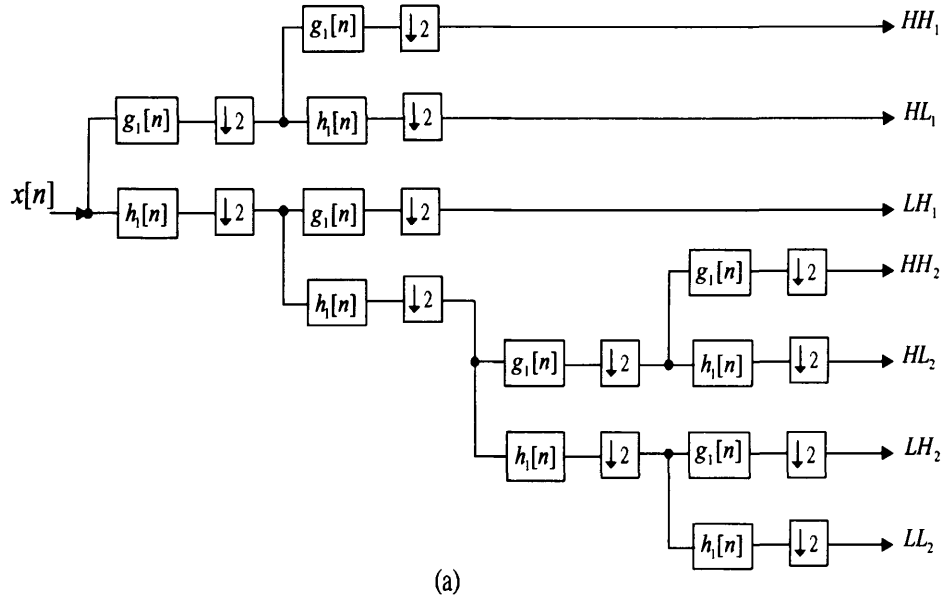

(a)

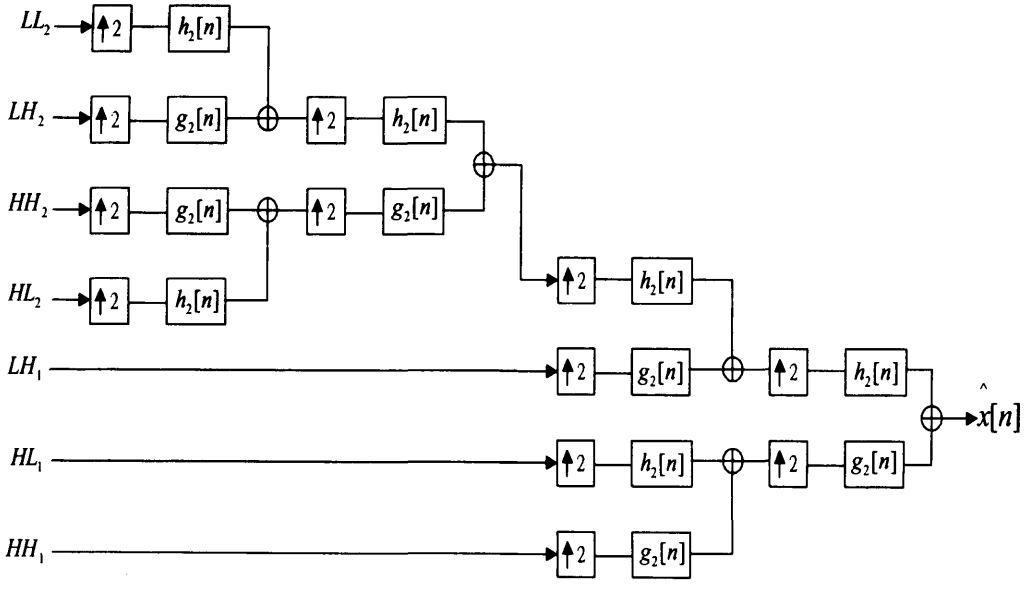

(b)

Figure 2.3. (a) 2-level forward wavelet filterbahk, (b) 2-level inverse wavelet filterbank, taken from [2].

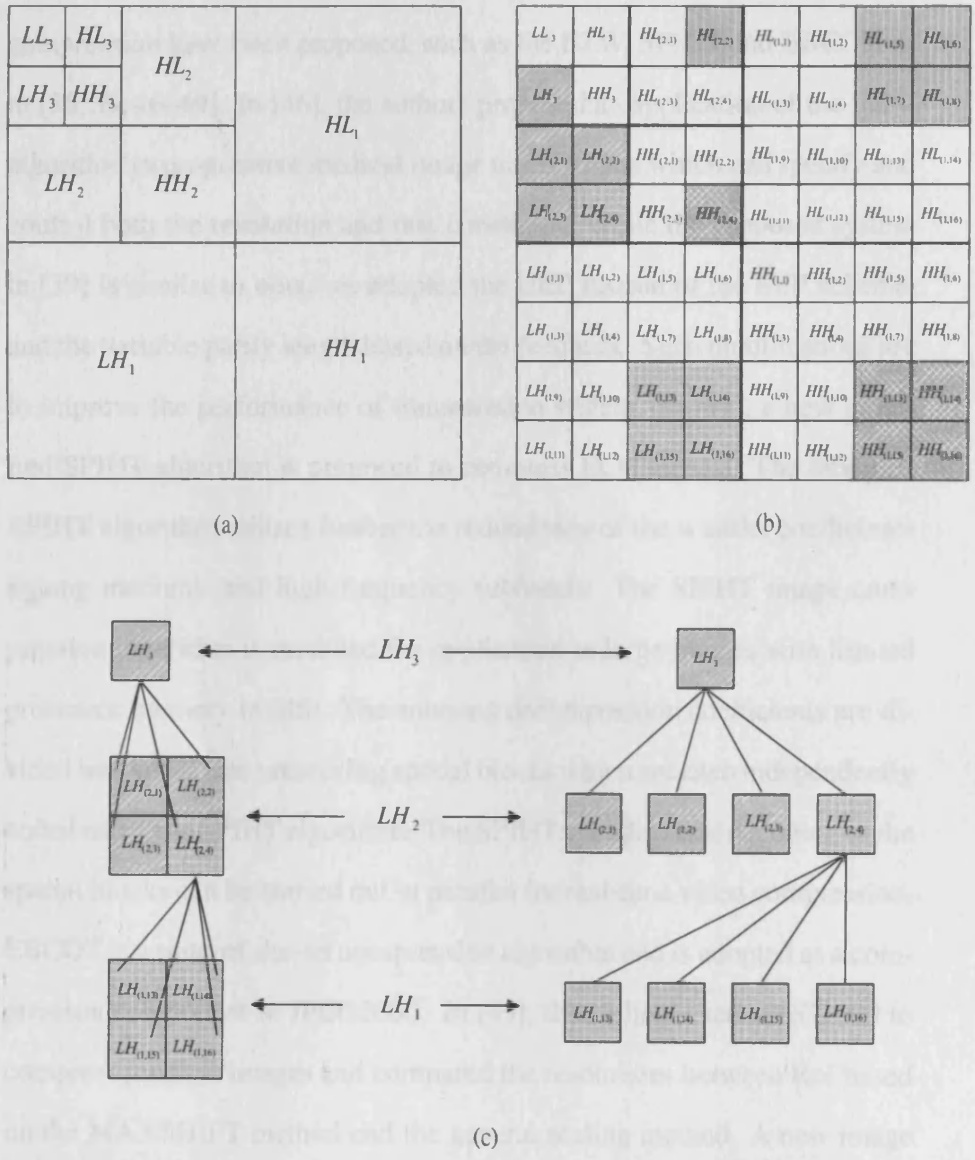

Figure 2.4. (a) Different subbands in an 8×8 block after 3-level WT, (b) Relations between wavelet coefficients in different subbands, and (c) The relations expressed as quad-tree structure .

The DWT has important applications in many domains, such as image compression, computer graphics, numerical analysis, radar target localization. In recent years, several wavelet-based coding algorithms for image compression have been proposed, such as the EZW, SPHIT and EBCOT, as in [36, 39, 46–49]. In [46], the authors proposed an application of the EZW algorithm in progressive medical image transmission which can specify and control both the resolution and rate constraint. While the proposed system in [39] is similar to ours, we adopted the UEP instead of the EEP scheme, and the variable parity length based on the feedback. Such modifications are to improve the performance of transmission system. In [47], a new modified SPIHT algorithm is proposed to compress ECG signals. The modified SPIHT algorithm utilizes further the redundancy of the wavelet coefficients among medium- and high-frequency subbands. The SPIHT image compression algorithm is modified for application to large images with limited processor memory in [48]. The subband decomposition coefficients are divided into small tree-preserving spatial blocks which are each independently coded using the SPIHT algorithm. The SPIHT encoding and decoding of the spatial blocks can be carried out in parallel for real-time video compression. EBCOT is a state-of-the-art compression algorithm and is adopted as a compression component in JPEG2000. In [49], the authors used JPEG2000 to compress medical images and compared the resolutions between RoI based on the MAXSHIFT method and the general scaling method. A new image compression algorithm is proposed based on EBCOT in [36]. The algorithm produces a bit-stream with a rich set of features, including resolution and SNR scalability together with a random access property.

Although the DWT is a powerful tool for signal and image processing, it has three serious disadvantages: shift sensitivity, poor directional-

ity, and lack of phase information [50]. The input signal shift causes an unpredictable change in transform coefficients, which mostly arises from downsamplers in the DWT implementation. Natural images are comprised of several different orientations, but the separable 2D DWT only has three orientations: horizontal, vertical and diagonal. Since the phase information is very useful in signal processing application, a new algorithm called complex wavelet transform (CWT) is proposed to overcome the disadvantages in the DWT. The Dual Tree Complex Wavelet Transform (DTCWT) is introduced and compared with the DWT in [51]. Although the DTCWT can detect the details over more than three directions compared with the DWT, it generates more redundancy. According to the experimental results in [52], the resolution of reconstructed image utilizing DTCWT is better than that obtained utilizing by the DWT. In [50], the authors proposed an algorithm called mapping-based CWT to overcome the three disadvantages of the DWT. The algorithm also possesses the additional benefits of flexibility and controllable redundancy. According to the authors, the proposed algorithm is one of a few CWT-based algorithms that can solve all the three disadvantages of DWT.

2.1.3 Haar wavelet transform and its application in image processing

Many kinds of mother wavelets have been developed by researchers. The most basic WT is the Haar wavelet transform (HWT) described by Alfred Haar in 1910 [53]. In our proposed scheme, we used 3-level HWT to achieve the WT as it is easier for hardware implementation than other kinds of WT. The HWT coefficients are defined below:

$$d_i = \frac{S_i - S_{i+1}}{2} \tag{2.1.12}$$

$$a_i = \frac{S_i + S_{i+1}}{2} \tag{2.1.13}$$

where d_i and a_i represent the coefficients of detail and approximation after the HWT. S_i is the element in the image and i is the location index. The process is begun by systematically averaging and differencing paired entries in a matrix and then entering the average in the first space of the resulting matrix. The process subsequently finds the difference between these paired entries and the average, and the result is entered as the halfway point. For example, the procedure for a one-dimensional discrete signal $x[n] = [10, 11, 12, 13, 14, 15, 16, 17]$ using 3-level HWT is as follows:

1. The averaging and differencing of each pair is shown below

Averaged	pair	Differenced
10.5	(10, 11)	-0.5
12.5	(12, 13)	-0.5
14.5	(14, 15)	-0.5
16.5	(16, 17)	-0.5

A new matrix is subsequently created after first-level HWT, i.e.

$$[10.5 \quad 12.5 \quad 14.5 \quad 16.5 \quad -0.5 \quad -0.5 \quad -0.5 \quad -0.5]$$

The averaged results are called approximation coefficients, and the differenced results are called detail coefficients.

2. We can repeat the process for only the averaged values (not differenced values), until only a signal averaged value or a number of data

layers is achieved. The final results after 3-level HWT are as follows.

x[n]	10	11	12	13	14	15	16	17
1st level	10.5	12.5	14.5	16.5	−0.5	−0.5	−0.5	−0.5
2nd level	11.5	15.5	−1	−1	−0.5	−0.5	−0.5	−0.5
3nd level	13.5	−2	−1	−1	−0.5	−0.5	−0.5	−0.5

Normally, an image can be considered as a two-dimensional matrix. In the proposed scheme, we decompose the image into an 8×8 block for the HWT to reduce computational cost. The HWT of a two dimensional matrix deals with each column of coefficients first, and then deals with each new row of coefficients. Accordingly, the result after the first level of Haar wavelet transform can be expressed as :

$$T_1 = N_1^T A N_1 \tag{2.1.14}$$

where A denotes the input matrix and T_1 is the result of the first level wavelet transformation. The result of the second level WT is $T_2 = N_2^T T_1 N_2$ and the result of the third level wavelet transform matrix is $T_3 = N_3^T T_2 N_3$. The 3-level wavelet transform matrix can thus be expressed as follows:

$$T = N^T A N \tag{2.1.15}$$

where $N^T = N_1^T N_2^T N_3^T$, $N = N_1 N_2 N_3$, respectively. N_1, N_2, N_3 are defined below:

$$N_1 = \begin{bmatrix} \frac{1}{2} & 0 & 0 & 0 & \frac{1}{2} & 0 & 0 & 0 \\ \frac{1}{2} & 0 & 0 & 0 & \frac{-1}{2} & 0 & 0 & 0 \\ 0 & \frac{1}{2} & 0 & 0 & 0 & \frac{1}{2} & 0 & 0 \\ 0 & \frac{1}{2} & 0 & 0 & 0 & \frac{-1}{2} & 0 & 0 \\ 0 & 0 & \frac{1}{2} & 0 & 0 & 0 & \frac{1}{2} & 0 \\ 0 & 0 & \frac{1}{2} & 0 & 0 & 0 & \frac{-1}{2} & 0 \\ 0 & 0 & 0 & \frac{1}{2} & 0 & 0 & 0 & \frac{1}{2} \\ 0 & 0 & 0 & \frac{1}{2} & 0 & 0 & 0 & \frac{-1}{2} \end{bmatrix}.$$

$$N_2 = \begin{bmatrix} \frac{1}{2} & 0 & \frac{1}{2} & 0 & 0 & 0 & 0 & 0 \\ \frac{1}{2} & 0 & \frac{-1}{2} & 0 & 0 & 0 & 0 & 0 \\ 0 & \frac{1}{2} & 0 & \frac{1}{2} & 0 & 0 & 0 & 0 \\ 0 & \frac{1}{2} & 0 & \frac{-1}{2} & 0 & 0 & 0 & 0 \\ 0 & 0 & 0 & 0 & 1 & 0 & 0 & 0 \\ 0 & 0 & 0 & 0 & 0 & 1 & 0 & 0 \\ 0 & 0 & 0 & 0 & 0 & 0 & 1 & 0 \\ 0 & 0 & 0 & 0 & 0 & 0 & 0 & 1 \end{bmatrix}.$$

$$N_3 = \begin{bmatrix} \frac{1}{2} & \frac{1}{2} & 0 & 0 & 0 & 0 & 0 & 0 \\ \frac{1}{2} & \frac{-1}{2} & 0 & 0 & 0 & 0 & 0 & 0 \\ 0 & 0 & 1 & 0 & 0 & 0 & 0 & 0 \\ 0 & 0 & 0 & 1 & 0 & 0 & 0 & 0 \\ 0 & 0 & 0 & 0 & 1 & 0 & 0 & 0 \\ 0 & 0 & 0 & 0 & 0 & 1 & 0 & 0 \\ 0 & 0 & 0 & 0 & 0 & 0 & 1 & 0 \\ 0 & 0 & 0 & 0 & 0 & 0 & 0 & 1 \end{bmatrix}.$$

The inverse HWT can be expressed as:

$$A = ((T^T)N^{-1})^T N^{-1} = (N^{-1})^T T N^{-1} \tag{2.1.16}$$

where the inverse of matrix N is $N^{-1} = N_3^{-1} N_2^{-1} N_1^{-1}$.

A hardware-oriented image coding processing scheme based on the HWT is presented in [54]. The procedure computes a variant of the HWT to gain the lowest circuit complexity hardware implementation. In our proposed system, we chose a 3-level HWT to perform the DWT for each subblock, due to its simplicity and it being faster and easier to implement than other DWT methods.

2.2 Joint Source-Channel Coding

In many image transmission applications, it is not only the end-to-end performance that is important, but also the performance during the transmission. For a reliable and efficient image transmission design, both source and channel coders are needed to achieve this. For source coding, state-of-the-art wavelet-based coding algorithms are EZW, SPIHT, and EBCOT. Data protection techniques, as the major component of channel coding, can be classified into four main categories [55]:

1. Automatic repeat request (ARQ) [23]: in this process, the receiver checks the received data and asks the transmitter to retransmit the message if errors are detected or packets are lost. However, ARQ can be used only in a feedback system and may not be acceptable in strict time constraint applications.

2. Error resilience and concealment techniques: in error resilience techniques, the bitstream is modified to make it more robust to channel

noise, such as interleaving, tiling, or packetization techniques. Error concealment techniques are used to exploit redundant information in a sequence to recover missing data.

3. Forward error coding (FEC) [23]: the extra redundant symbols are added to the transmitted data, allowing the receiver to detect and correct errors caused by the transmission channels. Such coding may be CRC, RS, RCPC, and LDPC coding.

4. Hybrid techniques: these combine any number of the above methods.

In practical transmission systems, a JSCC scheme has better performance and more robustness than schemes with separate source and channel coding designs. Generally, system designers select prefabricated components for the source coder, and the channel coder and must achieve the best performance within these constraints. A major step in designing a JSCC scheme is to model the distortion introduced in the received image due to quantization and channel errors. This distortion is then used either as an objective function to be minimized or as a constraint in the design of a JSCC scheme [34]. The error protection strategy (EPS) algorithm optimally allocates a transmission rate budget for JSCC schemes. In [56], JSCC approaches are classified into four broad categories:

1. joint source-channel coders: where the source and channel coding operations are truly integrated.

2. concatenated source-channel coders: which allocate a fixed bit rate between a cascaded source coder and a channel coder.

3. unequal error protection source-channel coders: in which the output

of the source encoder is afforded unequal protection based on the effect of errors on the reconstruction sequence.

4. constrained joint source-channel coders: where a given source and/or decoder is modified to account for the presence of a given noisy channel.

For many applications, the channel condition cannot be predicted precisely before the transmission. Accordingly, as JSCC techniques usually require adequate knowledge about the transmission channel, a channel condition mismatch could cause devastating decoding effects. It is therefore highly desirable that JSCC applications are able to tolerate a certain amount of residual error caused by nonergodic channel behavior or from other error sources [57]. Generally, the JSCC scheme is combined with the rate allocation algorithm to achieve an efficient transmission system. The rate allocation algorithm is used to trade off the transmission rate between source coding and channel coding to obtain the best visual quality with the lowest bit rate. The UEP feature is another feature added to the JSCC transmission system. The main idea behind the UEP is that it provides different levels of data protection based on the importance of the transmitted data. In our proposed system, the UEP feature is based on the data location in the transmitted image and transmission channel condition.

In [58], the authors proposed a concatenation of an outer cyclic redundancy check (CRC) code for error detection and an inner rate-compatible punctured convolutional (RCPC) code for error correction in order to protect the SPIHT bitstream to achieve an efficient progressive JSCC system. The SPIHT compressed bitstream is segmented into blocks of fixed length for the error resilience model and the EEP is employed, not the UEP scheme. The decoding is stopped when the first uncorrectable error is detected. The

JSCC scheme in [59] is the same as in [58], but [59] provides about 0.3 dB improvement over the method in [58] with the same source and channel coders because the UEP is used to replace the EEP. The authors in [60] proposed a hybrid coder that combines the packetized zerotree wavelet (PZW) coder in [61] and CRC/RCPC coders in [58], and showed that the proposed scheme had better performance than that introduced in [58, 61] in the varying channels. This proposed scheme was improved by [62] using an optimal packetization scheme and CRC/RCPC to replace the PZW. In [63], the work of [58] is extended to fading channels by adding a second layer of protection using RS codes in the framework of product codes. The proposed scheme in [62] uses RS and RCPC as an FEC scheme and provides a linear-time algorithm, similar to that used in [63], for the efficient selection of both RS and RCPC code rates to improve the hybrid approach of [60]. In [64], an efficient rate allocation is proposed based on the available source rate criterion from [65]. It achieves optimal protection with reduced complexity for the SPIHT image coder. In [41], the authors proposed a linear-time algorithm for computing a UEP scheme that maximizes the average of the expected number of correctly received source bits over a set of intermediate transmission rate in a JSCC scheme.

In [66], the authors proposed a progressive time-varying source-channel coding system for transmitting images over wireless channels. The core result was a systematic method of instantaneous rate allocation between the progressive source coder and channel coder. In [4], the authors used the sequence maximum a posteriori method to design a joint source channel decoder under the Gilbert-Elliott channel (GEC) and estimate the parameters of the GEC model through the hidden Markov model. Based on [59], the authors in [67] adopted the JSCC technique to develop a transmission sys-

tem using different channels, such as BSC, GEC, and fading channels using finite-state Markov channel (FSMC). Employing an effective tool called error sequence analysis, they analytically obtained the probability distribution of the error sequence and used a concatenation of RCPC and CRC codes to form a UEP scheme and find the optimal rate allocation solutions for progressive image transmission over noisy channels based on the FSMC model. The authors in [68] proposed a JSCC method for transmission of images over fading channels and demonstrated the application of rate-compatible low-density parity-check (RC-LDPC) codes constructed by the progressive edge-growth algorithm. They used the UEP to protect the images over fading channels.

The JSCC system with feedback channel is proposed in [69–71]. The feedback signal can shift the optimal rate allocation point, resulting in higher rates for error-correcting codes and smaller overall distortion. According to the simulation results on both memoryless and fading channels, the system with feedback channel shows improvement in PSNR compared to a similar system without feedback.

The JPEG2000 is being widely used because it is a state-of-the-art compression algorithm [19]. The authors in [72] used a Viterbi-algorithm (VA)-base rate allocation approach to create a transmission system utilizing turbo codes and JPEG2000 to simulate performance over a BSC. A similar algorithm was used in [73]. However, the algorithm discussed in [72] is simpler than in [73] because it starts from a rate-optimal solution, and converges to a local distortion optimal solution, and also has better quality of the reconstructed image than that of [58]. In [74], the JPEG2000 as source coder and RCPC as channel coder are used to form a JSCC scheme for image transmission. A combination of the JPEG2000 and rate-compatible punctured turbo

(RCPT) codes forms the JSCC scheme in [75] for the parallel transmission of scalable images in multichannel systems. In [31], the authors proposed a JSCC scheme with UEP for transmission of JPEG2000 codestreams over memoryless channels. The proposed scheme combines the FEC capability provided by channel codes, together with the error detection and localization functionality provided by the JPEG2000 error resilience tool in an effective way.

Presently, with current state-of-the-art source-coding technology, many communication channels are now capable of delivering several compressed images or video sequences concurrently. This makes it possible for some applications to transmit multiple images together sharing a common channel. In [33], a JSCC algorithm is proposed for the transmission of multiple image sources over memoryless channels. The proposed algorithm uses a quality scalable image coder to optimally allocate a limited bit budget among all the sources to achieve the optimal overall distortion reduction for the multiple reconstructed images.

In our proposed system, we adopt a 3-level HWT and EZW for source coding and the RS codes are adopted as channel coding to achieve a JSCC scheme. The reason for selecting the Haar wavelet is because it is simpler, needs lower computation time, and is easier to implement into portable devices. The RS codes are block-based and efficient burst error correcting codes used widely in digital communication and storage.

2.2.1 Embedded zerotree wavelet and its applications

The EZW is briefly introduced in this subsection. The EZW was proposed by Shapiro [16] and has become a popular image compression algorithm in various communication systems. The EZW was specifically designed to

be used with the WT and is a simple, efficient, and flexible compression algorithm for low bitrate image coding. The EZW coders work based on the following steps:

1. After WT, the wavelet coefficients are distributed in various subbands. The most important coefficients are located in the lowest subbands, and the order of importance of the subbands can also be obtained.

2. Larger wavelet coefficients are more important than smaller wavelet coefficients. Generally, most larger wavelet coefficients are in the lower subbands.

3. The EZW encoder can terminate the encoding at any point according to the pre-set parameters, such as for a given bitstream and the amount of received data. More details can be added and a higher resolution of the reconstructed image can be obtained.

The EZW suits progressive data transmission since it allows hierarchical encoding and decoding by means of various threshold values. Accordingly, the first step in the EZW algorithm is to determine the initial threshold. In order to obtain a perfectly reconstructed image we need to repeat the process by lowering the threshold until the threshold has become smaller than the smallest coefficient value, or the iteration is stopped by request. The initial threshold t_0 is defined below:

$$t_0 = 2^N, \quad N = \log_2\{max(|\gamma(x,y)|)\} \tag{2.2.1}$$

where max(·) refers to the maximum coefficients in the subblock and $\gamma(x,y)$ represents the coefficient with (x,y) coordinates. After the initial threshold t_0 is found, the EZW algorithm compares the initial threshold t_0 with each coefficient in a predefined scan order as shown in Fig. 2.5.

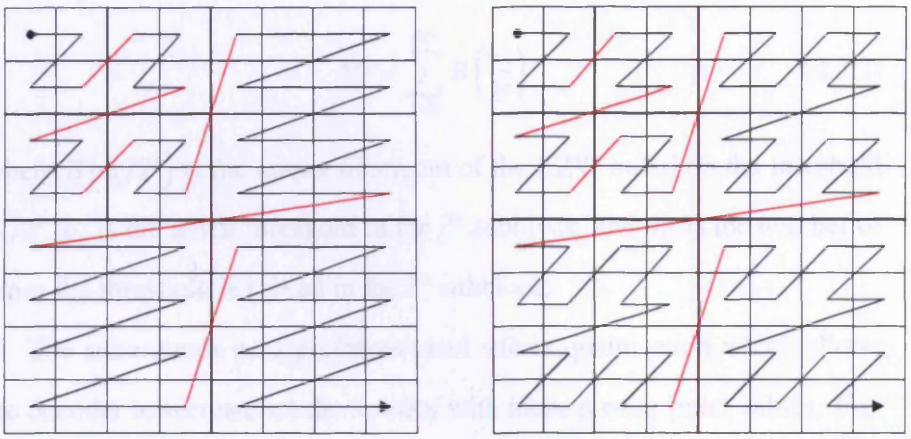

Figure 2.5. Scan order in the EZW, (a) raster scan, and (b) Morton scan. [3]

Table 2.1. Definition of symbols

Symbols	Description
p	$\gamma(x,y) \geq t_n$, called significant coefficients at threshold t_n
n	$\gamma(x,y) < 0$ and $\lvert\gamma(x,y)\rvert \geq t_n$, called negative significant
z	$\gamma(x,y) < t_n$, but some of its descendants have a value greater than t_n, called isolated zero.
t	$\gamma(x,y) < t_n$, and all its descendants have magnitudes less than t_n, called zerotree zero.
1,0	Refinement bits for reconstructing image

In our proposed scheme we adopt a Morton scan. In each scan there is a dominant pass and subordinate pass. The dominant pass generates a series of symbols and the subordinate pass quantizes all significant coefficients. The definitions of the symbols are shown in Table 2.1:

The final threshold level determines the length of the bitstream output. Thus, the length of the output bitstream M_i is related to the number of times the threshold is defined as:

$$M_i = \sum_{k=0}^{n_{T_i}} B\left(\frac{t_{0_i}}{2^k}\right) \tag{2.2.2}$$

where $B\left(t_{0_i}/2^k\right)$ is the output bitstream of the EZW based on the threshold $t_{0_i}/2^k$. t_{0_i} is the initial threshold in the i^{th} subblock, and n_{T_i} is the number of times the threshold is halved in the i^{th} subblock.

The subordinate pass performs pixel values quantization which allows the decoder to reconstruct the symbol with more precise pixel values. Fig. 2.6 and Fig. 2.7 present examples of 8×8 blocks for the EZW process.

The authors in [16, 39, 46, 76] have used the DWT and EZW in their proposed system.

2.2.2 Reed-Solomon codes and their applications

In real world applications, the decoder often receives erroneous data by means of physical transmission channels. Therefore, we need a suitable channel coding strategy to effectively protect the transmitted data. RS coders are popular and have a wide range of applications, ranging from deep-space communication to compact disk (CD) and are easy to implement into portable devices. In this subsection, we briefly introduce the fundamental definition of RS codes. RS codes are block-based error correcting codes developed by Irving S. Reed and Gustave Solomon in 1960 [77] and widely used in wireless communication and storage systems. RS codes are non-binary cyclic codes with symbols made up of m-bit sequence, and are very effective in correcting random burst errors. The RS coder is a coding scheme which works by first constructing a polynomial from the data symbols to be transmitted and then sending an over-sampled plot of the polynomial instead of the original symbols themselves. The meanings of symbols in RS codes

63	-34	49	10	7	13	-12	7
-31	23	14	-13	3	4	6	-1
15	14	3	-12	5	-7	3	9
-9	-7	-14	8	4	-2	3	2
-5	9	-1	47	4	6	-2	2
3	0	-3	2	3	-2	0	4
2	-3	6	-4	3	6	3	6
5	11	5	6	0	3	-4	4

The initial threshold is:

$N = \log_2(63) = 5;$

$t_0 = 2^5 = 32$

The first refine value is:

$R_0 = (63+32)/2 = 48$

(a)

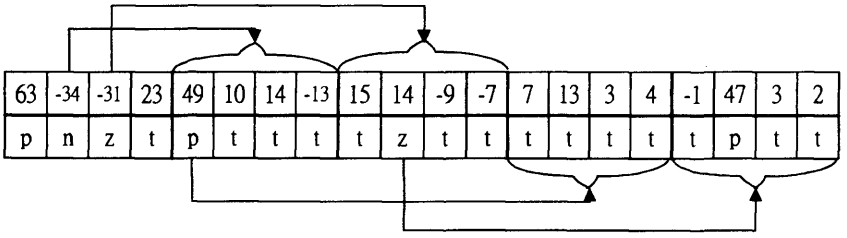

(b)

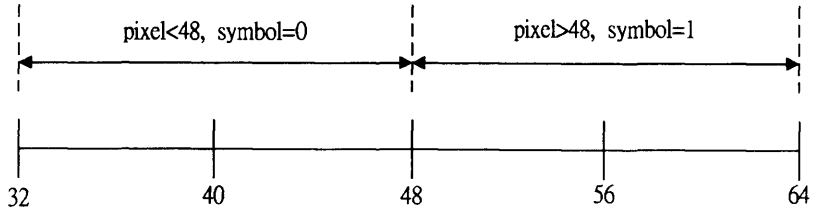

(c)

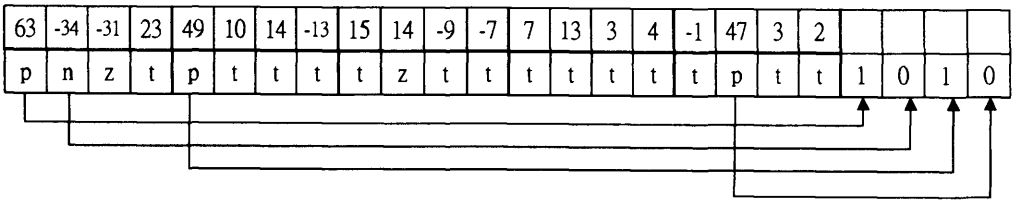

(d)

Figure 2.6. Example of the EZW process, (a) 8 × 8 block data, (b) the first dominate pass output under t_0, (c) the reconstruction value refined at R_0, and (d) the compression output after the first dominate and subordinate pass [2].

0	**0**	**0**	10	7	13	-12	7
-31	23	14	-13	3	4	6	-1
15	14	3	-12	5	-7	3	9
-9	-7	-14	8	4	-2	3	2
-5	9	-1	**0**	4	6	-2	2
3	0	-3	2	3	-2	0	4
2	-3	6	-4	3	6	3	6
5	11	5	6	0	3	-4	4

(a)

The next threshold is:

$N = \log_2(63) = 5;$

$t_1 = t_0 / 2 = 32/2 = 16$

The second refine value is:

$R_1 = R_0 / 2 = 48/2 = 24$

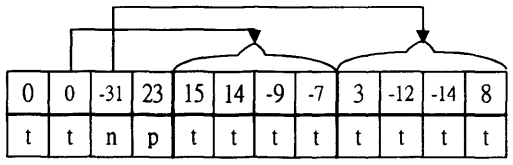

(b)

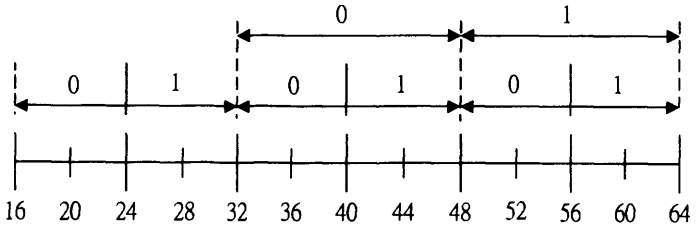

(c)

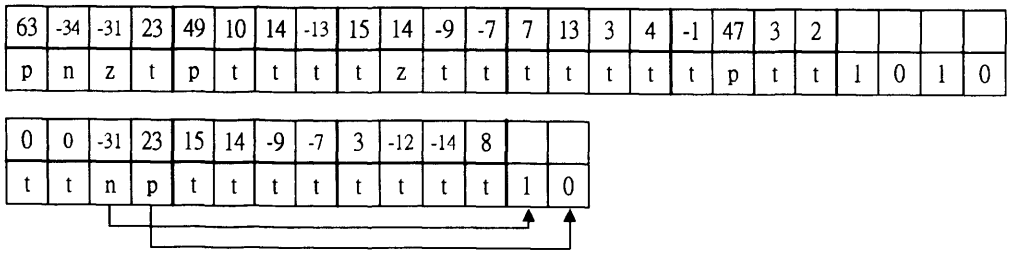

(d)

Figure 2.7. Compression continued based on the new threshold t_1, (a) some coefficients are replaced by 0 after the first compression process, (b) the second dominate pass output under the threshold t_1, (c) refine the reconstruction value refined at R_1, and (d) the compression output after the second dominate and subordinate pass [2].

Table 2.2. Definition of parameters in RS codes

Symbols	Meaning
m	Number of bits per symbol.
n	Number of symbols per codeword, $n \leq 2^m - 1$.
k	Number of symbols per message, $k < n$.
t	Error-correction capability of the code, $t = (n - k)/2$.

are shown in Table 2.2 [23]:

In an RS(n, k) code, k is the number of data symbols being encoded and n is the total number of symbols in the codeword. Where $n = k+2t$, t is the number of error symbols which can be corrected, and $2t$ is the number of error symbols that can be detected. The specification for the RS coder in our proposed scheme is set as RS(255, k), and the parity length $2t$ is variable. The RS(255, k) design process is as follows:

- RS(255, k) encoder design: The Galois Fields (GF) concept is used in the design of RS codes. From the specification of RS(255, k), the symbol length in each codeword is 255 and each symbol can be expressed by $m = 8$ bits. In this case, the linear feedback shift register (LFSR) circuit is adopted to generate the elements of GF(2^8) based on the selected primitive polynomial $p(x) = x^8 + x^4 + x^3 + x^2 + 1$. The LFSR for generating a GF(2^8) code is as in Fig. 2.8:

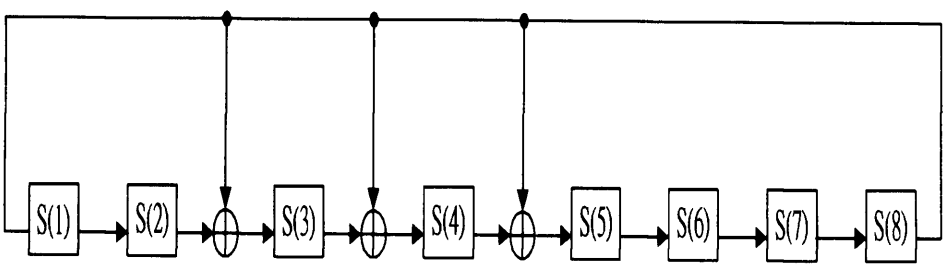

Figure 2.8. LFSR circuit for generating the elements of GF(2^8)

The initial condition for [S(1),S(2),S(3),S(4),S(5),S(6),S(7),S(8)] is set as [10000000]. ⊕ indicates logical AND operation. In each clock cycle, a new S value is generated as an element of GF. After 255 cycles, the LFSR circuit generates 256 elements for GF(2^8). Thus, the GF(2^8) has 256 roots. This can also be expressed as $\{0, 1, \alpha, \alpha^2, \alpha^3, \cdots, \alpha^{254}\}$. Each element can be expressed as:

$$\alpha^i = \alpha_{i,0} + \alpha_{i,1}x + \alpha_{i,2}x^2 + \alpha_{i,3}x^3 + \alpha_{i,4}x^4 + \alpha_{i,5}x^5 + \alpha_{i,6}x^6 + \alpha_{i,7}x^7 \quad (2.2.3)$$

After the elements are generated, the next step is to find the generator polynomial for $2t$ capability of error-detecting. The degree of generator polynomial g(x) is based on the error-detecting capability and defined as follows:

$$g(x) = (x + \alpha)(x + \alpha^2)(x + \alpha^3) \cdots\cdots\cdots (x + \alpha^{2t}) \quad (2.2.4)$$

$$= g_0 + g_1 x + g_2 x^2 + g_3 x^3 + \cdots\cdots + g_{2t-1} x^{2t-1} + g_{2t} x^{2t}$$

Accordingly, the RS encoder circuit for a $2t$ error-detecting capability is designed as Fig. 2.9, where g_{2t}=1:

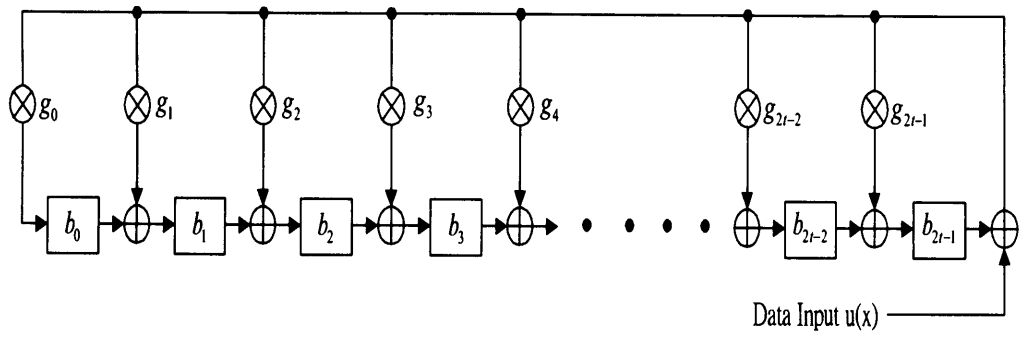

Figure 2.9. RS encoder circuit for $2t$ capability.

where $\otimes$ indicates the multiply operation. Thus, for encoding, each code polynomial $v(x)$ in an (n, k) cycle code is expressed as below:

$$v(x) = u(x) \cdot g(x) = (u_0 + u_1 x + \cdots + u_{k-1} x^{k-1}) \cdot g(x) \qquad (2.2.5)$$

where $u(x)$ is the input message codes. The multiplier circuit based on the primitive polynomial $p(x) = x^8 + x^4 + x^3 + x^2 + 1$ is designed as in Fig. 2.10.

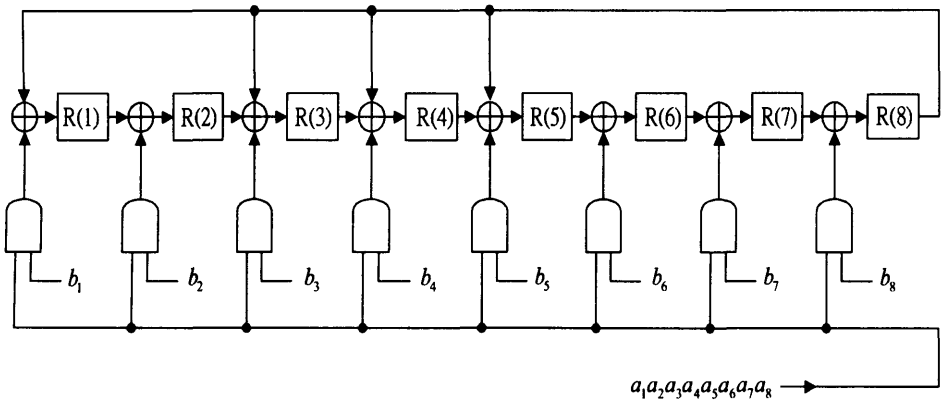

Figure 2.10. The multiplier circuit, $R = a \cdot b$, based on the primitive polynomial $p(x) = x^8 + x^4 + x^3 + x^2 + 1$.

In Fig. 2.10, the multiplier is used in both the RS encoder and decoder.

- The RS(255, k) decoder design process:

  The RS decoding process is very complex in comparison with the encoder part. Decoding of an RS code requires determination of both locations and values of the error symbols. First, we assume that the transmitted code polynomial $v(x)$ is as below:

$$v(x) = v_0 + v_1 x + \cdots + v_{n-1} x^{n-1} \qquad (2.2.6)$$

and the received transmitted code polynomial in the RS decoder is as below:

$$r(x) = r_0 + r_1 x + \cdots + r_{n-1} x^{n-1} \tag{2.2.7}$$

Therefore, the error pattern is:

$$e(x) = r(x) - v(x) = e_0 + e_1 x + \cdots + e_{n-1} x^{n-1} \tag{2.2.8}$$

where $e_i = r_i - v_i$ is a symbol in GF(q). Suppose the error pattern $e(x)$ contains v errors with $0 \leq j_1 < j_2 \cdots < j_v \leq n-1$. The $e(x)$ can be rewritten as:

$$e(x) = e_{j_1} x^{j_1} + e_{j_2} x^{j_2} + \cdots + e_{j_v} x^{j_v} \tag{2.2.9}$$

where $(e_{j_1}, e_{j_2}, \cdots, e_{j_v})$ denote the error values and $(x^{j_1}, x^{j_2}, \cdots, x^{j_v})$ are error locations. There are four steps to be taken to decode the RS code.

- Compute the syndrome $(S_1, S_2, S_3, \cdots, S_{2t})$.
- Evaluate the error-location polynomial $\sigma(t)$.
- Determine the error-value evaluator $Z_0(x)$.
- Evaluate error-location numbers and error values and perform error correction.

■ Syndrome computing:

As with binary BCH codes, the syndrome S is a $2t$-tuple over GF(q^m):

$$(S_1, S_2, \cdots, S_{2t})$$

According to $r(x) = v(x) + e(x)$, we have

$$S_i = v(\alpha^j) + e(\alpha^j) = e(\alpha^j) \tag{2.2.10}$$

Therefore, based on equation (2.2.10), we can rewrite the following set of equations:

$$S_1 = e_{j_1}\alpha^{j_1} + e_{j_2}\alpha^{j_2} + \cdots + e_{j_v}\alpha^{j_v}$$

$$S_2 = e_{j_1}(\alpha^2)^{j_1} + e_{j_2}(\alpha^2)^{j_2} + \cdots + e_{j_v}(\alpha^2)^{j_v}$$

$$\vdots$$

$$S_{2t} = e_{j_1}(\alpha^{2t})^{j_1} + e_{j_2}(\alpha^{2t})^{j_2} + \cdots + e_{j_v}(\alpha^{2t})^{j_v}$$

■ Evaluate the error-location polynomial $\sigma(x)$

If $\sigma(x)S(x)$ is divided by x^{2t}, the remainder is $[\sigma(x)S(x)]_{2t}$.

$$\sigma(x)S(x) \equiv [\sigma(x)S(x)]_{2t} \quad mod \quad x^{2t}$$

$$= Z_0(x) \quad mod \quad x^{2t}$$

which is called the key equation in the decoding of BCH codes. Here, *mod* refers a remainder function. There are two methods to solve the key equation: Berlekamp and Euclidean algorithms [23]. We adopted the Berlekamp algorithm in the RS decoder because the Berlekamp decoding algorithm has more efficiency than Euclidean [23]. Assum-

ing that the error-location polynomial $\sigma(x)$ is defined as:

$$\sigma(x) = (1-\beta_1 x)(1-\beta_2 x)\cdots(1-\beta_v x) \tag{2.2.11}$$

$$= \sigma_0 + \sigma_1 x + \sigma_2 x^2 + \cdots + \sigma_v x^v.$$

$$= 1 + \sigma_1 x + \sigma_2 x^2 + \cdots + \sigma_v x^v.$$

The following set of equations relate the coefficients σ_i of $\sigma(x)$ and the syndrome components S_i:

$$S_{v+1} + \sigma_1 S_v + \sigma_2 S_{v-1} + \cdots\cdots + \sigma_v S_1 = 0$$

$$S_{v+2} + \sigma_1 S_{v+1} + \sigma_2 S_v + \cdots\cdots + \sigma_v S_2 = 0$$

$$\vdots$$

$$S_{2t} + \sigma_1 S_{2t-1} + \sigma_2 S_{2t-2} + \cdots\cdots + \sigma_v S_{2t-v} = 0$$

The above equations are known as generalized Newton's identities. We need to find the minimum degree polynomial $\sigma(x)$ whose coefficients satisfy these generalized Newton's identities. If we can find $\sigma(x)$, that means we can determine the error values and locations. In the u^{th} step, we can determine a polynomial of minimum degree,

$$\sigma^{(u)}(x) = \sigma_0^{(u)} + \sigma_1^{(u)} x + \cdots + \sigma_{\ell_u}^{(u)} x^{\ell_u} \tag{2.2.12}$$

whose coefficients satisfy the following $u - \ell_u$ identities. This means

$$S_{\ell_u+1} + \sigma_1^{(u)} S_{\ell_u} + \cdots + \sigma_{\ell_u}^{(u)} S_1 = 0$$

$$S_{\ell_u+2} + \sigma_1^{(u)} S_{\ell_u+1} + \cdots + \sigma_{\ell_u}^{(u)} S_2 = 0$$

$$\vdots$$

$$S_u + \sigma_1^{(u)} S_{u-1} + \cdots + \sigma_{\ell_u}^{(u)} S_{u-\ell_u} = 0$$

An iterative algorithm is required for finding the error-location polynomial $\sigma(x)$. The first step of the iterative process is to find the minimum polynomial $\sigma^{(1)}(x)$ whose coefficients satisfy the first Newton's identity. The next step is to test whether the coefficients of $\sigma^{(1)}(x)$ also satisfy the second Newton's identity. If yes, then:

$$\sigma^{(2)}(x) = \sigma^{(1)}(x)$$

If no, we need to add a correction term to $\sigma^{(1)}(x)$ to form $\sigma^{(2)}(x)$. The process of finding the minimum of the polynomial then iterates until $\sigma^{(2t)}(x) = \sigma(x)$. Thus, the final $\sigma(x)$ equation is the desired error-location polynomial.

■ Next it is crucial to determine the error-value evaluator $Z_0(x)$ and correct the error data.

To correct the error values, we have to find the roots of the error-location polynomial. Substituting $\alpha, \alpha^2, \cdots, \alpha^{2^m-1}$ into the error-location polynomial, where $m = 8$ for RS(255, k), if $\sigma(\alpha^{tt}) = 0$, $1 \leq tt \leq 2^m - 1$, this means α^{tt} is a root of $\sigma(x)$. The error-location is the reciprocal of the root. Next, we have to find the error-value which is in the error

location. Based on $Z(x) = \sigma(x) \cdot S(x)$, $Z(x)$ is

$$Z(x) = (1+\sigma_1(x)+\sigma_2 x^2+\cdots+\sigma_v x^v)(S_1+S_2 x+\cdots+S_{2t}x^{2t-1}) \quad (2.2.13)$$

$$= S_1+(S_2+\sigma_1 S_1)x+(S_3+S_2\sigma_1+S_1\sigma_2)x^2+\cdots+(S_v+S_{v-1}\sigma_1+S_{v-2}\sigma_2+\cdots+S_1\sigma_{v-1})x^{v-1}$$

where $\sigma(x)$ is the error-location polynomial, $S(x)$ is the syndrome polynomial, and $Z(x)$ is called the error-value evaluator. The corrupted data in the error-location is computed as:

$$\delta_k = \frac{Z(\beta_k^{-1})}{\beta_k \prod_{i=1,i\neq k}^{v}(1-\beta_i\beta_k^{-1})} \quad (2.2.14)$$

where β_k is the kth error-location. The value of δ_k expresses the corrupted data in the error-location β_k. The corrected data will therefore be added to the received message to correct the error data.

Several researchers such as [63, 78] have adopted RS coders as FEC. In [63], an RS code was added to each packet to protect it against the errors caused by memoryless and fading channels. In [78], the RS coders were used to protect the source coded video bitstream in a JSCC scheme. Since burst packet losses occur frequently in transmission, the researchers in [79] proposed a data recovery method that generates redundant data using a combination of RS codes and convolution of neighboring blocks to protect transmitted images. The proposed method exhibited better performance than when RS codes are only used, but it results in an extra small amount of redundancy.

2.3 Progressive Image Transmission

Unlike in conventional image transmission systems, PIT techniques allow a low-resolution approximate image to be first transmitted and then the received background image is progressively improved over a number of transmission passes. The decoder has therefore at each stage an approximation of the full resolution image, rather than a part of it only. The advantage of PIT is that the gross structural information of the image appears immediately at the beginning of transmission so that it is possible for the user to make a decision on whether further transmission is necessary. The PIT scheme is particularly useful for transmitting large images in narrowband channels at minimum cost. Progressive transmission can be classified into three categories [80]: spatial domain [81], transform domain [82], and pyramid-structure [83]. The bit-plane method (BPM) is the simplest way to implement the PIT system. The image does not rely on any encoding process and the transmitter transmits one bit for each pixel in each round and the transmitted bits are arranged from the most significant bit (MSB) to the least significant bit (LSB). The final transmitted image is therefore the same as the original. In the transform domain, an image undergoes block compression, such as using EZW, SPIHT, and the compressed symbols are transmitted progressively in an importance order. In the pyramid-structure domain, the data in different levels in a pyramid structure is transmitted progressively, therefore, the decoder image can be reconstructed by transmitting the pyramid data structure from the top level to the bottom level. In [84], in the spatial domain, the authors proposed a guessing by neighbors (GBN) method based on an interleaving strategy. On average, only 50% of the image data is transmitted in the GBN method, the remaining 50% is interpolated by guessing the average values of the neighborhood pixels.

The GBN approach produces better results compared to the BPM approach. In [80], the authors proposed a new GBN method based on the old GBN method. The new GBN method provides a multiple resolution for each pixel box. According to the experimental results, the new GBN method had better performance in terms of both PSNR and compression ratio than the old GBN method.

However, progressive transmission is problematic in the presence of noisy channels. In practice, progressive transmission over noisy channels has to be accompanied by appropriate channel coding or JSCC, and other properties, such as UEP and RoI, to achieve an efficient PIT scheme. PIT based on the transform domain method is adopted in our proposed system. The input image undergoes block transform, EZW based on DWT, and the transformed coefficients are transmitted progressively in a relative importance order by a preset scan order. The properties of being progressive and emphasis on the region of interest are exploited simultaneously to achieve better efficient transmission in our proposed system. The two united features not only allow a faster transmission, but also sufficient resolution of the desired region in a limited capacity channel.

2.3.1 Region of interest

In this subsection, we describe a communication protocol for interactive image transmission, with the emphasis on the RoI in a narrowband network system. The aim of utilizing the RoI is to allow users to recognize the desired part as quickly as possible since important diagnostic information may occupy part of the medical image called the RoI. The information in the RoI is often transmitted using a lossless compression technique to ensure that the physicians (or other users) have access to the entire and correct

diagnostic information in a shorter time. The information is transmitted after applying a lossy compression. However, the overall resolution can be increased gradually. In our proposed scheme, the location of the RoI within the image and its radius can be selected by the user through a user friendly interface.

As an example, Fig. 2.11 shows three areas: RoI, R1 and R2. The RoI is centered at point (x_0, y_0). The importance of information in area R2 is the lowest and that of the RoI is the highest. The quality of the reconstructed subblocks and consequently the compression rate therefore depends on the size of the embedded coefficients.

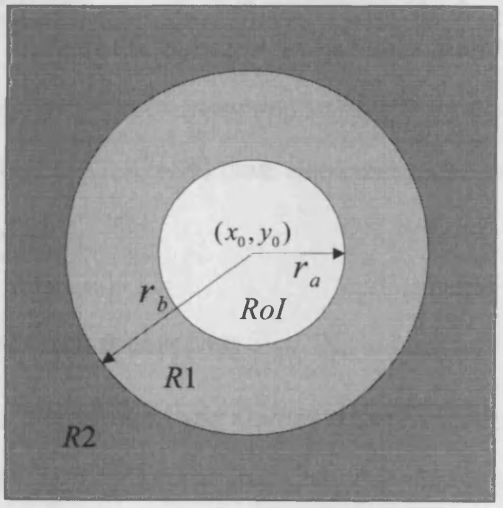

Figure 2.11. Areas of different priorities in an image used in the proposed scheme.

This is set by the distance from the center of the RoI. Based on the assigned parameters for EZW, the data in each subblock will be compressed at different rates depending on the location of the subblock. As an example, the areas in the reconstructed image can be defined as:

$$\text{For RoI:} \quad \sqrt{(x-i)^2+(y-j)^2} \le r_a$$

$$\text{For R1:} \quad r_a < \sqrt{(x-i)^2+(y-j)^2} \le r_b$$

$$\text{For R2:} \quad \sqrt{(x-i)^2+(y-j)^2} > r_b$$

where x and y are the coordinates of the center of the RoI assigned by the physician using a mouse click. Thereafter, both values are sent back to the host. The values of r_a and r_b are the radius of the RoI and R1, and i and j express the $x-y$ Cartesian coordinate of the subblock centered at (i, j). In the successive progressive stages, the values of r_a and r_b gradually expand to include a larger area and finally the whole image, and therefore create the reconstructed image of a higher quality. In our proposed algorithm, the first transmitted image is the background low resolution image. Then, the reconstruction is progressively continued starting from the RoI.

The authors in [85–87, 87–89] have also considered the RoI and the related procedures.

2.3.2 Unequal error protection

When the data is transmitted over a noisy transmission channel, we have to add redundant data to protect it and achieve a reliable transmission. Simultaneously, it is desirable to compress the transmitted data to reduce the redundancy and achieve an efficient transmission. Obviously, the two methods are different but often coexist to form an efficient and reliable transmission system. From an efficient communication point of view, the error code should be as short as possible, but if too short, an acceptable quality of the decoded images may not be achieved. Classical theoretical framework for communication systems assumes that all information is equally

important, and uniform error protection is provided to protect all messages over the noisy channels. Nevertheless, wavelet-based image compression algorithms and error resilient techniques are widely used in practical communication systems and in these compression algorithms, each compressed coefficient represents different levels in the image, making it easy to recognize the order of importance of the compressed coefficients. Moreover, based on tiling and packetization techniques, we can assume which block or messages packet is more important. Based on the above concepts, we can provide different amounts of data protection for different transmitted bitstreams.

Generally, error protection can be divided into two categories: EEP and UEP. In EEP, the entire bitstream receives the same amount of protection from a channel coder. UEP schemes, however, apply different amounts of protection to different sections of a bitstream, and can effectively shift uncorrectable bit errors toward the less importance sections. As a consequence, a better performance is likely to achieved with UEP than with EEP. UEP therefore attracts more attention because it takes advantage of the hierarchical structure of the source data. A UEP scheme using RCPC was proposed for SPIHT in [59] and produced an improvement of around 0.3 dB over the EEP employed in [58].

The packetization technique is used for robust image transmission. There are two types of packetization according to packet size form: fixed and variable length. Each type has its advantages and disadvantages. UEP was adopted in [90] and variable packet length was used for the following reasons: 1) in rate-distortion at low bit rate, the variable length scheme is more efficient than a fixed length scheme; 2) a priority on the specific tree structures can be imposed by using the packet length; and 3) a fixed length packet

may cause severe overhead for some trees. UEP with fixed packet length was adopted in [41]. The types of EEP and UEP with variable/fixed length schemes are shown in Fig. 2.12.

In our proposed transmission system, we adopt UEP with the packet fixed length scheme, the same as that in Fig. 2.12(C) to provide appropriate data protection with minimum overhead. The amount of data protection is not only based on the order of information importance, but also depends on the physical transmission channel conditions. Such a scheme significantly increases the efficiency.

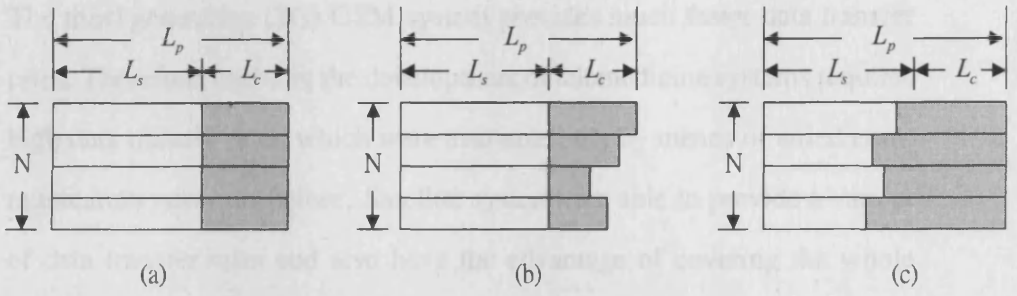

Figure 2.12. Error protection schemes, where L_p indicates packet length, L_s is the sources code length, L_c is the parity length, and N is the number of packets, (a) an EEP structure, (b) a UEP structure; the L_s are fixed, but L_p and L_c are variable, and (c) a UEP structure; L_p is fixed, but L_s and L_c are variable.

2.4 Transmission of Encoded Data

There are two types of communication networks: wired and wireless. The fixed wired Ethernet connections are not prone to interference and fluctuations in available bandwidth because of realistic wire connection. Compared with wireless, the wired networks are faster, more reliable, and more secure. In the wireless network, the transmission of signals is modulated by elec-

tromagnetic waves and transmitted through air to the destination. Since the wireless transmission media is air, generally, wireless networks have lower bandwidth but are easier to setup and manage. However, the signals transmitted in air are more prone to interference.

Due to the increasing demand for healthcare, medical treatment, message exchange, and consultation, and the growing number of emergency cases, wireless systems are highly demanded in clinical environments. Those technologies used in wireless telemedicine systems include the Global System for Mobile Communication (GSM), General Packet Radio Service (GPRS), satellite communication links, and wireless local area networks (WLANs). The third generation (3G) GSM system provides much faster data transfer rates. Therefore, enabling the development of telemedicine systems requires high data transfer rates, which were available only by means of wired communication networks before. Satellite systems are able to provide a variety of data transfer rates and also have the advantage of covering the whole globe. The WLAN is a flexible data communications system implemented as an extension of wired local area networks (LANs). WLANs transmit and receive data over the air, minimizing the need for wired connections. However, the transmitted data is influenced by interference from air transmission channels and can cause degraded quality of the information. The main problems associated with wireless channels are noise and fading. The occurrence of interference is random and unpredictable. In [91], the authors proposed emerging applications of wireless information-technology in health systems. In [92], the author describes transmission problems which are caused by the wireless channel, channel characteristics and diversity techniques, and proposes diversity techniques as one way to overcome fading and noise problems in wireless communication systems. Wireless com-

munication channels suffer from many impairments, such as thermal noise, path loss and fading, shadowing due to the presence of fixed obstacles in the radio path, and rapid movement of mobile reflectors. In a typical wireless communication environment, due to scattering by different objects, multiple propagation paths from a transmitter to a receiver often exist. The receiver therefore receives signals from different paths and undergoes different attenuations, distortions, delays, and phase shifts. To tackle these problems, different kinds of diversities are commonly employed in wireless communication systems to fully exploit the existing information and transmission capacity: frequency diversity [93], time diversity [94], and space diversity [95]. The diversity approaches increase the efficiency and enhance the quality of the reconstructed data in the receiver.

2.5 Conclusions

In this chapter, a comprehensive survey of the existing algorithms in PIT and JSCC has been presented. In addition, the major tools to be utilized in our proposed system, including HWT, EZW, RS, RoI concept and feedback scheme have been addressed. For the purpose of telemedicine, we consider not only limited channel capacity or memory and computational complexity, but also ease of implementation into portable devices. In addition, the important concepts of EEP and EUP have been reviewed and the survey has shown that it is crucial to integrate both source and channel coding components within an image transmission system, including feedback. The feedback enables an interaction between the transmitter and the receiver, and also influences the priority of the image region to be coded. It is also affected by the status of the transmission channel.

Chapter 3

ESTIMATING CHANNEL ERROR USING A RECEIVED DATA SEQUENCE

When considering the image transmission over a noisy channel, the challenge in transmitting data is to minimize the corrupted data caused by the channel errors. Several techniques can be employed: 1) error resilience techniques, 2) FEC-based protection algorithms, and 3) error concealment techniques. Although transmitted images are becoming more robust due to these algorithms, the success or failure of decoding is determined by the error detection mechanism. Many JSCCs methods with rate allocation have been described in section 2.2 of Chapter 2. In such JSCC methods, the channel code rate is carefully chosen to match the properties of the source coders and the conditions of the transmission channel. The rate allocation naturally depends on the BER of the channel and is known to the transmitter before transmission. However, in real-world environments, channel conditions frequently change over time and are still unknown in the transmitter part. Thus, FEC-based systems might not be able to perfectly adapt their error-protection strategy to the actual channel conditions, because the required appropriate level of FEC depends on an accurate estimation of the

channel's behavior. While systems using FEC can provide good protection for known channel conditions, if a precise statistical description of the channel is unavailable, then one typically designs FEC code for the worst possible channel that can be anticipated.

Another useful method used in the transmission system is the feedback scheme, which tries to send back the decoding results from the receiver to the transmitter. Using FEC with the feedback scheme allows the transmitter to receive information about the practical transmission channel. Thus, the transmitter has another opportunity to adjust its error-protection strategy for next transmission according to feedback information. In [70], the received packet decoding result, success or failure, is conveyed back to the encoder by sending one bit through the feedback channel. The encoder stops transmission for the current packet and proceeds with the transmission of the next packet if the decoding is successful. Otherwise, the encoder provides a stronger channel code according to the decision policy to decode the packet again. According to the results in [70], the use of a feedback channel can significantly improve the average PSNR of the received image, compared to a system without feedback channel. In [69] a feedback signal was shown to be able to shift the rate allocation point to receive a better performance. The simulation results showed that a transmission system with a feedback signal resulted in up to 1 dB improvement in PSNR compared to a transmission system without a feedback signal. Hence, the feedback scheme can not only be used for retransmission but also to estimate the state of the current channel. In [96], the authors investigated the JSCC scheme with and without feedback signals. In this work, the authors developed an empirical model of decoded BER in terms of the channel code rate for the progressive source-channel rate allocation problem. In general, the presence of feed-

back changed the optimal rate allocation, resulting in higher code rates for error-correcting codes and smaller overall distortion. Simulation results for memoryless and fading channels in [96] indicated that the feedback signal provides up to 1 dB improvement in PSNR. Obviously, the image transmission system with a feedback channel shows better performance than a transmission system without a feedback channel, because the encoder side has more information about the state of the current channel. However, in order to take full advantage of feedback, some delay needs to be tolerated. The delay time can be ignored in a high speed transmission, regardless whether encoding is implemented or not.

Based on the above results, it can be deduced that the performance of transmission system is affected by the channel information. Accordingly, I attempted to capture as much information as possible about the practical transmission channel in order to provide an adaptive protection of the transmitted data. However, it is a big challenge to estimate exactly the practical channel transmission because there are still many unknown events. In the next sections, we provide background knowledge about the BSC and wireless channel model, and present a method for estimating the channel state.

3.1 Wireless Channel Model

The channel model is used to represent the practical transmission channel designed for simulating the transmission systems. Normally, the channel model is classified as either memoryless or memory. When signalling through the channel, the channel is called a memoryless channel if the output signal depends only on the input signal. If the output signal depends on both current and previous signals this kind of channel is called a memory transmission channel.

A BSC model is the simplest communication channel model for a memoryless channel. The BSC is a binary channel which can transmit only one of two symbols, 0 or 1, over a transmission channel, and it has one parameter only, the bit error rate (BER), to describe the error condition. In a BSC, the error probabilities of sending a one but receiving a zero, and alternatively sending a zero but receiving a one, are the same; accordingly, the BER can be found as probability of one bit being received in error. The BSC model is a very popular channel model because it significantly simplifies the analysis. The Additive White Gaussian Noise (AWGN) channel is another memoryless channel, where the distortion of one bit is independent of all other bits in the data stream. In the AWGN channel model, the distortion in the transmission channel is due to the addition of a zero-mean Gaussian random value to each bit.

The BSC model is defined as follows: The input data transmitting over the BSC is a string of binary bits. Assume the BSC is a noisy channel, and the probability of p changing the transmitted data from zero to one and from one to zero is the same, i.e. $P(0|1) = P(1|0) = p$ and $P(1|1) = P(0|0) = 1-p$.

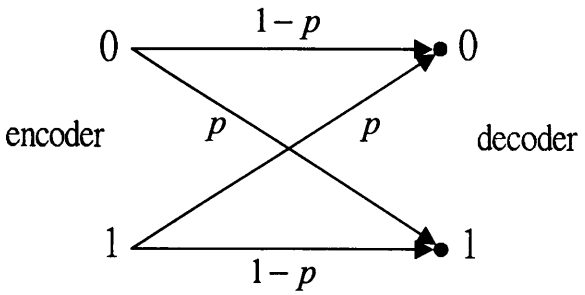

Figure 3.1. Definition of probabilities of error in a BSC model.

In this case, the overall error is simply calculated as:

$$p(error) = \sum_{i \neq j} P(j|i)p(i) \tag{3.1.1}$$

The AWGN channel is another simple and popular channel model for the analysis of the performance of an image transmission system over a memoryless channel. The AWGN channel for a discrete memoryless channel can be described as:

$$\mathbf{y}[n] = \mathbf{x}[n] + \mathbf{z}[n]$$

where $\mathbf{x}[n]$ is the input data at the discrete time event index n, $\mathbf{z}[n]$ is the additive Gaussian noise in the channel, and $\mathbf{y}[n]$ is the channel output.

In a real-world channel, error events are generally not independent. Thus, we need a channel model that can handle memory. For wireless communication, the simplest and most popular discrete memory model is the Gilbert-Elliott channel (GEC) [97]. A two-state Markov model is well known as a GEC model. This model is widely used in representing the error characteristics of a wireless channel between two stations. The two states are: the good state and the bad state. In the good state, the errors occur with low probability P_G, such as $P_G \approx 0$, while in the bad state the errors occur with high probability P_B, such as $P_B \approx 0.5$. Both P_G and P_B are assigned by designers to simulate the noisy channel state. The channel is in the good state most of the time, but on occasional shifts to the bad state owing to a change in the transmission characteristic of the channel. Each state can be treated as a BSC model. In a BSC model the BER is used to express the amount of errors in it. Sometimes, more complex models with three or more states are needed. Due to the underlying Markov nature of the channel, it has memory that depends on the transition probabilities between the states. The FSMC

models have been shown to be good approximations for binary transmission over slow varying flat fading channels [98]. Details about discrete channels with memory can be found in [99]. The transition probabilities from one state to the other are represented by b and g, as shown in Fig. 3.2; $(1 - b)$ and $(1 - g)$ are the probabilities of staying at the good state and bad state respectively. The average bit error rate produced by the GEC is [100]:

$$BER_{avg} = \frac{gP_G + bP_B}{g + b} \tag{3.1.2}$$

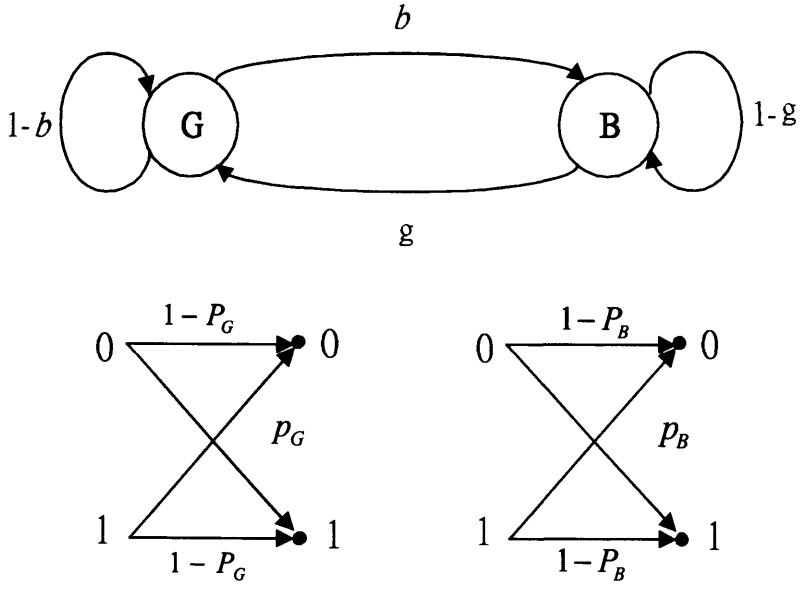

Figure 3.2. GEC model, P_G and P_B are the channel crossover probabilities in the good and bad states, and g and b are transition probabilities between states [4].

In wireless mobile communications, the most popular channel model is the Rayleigh flat-fading channel. Rayleigh flat-fading models assume that the magnitude of a signal that has passed through a communication channel

varies randomly, or fades according to a Rayleigh distribution. Such models are well suited for radio communications, where the transmitted signal reaches the receiving antenna via multiple paths, and the delay between the received paths is short compared to a bit interval. No dominant propagation along a line of sight between the transmitter and receiver is considered.

Another channel model commonly used in packet-switched networks is the erasure channel. If the input data are partitioned into packets, so that either all symbols within a packet are received or all are lost, this is called packet erasure channel. The simplest of such model is memoryless and it assumes that the packets are lost randomly.

3.2 Directly Estimating the State of the Transmission Channel

A bit error uncorrectable in the decoder often leads to a complete loss of synchronization and often makes the reconstruction impossible. Although increasing the parity length provides more data protection, it also increases the overhead in transmission channel. The parity length selection is the main point for an efficient and reliable image transmission system design. Researchers have therefore proposed many methods and algorithms to achieve this. These include JSCC, variable parity length, UEP, and feedback schemes. However, in these algorithms the channel state is assumed known, which may not be the current channel condition. In the image transmission without feedback system, collapse of the reconstructed image is possible if the data is not well protected. On the other hand, if we offer much data protection over a low noise channel, the transmission system becomes less efficient and the overhead information in the bandlimited channel increases. It is very difficult to provide an adequate data protection under an unknown channel state. Thus, in order to reduce the possibility of data collapsing,

another method has been proposed to address this problem. This approach sends a sequence of signals called the training signal sequence first, and then compares the original training signal with the received signal and evaluates the channel errors. However, this may not be acceptable in the real world application because it causes a long delay.

A feedback system is another solution which has shown better performance compared to a channel without no feedback, because a decoding result (success or failure) can be sent back from the receiver to the transmitter through the feedback channel. Therefore, the transmitter has the opportunity to change the parity length for data protection in the subsequent transmission. However, the feedback information only indicates that the parity length is enough or not for data correction; it neither shows the exact channel state, nor provides any rough estimation of channel data. For lowering the system complexity, in some cases, the transmitter may regard the noisy channel as the worst case and provide the largest parity length for the next transmission data if the decoding failure is acknowledged. Thus, the main problem is that the encoder has no exact or even rough information about how many errors are caused by the noisy channel.

To design an image transmission over noisy channels, the best performance can be achieved if the parity length is adaptive and variable, according to the channel state. To achieve this goal, we have to capture more accurate information about the channel condition. Although it is difficult to measure the channel error in real applications, in the next subsection, we present a simple method to evaluate the channel state. This algorithm detects, assigns and calculates the amount of header information errors caused by the channel and sends back to the transmitter. This information is used by the proposed adaptive procedure in the transmitter to readjust the parity

and therefore enhance the system reliability.

3.2.1 Algorithm development

An algorithm, for direct estimation of the state of the transmission channel was developed specifically for our proposed transmission system based on the nature of WT and EZW coding. This algorithm is able to detect the corrupted header information, count the amount of the corrupted header value and reassign new values to such a header information. The output of EZW compressed symbols consists of header and compressed symbols. The header information represents the number of compressed symbols per compression process followed by the compressed symbols. In detecting the corrupted header information, the algorithm checks the value which holds the header information position, and then assigns a new value based on the decision policy if the corrupted data is detected. Assigning new values reduces the probability of collapsing the reconstructed images and therefore allows the detection process to continue. The corrupted header data amount is sent back to the transmitter via feedback channel to evaluate the channel state. Although it is hard to evaluate exactly the current channel conditions under various noise levels, I attempted to capture the channel state more precisely using the proposed technique, since the transmission system should have better performance if the transmitter has more information about the channel state. According to the experimental results, the developed algorithm had better performance in a less noisy channel than in a more noisy channel and was more able to capture the channel state.

The proposed algorithm was developed in the following steps:

- The original images were segmented into subblocks. We could therefore find out the amount of data in each block. For example, an 8×8

subblock was used in our proposed scheme, and the amount of data was 64 in each subblock.

- DWT and EZW were performed. The EZW encoded each subblock independently. Accordingly, the number of EZW compressed output symbols was between 4 and 64, and was also divisible by 4 in the 8×8 subblocks.

- The EZW compressed output symbols consisted of the number of compressed symbols and header followed by the compressed symbols. The output of EZW compressed symbols over a channel was formatted as in Fig. 3.3.

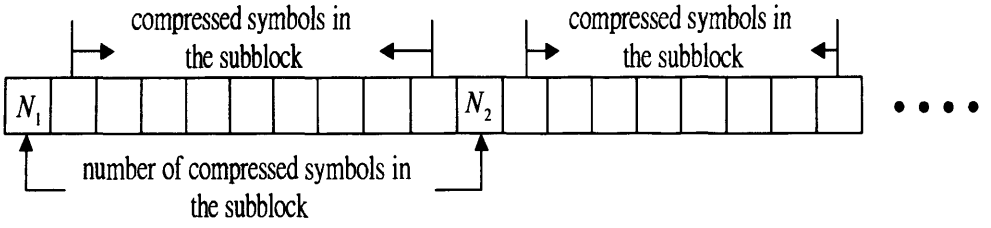

Figure 3.3. Format of the EZW plus the symbol number information transmitted over the channel.

We could enforce some constraints from the header information, such as $4 \leq$ header information ≤ 64 and that the header value is divisible by 4 for the case of 8×8 subblocks. Such constraints could be changed according to the size of subblocks and used as the criteria to check the header values if they have been corrupted. A flowchart of the algorithm to directly estimate the state of the transmission channel is shown as Fig. 3.4.

The detailed information in the flowchart is explained below:

- Is the header address out of the range of data length? If not, then

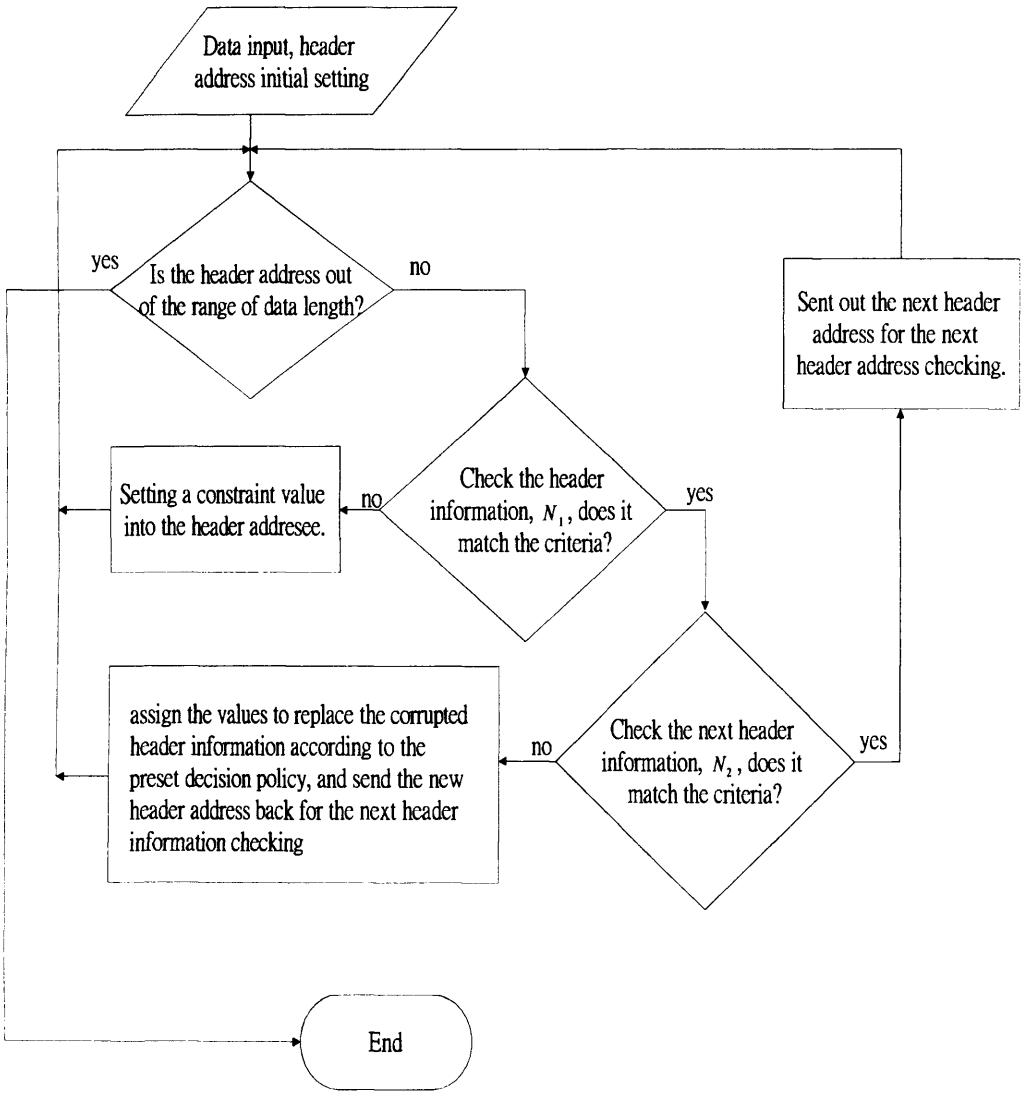

Figure 3.4. Flowchart of the direct state estimation of the transmission channel algorithm.

the algorithm will be continued until the header address is out of the range of input data length.

- Check the header information, N_1, to see if it matches the criteria. Here, the checking criteria are: $4 \leq$ header information ≤ 64 and the header value is divisible by 4 because only 8×8 subblocks are used in our proposed scheme. Therefore, N_1 is considered to be probably clear header information if it can pass the detection criteria.

- Check the next header information N_2 to see if it matches the criteria. Check the next header information N_2 to ascertain whether the previous header information N_1 is corrupted or not. The position of N_2 is based on N_1 and is equal to N_1 address plus $N_1 + 1$. A double detection method is used to avoid the situation where N_1 has passed the detection criteria but N_2 has not passed the detection criteria. Such situation indicates that maybe N_1 is corrupted. Accordingly, N_1 is considered to be clear header information only if both N_1 and N_2 pass the detection criteria. The amount of corrupted data is incremental once the corrupted N_2 is detected. The final amount of corrupted header information is used to indicate the state of the noisy channel.

- Assign the a new value to replace the corrupted header information according to the preset decision policy and send the new header address back for the next header information checking. In the case of N_2 not passing the detection criteria, a new value is assigned to replace the corrupted header information and the data structure is rearranged by the preset decision policy. In the decision policy algorithm, each symbol is detected until a symbol can pass the criteria. The symbol that has passed is considered to be the header information, not the

transmission data. The distance d between N_1 and the information N (which has passed the criteria) is then estimated. The output of EZW compressed symbols are represented by p, n, z, t, where, in this case p=112, n=110, z=122, and t=116 and is expressed in ASCII codes. Because the length of the EZW output compressed symbols is divisible by 4, four possible formats exist in between N_1 and N. We can therefore rearrange the data structure based on the remainder m of $(d-1)/4$. Each new data structure is described as follows:

- m=0: referring to condition m=0, we assume N_1 is corrupted and no other header information exist in such data structure. N_1 will then be replaced by d-1 and the address of the N sent out for the next detection. This is shown as in Fig. 3.5(a).
- m=1: this is the case where N_1 is correct and N_2 is corrupted. We therefore assign a new value to replace the corrupted information N_2 according to the considered decision rule. The new value is equal to $d-2-N_1$ under the $d-2-N_1 > N_1$ condition. This is shown in Fig. 3.5(b).
- m=2: under the m=2 condition, we assume N_1 is correct and N_2 is corrupted. We also assume there exists another header information in distance d. The decision is therefore: N_1 is correct, N_2 is replaced by 4, and the other header value, N_3 is $d-N_1-7$. The N_3 address is equal to the N_2 address plus five. [see Fig. 3.5(c)].
- m=3: in this situation, we assume N_1 is correctly received and N_2 is corrupted, and two other headers exist in distance d. N_2 is therefore set to 4, and the other two headers, N_3 and N_4, are set to 4 and $d-N_1-12$, respectively. The address of N_3 is equal to

the N_2 address plus five and the address of N_4 is equal to the N_3 address plus five. This is shown in Fig. 3.5(d).

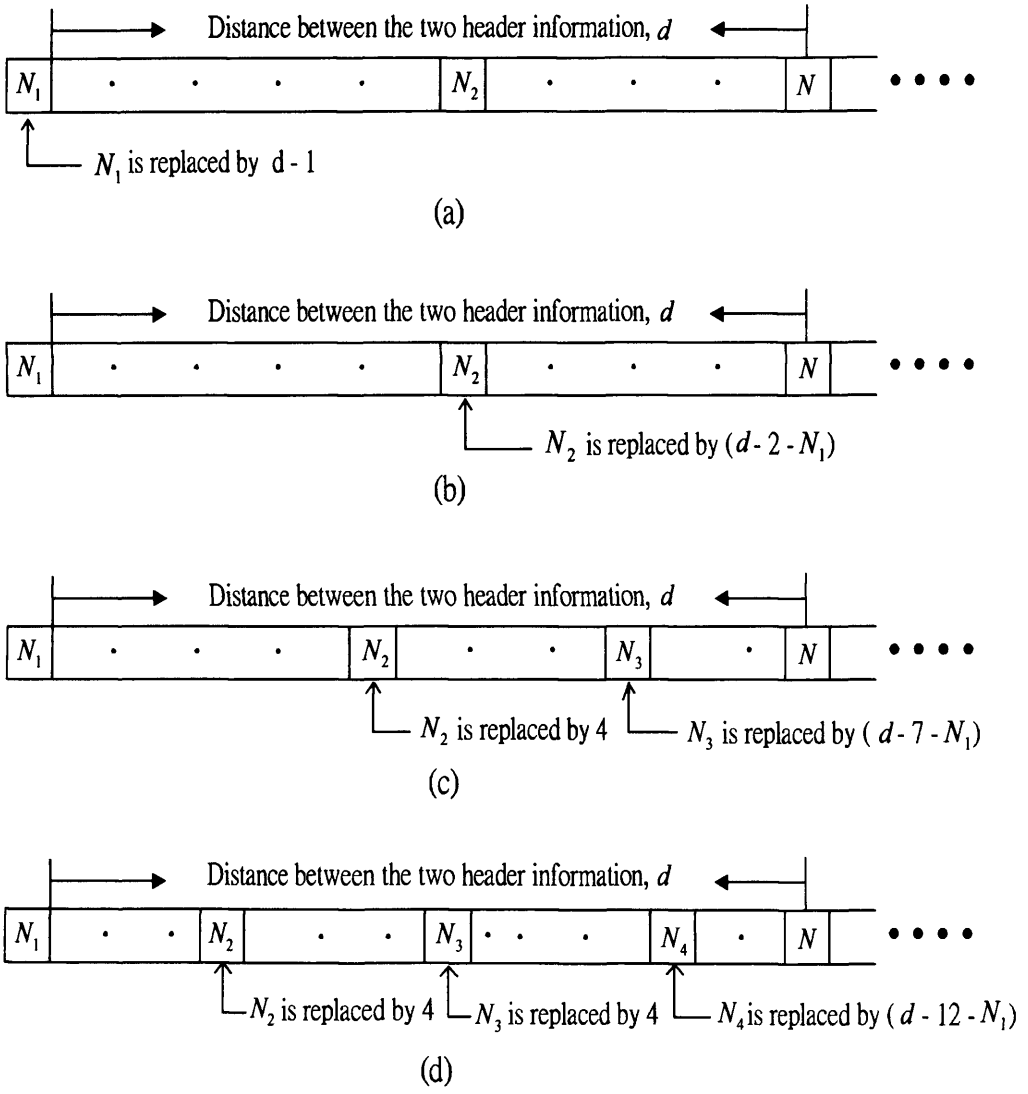

Figure 3.5. Based on the decision rule new header values are assigned in four types of data structure: (a) N_1 is considered corrupted, but N_2 is considered correct under the m=0 condition, (b) in the m=1 condition, N_1 is considered correct, but N_2 is considered corrupted, (c) in the m=2 condition, N_2 is replaced by four, N_3 is created and is set to $d - N_1 - 7$ according to the data structure and criteria, and (d) reassigning the data structure in the m=3 condition, N_2 and N_3 are replaced by 4, and N_4 is replaced by $d - N_1 - 12$.

3.2.2 Experimental results

The proposed algorithm is simulated for both BSC and flat fading Rayleigh channels. The BSC is the simplest channel model, since only zeros and ones are conveyed in the channel. We can therefore simplify the analysis and thereby facilitate fast software implementation. However, flat fading Rayleigh noise is often present in mobile communication channels, therefore, we simulated both BSC and flat-fading channel models and tested the performance of the proposed techniques against both models. RS(255,k) is used in the proposed scheme. The RS codes correct the symbol error and not the bit error. The BER used here was not the output BER but an experimental setup to denote the noise level in the channel. For example, 7 error bits were generated when the BER was set at 0.003, because RS codes are systematic linear block codes. When the errors are uniformly distributed the average parity length is 14 for a 255 length code length. Accordingly, the parity length in the RS coder should be at least 14 symbols in the worst case scenario in order to be able to correct the data errors. The RoI and UEP schemes were also included in this simulation.

Fig. 3.6 shows the frequency of the set of parity lengths in 10 trials for when the BER was set at 0.003 equivalent to the occurrence of 7 errors. The results showed that the proposed algorithm had channel state information very near to the practical channel state in nine of the ten trials. Since data in the RoI was the most important data in the overall image; the length of parity codes was longer than that for the data outside RoI. The output image format was based on Fig. 2.11 in Chapter 2. In the proposed algorithm, the codeword length of RS codes was 255 and the number of error bits was generated at random.

The parity lengths were found by averaging the results of 10 trials under

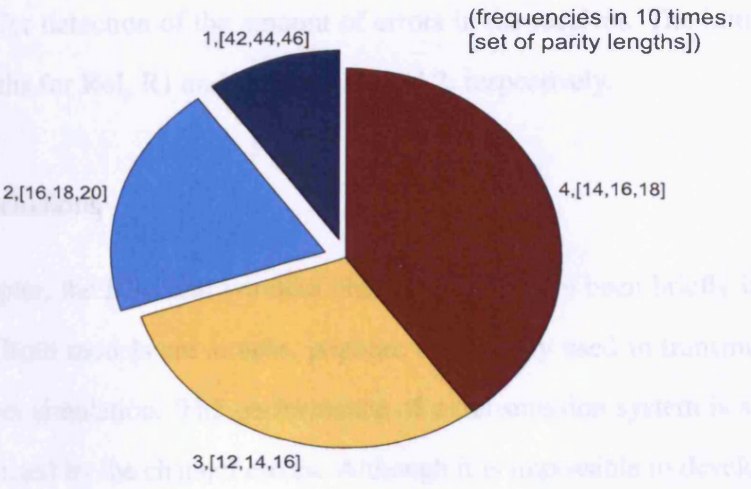

Figure 3.6. Average distribution (frequency) of the set of parity lengths in 10 trials for BER=0.003. [i, j, k] refers to three parity length i, j and k corresponding to three regions in the image.

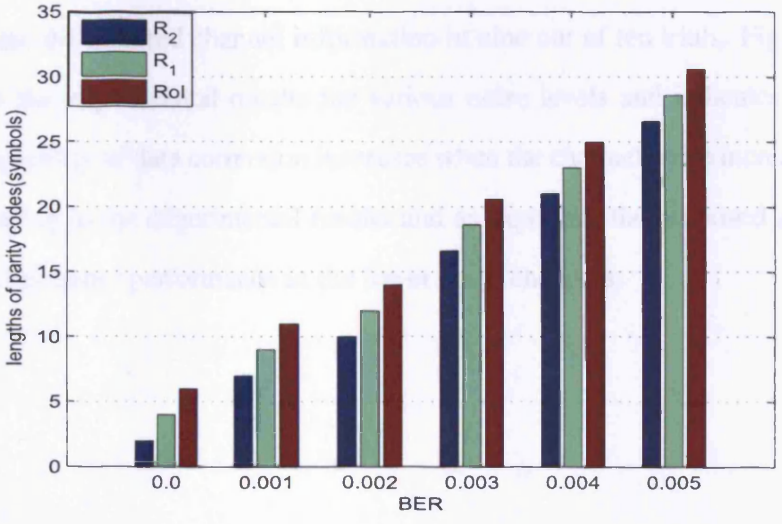

Figure 3.7. Lengths of the parity codes based on various channel noise levels.

various noise-levels (see Fig. 3.7). These were estimated by the algorithm developed for detection of the amount of errors in the receiver. The initial parity lengths for RoI, R1 and R2 are 6, 4, and 2, respectively.

3.3 Conclusions

In this chapter, the BSC and wireless channel model have been briefly introduced. Both models are simple, popular, and widely used in transmission channel simulation. The performance of a transmission system is seriously affected by the channel errors. Although it is impossible to develop an algorithm which can estimate exactly the channel state because of too many unknown events, an algorithm which directly estimates the state of transmission channel was developed to capture more accurately the channel conditions. The proposed algorithm is simple and implementable and was simulated for both BSC and Rayleigh channels. Based on the experimental results in Fig. 3.6, it was demonstrated that the proposed algorithm could estimate the required channel information in nine out of ten trials. Fig. 3.7 shows the experimental results for various noise levels and indicates that the capability of data correction increases when the channel noise increases. According to the experimental results and as expected, the proposed algorithm has better performance in the lower noise channels.

Chapter 4

A COMPRESSIVE SENSING APPROACH FOR TRANSMISSION OF IMAGES

In this chapter, a compressive sensing approach as a source coding technique for progressive transmission of images is proposed. Hierarchical alternative least squares (HALS) based compressive sensing (CS) is used for adaptive selection of the wavelet coefficients and nonlinearly thresholding the transform coefficients. CS is a relatively new coding paradigm which seeks to capture only the significant coefficients in the signal by a random matrix, and then uses nonlinear recovery algorithms (based on convex optimization) to reconstruct the signal with as few measurements as possible. In this chapter, we have evaluated both EZW and CS algorithms and compared with CS and EZW in the progressive transmission of images mentioned in previous chapters. Generally, the CS algorithm is easier to use, more efficient, provides better resolution, and entails lower computation. Under a similar compression rate, the resolution of reconstructed image utilizing the CS algorithm is better than that obtained when the EZW algorithm is used.

The overall JSCC system block diagram is the same as that depicted in Fig. 2.1 in Chapter 2.

4.1 Introduction to Compressed Sensing

Generally, in conventional image compression techniques based on transform domain, the images are transformed into a domain where the correlation among the samples becomes minimum and the signal energy is distributed among a small number of samples only. This procedure acquires the full signal, computes the complete set of transform coefficients, encode the largest coefficients and discard all the others. The compression is fundamentally achieved when a small set of transform samples (coefficients) are selected and the image is decoded (reconstructed) using these coefficients and an inverse transformation. CS also known as compressed sensing, developed by Candes and Donoho [101, 102], shows that a direct reconstruction using a smaller observations/samples is indeed possible if the data in that particular domain is sufficiently sparse. This allows sampling of the data at rates less than Nyquist rate. This technique combines two key ideas: sparse representation based on wisely choosing a linear basis for image; and incoherent measurements of the signal to extract the maximum amount of information from the image using a minimum amount of measurements. The key requirement of a successful CS system is sparsity which requires a significant number of signal samples in the sparse domain to be zero. Sparse signals have a small number of non-zero samples compared to their length. Although sparsity might exist in other basis rather than the present domain, it is an essential characteristic of a signal to make it suitable for applying CS. CS provides a different compression method to build the data compression directly into data acquisition and provides a great reduction of sampling rate, power consumption and computational complexity to acquire and represent a sparse signal [103]. As this theory has a direct connection with sparse signal recovery, many researchers attempted to take the advantage

of CS in related applications. Some applications for medical imaging are in [104, 105].

4.1.1 Mathematical expression of CS

Consider **x** is a real-valued, finite-length, one-dimensional and discrete-time signal, which can be viewed as an $N \times 1$ column vector in $\Re^N$ with elements $x[n]$, n=1, 2,... N. Assume that the basis is orthonormal, using the $N \times N$ basis matrix $\Psi = [\psi_1|\psi_2|\cdots|\psi_N]$ with the vector ψ as columns of Ψ. Any signal in the space of real numbers, $\Re^N$, can be represented as sum of weighted $N \times 1$ vectors and expressed as

$$\mathbf{x} = \sum_{i=1}^{N} s_i \psi_i \quad or \quad \mathbf{x} = \Psi \mathbf{s} \tag{4.1.1}$$

where **s** is the $N \times 1$ column vector of the transform coefficients $s_i = \langle x, \psi_i \rangle$, Obviously, **x** and **s** are equivalent representations of the signal, with x in the time or space domain and s in the Ψ domain. If the signal **x** is K sparse, which means there are k non-zero coefficients and therefore, the K largest coefficients are encoded and the $(N-K)$ smallest coefficients are discarded. If the representations in equation (4.1.1) has a few large coefficients and many small coefficients, $K << N$, the signal **x** is compressible.

Assume that we have a set of few non-adaptive linear measurements obtained from the entire input image, the aim in compressed sensing is to reconstruct the entire signal accurately and efficiently from those measurements. The purpose of CS is to recover the sparse signal x by taking random measurements less than N. For taking CS's measurements, we first let measurement matrix Φ denote an $M \times N$ with $M << N$. The Φ should be uncorrelated with Ψ. The choice of the test function, Φ_k, allows us to choose

in which domain we gather information about the image. For example, if Φ_k are sinusoids at different frequencies, we are essentially collecting Fourier coefficients, if they are delta ridges, we are observing line integrals, and if they are indicator functions on squares, we are back to collecting pixels. Imagers that take these generalized kinds of samples are often referred to as coded imaging system, as the measurement $y_1, \cdots, y_m$ are in some sense a coded version of the image X rather than direct observations. Various types of measurements can be found in [106–108]. Therefore, the number of measurements, M, and each measurement y_k in our acquisition system is an inner product against a different test function ϕ_k and shown in Fig. 4.1:

$$y_1 = \langle x, \phi_1 \rangle, \quad y_2 = \langle x, \phi_2 \rangle, \cdots, y_k = \langle x, \phi_k \rangle. \quad k = 1, \cdots, M. \tag{4.1.2}$$

$$\mathbf{y} = \Phi\mathbf{x} = \Phi\Psi\mathbf{s}$$

Figure 4.1. Compressive data acquisition [5].

We choose ϕ_k in such a way to minimize the number of measurements M needed to reconstruct $\mathbf{x}$. One idea is that we reconstruct the image by finding the closest image that matches the observed projection onto the span

$\{\phi_1, \cdots, \phi_m\}$. The reconstructed image $\hat{\mathbf{x}}$ is [109]

$$\hat{\mathbf{x}} = \Phi^*(\Phi\Phi^*)^{-1}\mathbf{y}. \tag{4.1.3}$$

where Φ is the linear operator that maps an image to a set of M measurements. Φ^* is its adjoint, and $\mathbf{y}$ is the M-vector of observed values. However, this type of linear-coded imaging system have a severe shortcoming, the measurement process is not adaptive, meaning that Φ is fixed and does not depend on the signal $\mathbf{x}$ and therefore, the same M transform coefficients are recorded for every image [109]. Therefore, to reconstruct $\mathbf{x}$ from $\mathbf{y}$, the number of measurements in $\mathbf{y}$ is almost equal to the number of coefficients recoded by a traditional transform coder. The sparsity and incoherence are the most important properties to make CS possible. CS exploits the fact that many natural signals are sparse or compressible in the proper basis Ψ. Incoherence implies that sampled waveforms have an extremely dense representation in Ψ. For solving the problem for Φ, we find that the ϕ_k should be completely unstructured and look more like random noise than any feature we would expect to see in the image.

The selected number of measurements is highly related to the level of sparsity; more sparsity allows us to take smaller M. The CS theory states that the signal could be recovered exactly if the number of measurements M obeys the condition $M_{min} \geq C\log(N/K)$ [101]. C is a constant and is an over-measuring factor greater than 1. Since $\mathbf{y}$ is lower dimension vector compared to $\mathbf{x}$, it is impossible to get exact $\mathbf{x}$ directly by the inverse transform of equation (4.1.2). In order to have an effective CS system, Φ and Ψ must be as incoherent as possible in their columns. This refers to the theory of Uniform Uncertainly Principle (UUP) [110]. The UUP states that

for any arbitrary k-sparse vector $\mathbf{h}$, the energy of the measurements $\Phi\mathbf{h}$ is comparable to the energy of $\mathbf{h}$ itself,

$$\frac{1}{2} \cdot \frac{N}{M} \cdot \|\mathbf{h}\|_2^2 \leq \|\Phi\mathbf{h}\|_2^2 \leq \frac{3}{2} \cdot \frac{N}{M} \cdot \|\mathbf{h}\|_2^2 \tag{4.1.4}$$

The proportion of the energy of $\mathbf{h}$ appearing as energy in the measurements is roughly the same as the undersampling ratio N/M [109], and so this is called an uncertainty principle. While $\mathbf{h}$ is entirely concentrated on a small set in sparse domain, it is spread out more or less evenly in the measurement domain. In order to understand how the UUP relates to sparse recovery problem, suppose that equation (4.1.4) holds for sets of size 2k. We measure our k-sparse vector as: $\mathbf{y} = \Phi s_0$, assuming $\Psi = I$ is an identity matrix. Is it possible to make any other k-sparse vector $s_0 \neq s$ that has the same measurements? The answer is no. If there were such a vector, then the difference $\mathbf{h} = s - s_0$ would be $2k$-sparse and $\Phi\mathbf{h}$=0. These two properties are incompatible with the UUP [109]. The UUP confirms that the connection between presenting basis matrix Ψ should be as much incoherent as possible with the sensing matrix Φ. The coherency measure between the Φ and the Ψ, sometimes called mutual coherency [110], can be expressed:

$$\mu(\Phi, \Psi) = \sqrt{n} \max_{1 \leq k, j \leq n} |\langle \phi_k, \psi_j \rangle| \tag{4.1.5}$$

$$1 \leq \mu \leq \sqrt{n}$$

In fact, mutual coherency is the largest correlation between any two columns of Φ and Ψ. $\mu = 1$ represents the minimum coherency. There are many pairs with good incoherency in the literature [110]. However, it is proven that random matrices are largely incoherent with any fixed bases. This is

a very important property that allows us to choose the measurement matrix non-adaptively [110]. The Φ is the canonical or spike basis $\varphi_k(t) = \delta(t-k)$ and Ψ is the Fourier basis, $\psi_j(t) = n^{-1/2}e^{i2\pi jt/n}$ are ideal examples. Since Φ is the sensing matrix, this corresponds to the classical sampling scheme in time or space. The time-frequency pair obeys $\mu(\Phi,\Psi)$=1 and, therefore, we have maximal incoherence. The second example can be wavelets bases as the sparse transform Ψ and noiselets [111] for measurement matrix Φ. The coherence between noiselets and Haar wavelets is $\sqrt{2}$ and that between noiselets and Daubechies D4 and D8 wavelets is, respectively, about 2:2 and 2:9 across a wide range of sample sizes N [110].

Another significant property for the CS signals is the theory of Restricted Isometry Property (RIP) that should be considered as an effective factor in the robustness of CS [110]. For each integer $k = 1, 2, \cdots$ the isometry constant $\delta_k << 1$ of a matrix Φ is defined as the smallest number such that:

$$(1-\delta_k)\|\mathbf{x}\|^2 \leq \|\Phi\mathbf{x}\|^2 \leq (1+\delta_k)\|\mathbf{x}\|_2 \tag{4.1.6}$$

where $\|\cdot\|$ refers to ℓ_2-norm. For $1 < p < \infty$, we denote $\|\cdot\|_p$ as the usual p-norm,

$$\|x_i\|_p := (\sum_{i=1}^{i=d} |x_i|^p)^{1/p} \tag{4.1.7}$$

ℓ_2-norm refers to the case where p= 2. This equation (4.1.6) holds for all k-sparse vectors [110]. Suppose now we only have the measurements $\mathbf{y}$ and the measurement matrix Φ in hand; we want to recover signal $\mathbf{x}$ from $\mathbf{y}$. Obviously, we are dealing with an underdetermined system with more unknowns than knowns ($N >> M$). In order to solve such a system appropriately, we have to consider sparsity constraints. In other words, we are always seeking for the sparsest solution either in sample domain $\mathbf{x}$ or

in sparse transform domain **s** which is proven to be unique [101]. The most straightforward solution is ℓ_0-norm which calculates the number of non-zero elements K in the sparse signal **s** can be expressed by:

$$\hat{\mathbf{x}} = arg\ min\|\mathbf{x}\|_0 \quad s.t. \quad \mathbf{y} = \Phi\Psi\mathbf{x} \tag{4.1.8}$$

Although solving equation (4.1.8) is an intractable problem in general, some greedy techniques such as MP (Matching Pursuit) and OMP (Orthogonal MP) [112] have been reported to find the sparsest vector. This is achieved either using ℓ_0 or ℓ_1-norm which is defined by replacing $\|\cdot\|_0$ with $\|\cdot\|_1$ in equation (4.1.8). It has been shown that we can have the sparsest unique solution by applying ℓ_1-norm optimization as well.

Solving equation (4.1.8) is also an intractable problem in general. However, there have been recent attempts to solve this problem directly using iterative methods [113]. The most feasible and commonly used methods in this case, are greedy techniques mentioned above. When the support **s** of the signal has been calculated, the signal **x** can be reconstructed from its measurements $\mathbf{y} = \Phi\mathbf{x}$ as $\mathbf{x} = (\Phi\mathbf{s})\mathbf{y}$, where $\mathbf{x} = \Phi\mathbf{s}$ is actually the measurement matrix Φ restricted to the columns indexed by **s**. On the other hand, it has been shown that we can reconstruct the sparsest unique solution by solving ℓ_1-norm optimization. It leads to a convex optimization problem which is solved by linear programming. Basis Pursuit (BP) is one of the major approaches of this type which relaxes the ℓ_0-minimization problem to an ℓ_1-minimization problem. Basis Pursuit requires a stronger condition on the measurement matrix than the simple injectivity on sparse vectors, but many kinds of matrices have been shown to satisfy this condition. In general, the ℓ_1-minimization methods provide solution guarantees and stability, but rely

on methods in Linear Programming which impose high complexity to the system. Moreover, since there is yet no known strongly polynomial bound, or more importantly, no linear bound on the runtime of such methods, these approaches are often not optimally fast.

The samples are nonadaptive and measure random linear combinations of the transform coefficients. Approximate reconstruction is obtained by solving the transform coefficients consistent with measured data and having the smallest possible ℓ_1 norm. [101, 110, 111, 114–116] demonstrate the feasibility of recovering sparse signals using a small number of linear measurements.

4.2 Hierarchical Alternative Least Squares

The fundamental idea underlying hierarchical alternative least squares (HALS) is based on compressive sensing and suggests that a sparse signal $\mathbf{x} \in \Re^J$ with a few significant samples m ($m \ll J$ nonzero coefficients) can be recovered almost perfectly using a lower dimensional signal. The CS model is described as:

$$\mathbf{Y} = \mathbf{AX} \tag{4.2.1}$$

where $\mathbf{X} = [\mathbf{x}_1, \mathbf{x}_2, ..., \mathbf{x}_N] \in \Re^{J \times N}$ represents an unknown family of J at least k-sparse source signals, and $\mathbf{Y} = [\mathbf{y}_1, \mathbf{y}_2, ..., \mathbf{y}_N] \in \Re^{J \times N}$ are the compressed signals obtained by applying a known projection matrix $\mathbf{A} = [\mathbf{a}_1, \mathbf{a}_2, ..., \mathbf{a}_J] \in \Re^{K \times J}$ (usually $K < J$) on the source signals. This means that each J-sample signal $\mathbf{x}_n$ (n-th column of the matrix $\mathbf{X}$) is represented by a K-sample signal $\mathbf{y}_n$ (n-th column of the matrix $\mathbf{Y}$). The primary objective is to reconstruct the sources represented by the rows of matrix $\mathbf{X}$ from $\mathbf{Y}$ by exploiting the

sparsity property in a suitable transform domain (such as wavelet in this case). This problem is nontrivial since the system of linear equations (4.2.1) is undetermined and generally provides an infinite number of solutions.

In [117], the iterative thresholding concept originally proposed in [118] has been followed. This has been modified to incorporate an adaptive non-linearly decreasing trend, (also known as shrinkage), which allows very successful reconstruction of sparse sources. The model is represented in the following form:

$$\mathbf{S} = \mathbf{A}^T\mathbf{Y} = \mathbf{A}^T\mathbf{A}\mathbf{X} = \mathbf{C}\mathbf{X} \tag{4.2.2}$$

where $\mathbf{S} = [\mathbf{s}_1, \mathbf{s}_2, \cdots, \mathbf{s}_N] \in \Re^{J\times K}$, $\mathbf{C} = [\mathbf{c}_1, \mathbf{c}_2, \cdots, \mathbf{c}_J] = \mathbf{A}^T\mathbf{A} = \in \Re^{J\times J}$.

The columns of $\mathbf{A}$ and $\mathbf{C}$ are normalized to unit length and the sparse sources $\mathbf{X}$ can be estimated when both $\mathbf{S}$ and $\mathbf{C}$ are known. In order to do this, the samples of $\mathbf{X}$ are estimated based on minimization of

$$D^{(j)}(\boldsymbol{u}^{(j)} \parallel \underline{\boldsymbol{x}}_j) = \frac{1}{2} \parallel \boldsymbol{u}^{(j)} - c_{jj}\underline{\boldsymbol{x}}_j \parallel_2^2 \tag{4.2.3}$$

where $\underline{\boldsymbol{x}}_j$ is the jth row of $\mathbf{X}$ and

$$\boldsymbol{u}^{(j)} = \underline{\mathbf{s}}_j - \sum_{r=1, r\neq j}^{J} c_{jr}\underline{\boldsymbol{x}}_r, \qquad j = 1, 2, ..., J \tag{4.2.4}$$

By taking the gradient and after some manipulation [117] and considering that $c_{jj} = 1$:

$$\underline{\boldsymbol{x}}_j \longleftarrow \boldsymbol{u}^{(j)} = \underline{\boldsymbol{x}}_j + \underline{\boldsymbol{r}}_j \tag{4.2.5}$$

where $\boldsymbol{r}_j$ is the j-th row of the residue matrix $\boldsymbol{R} = \boldsymbol{S} - \boldsymbol{C}\boldsymbol{X}$ which is updated as [117]:

x	0.0	0.1	0.2	1.0
$\psi(x)$	1.0	0.8	0.4	0.0

$$\boldsymbol{R}^{(i+1)} = \boldsymbol{R}^{(i)} - \boldsymbol{c}_j(\underline{\boldsymbol{x}}_j^{(i+1)} - \underline{\boldsymbol{x}}_j^{(i)}) \tag{4.2.6}$$

After each update of $\underline{\boldsymbol{x}}_j$ and before each update of $\boldsymbol{R}$, a shrinkage rule based on adaptive thresholding is applied to the estimated $\underline{\boldsymbol{x}}_j$ values as follows:

$$\underline{\boldsymbol{x}}_j \longleftarrow \boldsymbol{P}_\lambda(\underline{\boldsymbol{x}}_j) \tag{4.2.7}$$

where $P_\lambda(\cdot)$ represents a suitable shrinkage rule/transformation and $\lambda = [\lambda_1, \lambda_2, ..., \lambda_N]$ is the adaptive threshold. This nonlinear shrinkage transformation is to enable the achievement of a unique sparse solution and also robustness to noise. A number of functions have been introduced in the literature as stated in [117], and it has been demonstrated that the best performance can be achieved using the non-negative Garrotte and Abramovich rules almost equivalently. Therefore, the latter one can be defined as

$$P_\lambda(\mathbf{x}) = sign(\mathbf{x})\sqrt{\mathbf{x}^2 - \lambda^2} \qquad \textbf{for} |\mathbf{x}| > \lambda \tag{4.2.8}$$

for any variable **x**, is used here.

In our source coding application, as for the EZW algorithm, we need to establish a thresholding criterion here. A monotonically non-increasing function $\psi(\cdot)$ has to be used, as for many CS algorithms, for the selected shrinkage rule. Such a function should comply to $\psi(0) = 1$ and $\psi(1) \approx 0$. Often, it decreases faster at the start and gradually becomes slower as the argument tends to 1. In practice, this function can be designed, for example, by the shape-preserving piecewise cubic Hermite interpolation with only four initial points as in [117]: Alternatively, an exponential function such as

$\psi(x) = exp(-\beta x), \beta > 0$, can be used. It has been shown that the algorithm [117] performs best when $3 \leq \beta \leq 5$.

4.3 Simulation Results

Both the EZW and the proposed HALS-CS algorithms have been applied to a 512×512 monochrome X-ray bone image. Fig. 4.2(a) is the test image. Figs. 4.2(b) and (c) show respectively the results of EZW and HALS-CS both for 100 times compression. Obviously, the quality of reconstructed image by HALS-CS is better than that by EZW. The image has diagnostic information in the region of a bone fracture as indicated in Fig. 4.3(a). To test the overall performance of the system, the error bits are generated by randomly inverting a certain percentage of bits in the EZW or CS bit streams. To verify the effectiveness of the system initially, the image regions are progressively transmitted in the four stages P_1 to P_4 using fixed parity length as mentioned in Chapter 2. During P_1, the background image is transmitted. Stages P_2 and P_3 are for the transmission of the RoI, R1, and R2. Stage P_4 is mainly for transmitting the details of the RoI. The transmission can continue to achieve the desired compression rate in the final stage. The results of both schemes for progressive transmission of the bone image for a fixed parity length are given in Figs. 4.3(b) and (c). The data for both methods were compressed approximately 50 times. The signal-to-noise ratio (SNR-defined as the square of the original image divided by the Euclidean norm of the difference between the original and the reconstructed image in dB) for EZW-based compression SNR was found to be SNR_{EZW} = 15.02 dB, whereas this ratio for the CS-based method was SNR_{CS} = 20.39 dB. With regards to peak signal to noise ratio (PSNR =max(X)) divided by the norm of difference between the original and the reconstructed image) for

EZW, this was found to be PSNR_{EZW} = 23.3 dB, whereas for the CS-based approach it was PSNR_{CS} = 29.8 dB.

In the second experiment, using the HALS-CS method, a feedback was provided and the parity length was varied. The reconstructed data becomes much less sensitive to the changes in the channel noise and the system performed much better for the regions closer to the RoI center. The results are shown in Fig. 4.3. The source compression rate was approximately equal to 50. This confirmed the adaptivity of the variable parity length scheme to changes in both the region content and the channel noise level. Obviously, the overall compression rate is based on change in parity length in order to provide protection for the data. On average, the increase was up to 25%. From Fig. 4.3 it is clear that the error for the RoI and its vicinity has been effectively mitigated and the overall system has been improved due to scalability of the system. Fig. 4.4 shows that the parity lengths in the proposed system are automatically adjusted based on both the three designated regions and the noise level in the transmission channel.

(a) (b) (c)

Figure 4.2. Source coding and decoding of 512×512 bone image: (a) original image, (b) using the EZW algorithm, and (c) using HALS-CS algorithm. In both cases, the data was compressed 100 times.

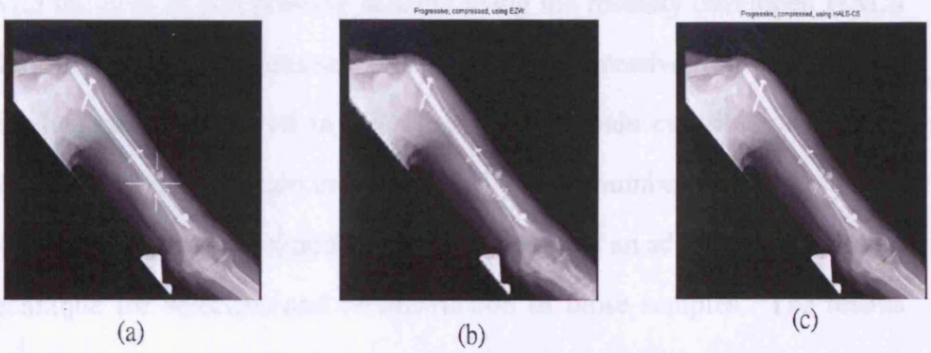

Figure 4.3. Progressive transmission of bone image; the RoI is at the point of bone fracture shown in (a), for (b) EZW and (c) HALS-CS algorithms for fixed parity length. The compression ratio is approximately 2%. In this experiment, the image was divided into subblocks of 16×16.

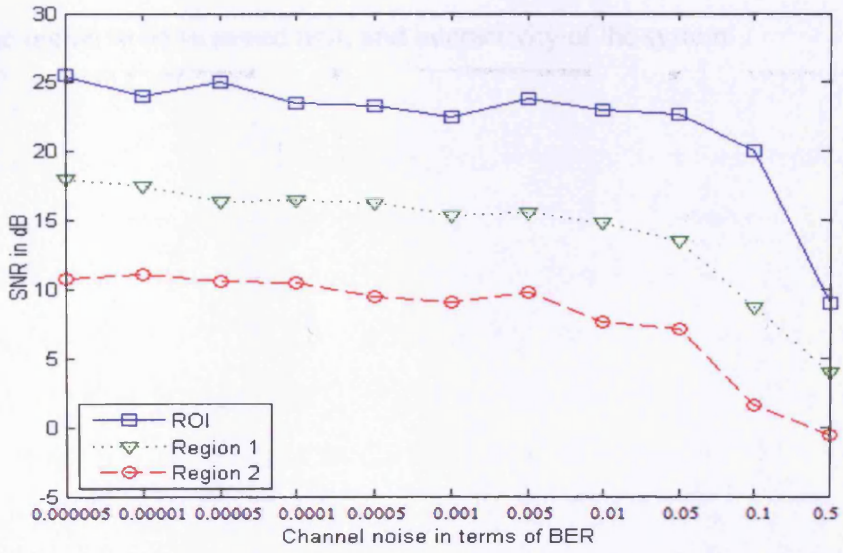

Figure 4.4. SNR for adaptive parity lengths for the three designated regions versus the noise level (in terms of bit-error rate or BER) in the channel.

4.4 Conclusions

With the help of compressive sensing using the recently developed HALS algorithm based on nonlinear thresholding a progressive transmission system has been introduced in this chapter. The main contributions of this work are: a) the selection and coding of a small number of samples (sampled below Nyquist rate) and b) the introduction of an adaptive thresholding technique for selection and reconstruction of those samples. The results have been compared with the previously introduced EZW with crisp thresholding and it has been shown that by using the new proposed technique, a much higher compression rate can be achieved for a high quality reconstruction of medical images. Generally, CS changes the rules of data acquisition, meaning that data is both captured and compressed. As a consequence, the CS algorithm will become increasingly important and widely utilized in the future. In addition, the feedback system provides flexibility in selection of the region to be streamed first, and interactivity of the system.

Chapter 5

PROPOSED PROGRESSIVE TRANSMISSION SYSTEM AND ITS IMPLEMENTATION

The proposed progressive medical image transmission with feedback system of Fig. 2.1 is implemented here and the outcomes are assessed. The proposed system consists of JSCC, UEP, and feedback (to exploit RoI and channel noise) modules. The JSCC scheme consists of a quantizer, entropy and channel coders to meet the target source rate, to achieve the required robustness in channel coding, and to find an optimal bit allocation between source and channel coding. In our JSCC scheme, a three-level HWT is adopted as a source coder and RS coders as channel coders. For medical image transmission, the UEP and both lossy and almost lossless compression methods based on HWT are adopted. The quality of the reconstructed medical images, especially for the RoI, should be acceptable. Which means having no visible error. This can be set as the constraint for the quantizer and the compression algorithm in advance. However, the quality of the reconstructed image is also affected by the channel state and proximity to the image RoI. An estimator for the noise level in the transmission channel is therefore developed. The noise estimate is sent back to the transmitter

through the feedback channel. The parity length is also varied to achieve an adaptive and efficient transmission system. The feedback signal in the proposed scheme updates the parity length without the need for retransmission of the data or addition of any extra overhead. The parity length is automatically adjusted by the feedback channel. Since the reconstructed image is divided into three areas for faster observation by the user, the UEP strategy is adopted to reduce the transmission channel load, and maintain the RoI region with minimum error. The proposed system is very user-friendly since the selection of the RoI, its size, overall code rate, and a number of test features, such as noise level, can be set by the user at both ends.

The principal idea behind all these methods is that in a progressive transmission framework, the receiver reconstructs the transmitted image at various bit rates, which makes fast and reliable retrieval of large images possible. That is to say, the quality of the reconstructed image is entirely dependent upon the volume of the received data and the images can be reconstructed in any reasonable bitrate. Further, the image subblocks are coded separately. Due to the high sensitivity to transmission noise, progressive transmission of images over noisy channels has to be accompanied by an appropriate channel coding, or a JSCC scheme. Any noise in the current communication system may be due to the electronic components, fading, Doppler shift for mobile systems, bad weather, interference, attenuation, etc. The RS codes utilized here are block-based error correcting codes which are widely used for channel coding. The RS(n, k) codes correct the symbol error and not the bit error. Accordingly, RS is suitable for burst error detection and correction. By utilizing our flexible system, minimum distortion of the transmitted images in a fairly short transmission time can be achieved. As the main contribution of this research, we adaptively con-

trol the lengths of parity codes simultaneously with respect to the selected region (i.e. longer lengths correspond to the areas closer to the centre of the RoI) and the amount of corrupted received data in the receiver.

A Matlab-based TCP/IP connection has been established to demonstrate the proposed interactive and adaptive progressive transmission system. The proposed system is simulated for both a binary symmetric channel (BSC) and Rayleigh channel. The experimental results verify the effectiveness of the design. A block diagram of the proposed system is shown in Fig. 2.1 in Chapter 2.

5.1 Description of the System

5.1.1 System analysis

Wireless transmission of medical images involves construction of an effective JSCC to not only preserve the diagnostic information but also to enable progressive streaming of the data from the host to the receiver. Thus, based on progressive encoding, we can compress a block into a bitstream with increasing accuracy. Traditionally, the input images are decomposed into many subblocks which can each be coded, compressed, and transmitted individually. First, the input image is segmented into a number of subblocks. An 8×8 subblock structure is adopted in our proposed system. Although larger subblocks compression rate is slightly better, the computation cost and the required memory size increases with the subblock size. For application in portable devices, memory and computation are of our concerns. WT decomposes each subblock into different time-frequency components. A 3-level HWT is utilized as the WT function in our proposed system.

After computing the HWT and quantizing the HWT coefficients, we

compress the quantized data in each subblock independently according to a variable thresholding mechanism governed by the EZW. The WT coefficients are coded into streams of four symbols, namely,($p, n, z, t,$) according to the threshold value, as detailed in section 2.2.1 of Chapter 2. EZW suits progressive data transmission, since it enables hierarchical encoding and decoding. The suitable approach in the EZW is to use a variable threshold and transmit only those coefficients to the decoder that are larger than the threshold. The first step in the EZW algorithm is to determine the initial threshold level t_0 and then repeatedly lower the threshold by half at a time until the threshold has become smaller than the smallest coefficient to be transmitted, or the iteration is stopped by request. Lowering of the iteration threshold by half at a time is used to determine the compression ratio and resolution in the subblock. The reconstructed image is divided into three areas, as shown in Fig. 2.11 in Chapter 2. Each area has a different resolution, which means the compression ratio in each subblock is based on the subblock location. The Morton scan is adopted as the scan order as shown in Fig. 2.5(b) in Chapter 2.

The RS (255, k) codes utilized here are block-based error correcting codes as detailed in section 2.2.2 of Chapter 2. The HWT and RS coders are utilized to achieve a JSCC scheme in our proposed system. In which, the parity length is adaptive and automatically adjusted by the channel state. In the proposed algorithm, the data in different image regions, as denoted in Fig. 2.11 in Chapter 2 for three regions, are protected by variable length parity codes as for the UEP. The data in the RoI is treated as the most important information and protected by longer length parity codes. Thus, according to the UEP, the ratio of parity to overall code length for the (n+1) regions

should be as follows:

$$C_{RoI} > C_{R1} > C_{R2} > \cdots > C_{Rn}. \tag{5.1.1}$$

where C_{RoI}, refers to this ratio for the RoI and so on. Further, the length of the parity code is affected by the noise in the channel, i.e. $C_{region} \sim (r, N)$, where r is the distance from the center of the RoI and N expresses the noise in the practical transmission channel.

An adaptive variable parity allocation requires the error between the transmitted image, $I(x, y)$, and the received image, $\hat{I}(x, y)$ to be minimized under the desired conditions. Suppose the error is defined as

$$\varepsilon = \|I(x, y) - \hat{I}(x, y)\| \tag{5.1.2}$$

where $\|\cdot\|$ is the Euclidean-norm. Generally, we want to have the optimum parity length such that:

$$C_{opt} = \min_{c} \varepsilon \quad subject\ to \quad \varepsilon \leq \varepsilon_T \tag{5.1.3}$$

where ε_T is an acceptable error level in the receiver. According to the above discussion, the parity length can be defined as:

$$C = g(r, \text{S/N}) = f(r, \text{BER}) \tag{5.1.4}$$

where S/N, BER and r respectively stand for signal-to-noise ratio, bit error rate and distance from the center of the RoI. The functions g and f are generally nonlinear functions which can be defined empirically based on examining the system for a number of trials. Fig. 5.3, $f \sim (\alpha_0 - \alpha_r)$ for a

fixed BER, where r is measured with respect to the number of pixels. From Fig. 3.7 in Chapter 3, it can be concluded that $f \sim (\beta BER + \beta_0)$ for a fixed proximity distance r. In more general applications, a more accurate and possibly complicated function may be adopted. For such applications, a reasonably accurate function can be modeled as

$$f(r, \text{BER}) = (\alpha_0 - \alpha_r)(\beta BER + \beta_0). \tag{5.1.5}$$

or

$$f(r, \text{BER}) = \mu_3 \text{BER} - \mu_2 r.\text{BER} - \mu_1 r + \mu_0. \tag{5.1.6}$$

where $\mu_i s$ are constant coefficients and can be easily found based on Fig. 5.3 and Fig. 3.7 in Chapter 3.

Fig. 3.6 in Chapter 3 shows the frequency of the set of parity lengths in 10 trials for when the channel noise is set to BER=0.003 equivalent to the occurrence of 7 errors in 2048 transmitted bits. As long as the error in the receiver remains higher than a threshold t_h, the length of parity increases. If the error falls below a level $t_l < t_h$ the parity length will also increase. These threshold levels are empirically selected by following the constraint in equation (5.1.3). In these cases, the parameters in equations (5.1.5) and (5.1.6) are approximately α_0=0.08, $\alpha = 2 \times 10^{-4}$, β_0= 5, $\beta = 5 \times 10^3$ and accordingly $\mu_0 = \alpha_0\beta_0$=0.4, $\mu_1 = \alpha\beta_0 = 10^{-3}$, $\mu_2 = \alpha\beta$=1, and $\mu_3 = \alpha_0\beta = 4 \times 10^{-2}$.

The performance of the system subject to different noise-levels is evaluated using the peak signal-to-noise ratio, PSNR, defined as:

$$\text{PSNR(dB)} = 10 \log_{10} \frac{A^2}{MSE} \tag{5.1.7}$$

where A=1 if the image $0 \leq I \leq 1$, and MSE is defined as:

$$MSE = \frac{\|\hat{I} - I\|_2^2}{\|\hat{I}\|_2^2} \tag{5.1.8}$$

where $\hat{I}$ represents the reconstructed subblock of the image, I is the subblock of the original input image, and $\|\cdot\|_2$ represents the Euclidean norm.

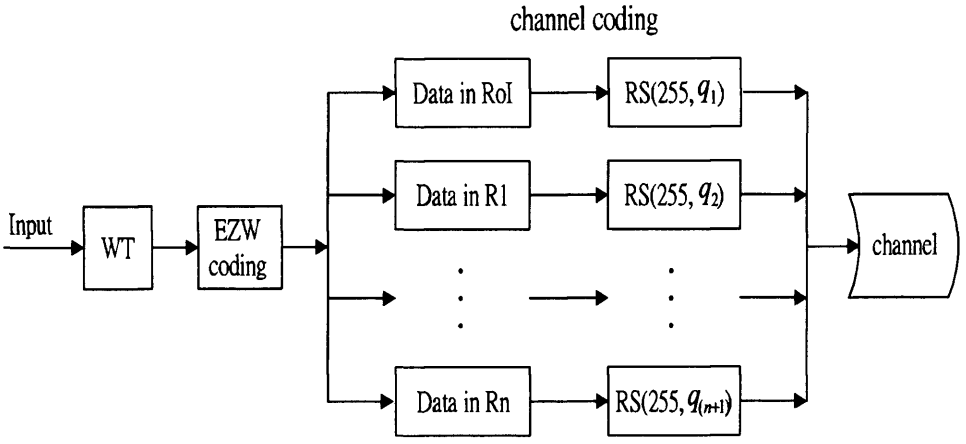

Figure 5.1. The transmitter including the proposed channel coding block diagram.

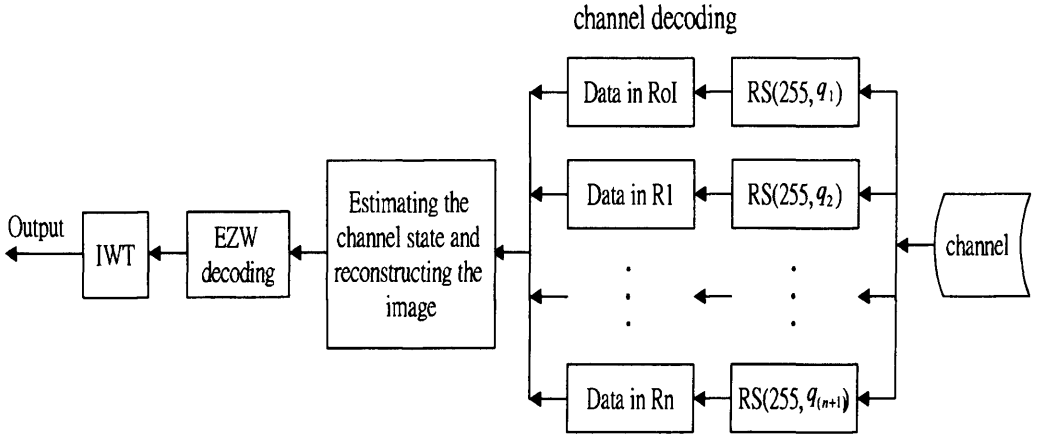

Figure 5.2. The block diagram for the receiver.

Figs. 5.1 and 5.2 show channel coding structures in our proposed system. The data in the same area is accepted as having the same data protection capability, and different data protection capability between areas. The two figures also show the UEP scheme.

5.1.2 Experimental results

The proposed system is simulated for both the BSC and flat-fading Rayleigh channel models. The BSC is the simplest channel model, which facilitates the analysis and enables a fast software implementation. Since wireless mobile communication channels are often considered to be with flat-fading Rayleigh noise, we simulated both the BSC and flat-fading channel models and tested the performance of the proposed technique against both models. RS(255, k) was used in the proposed scheme. The RS codes correct the symbol error and not the bit error. The noise in the simulated channel was considered such that a BER of 0.01 was set in the receiver end. When the errors are uniformly distributed, the average parity length is 42 for a 255 length code length. This recovers the RoI perfectly when either the BSC or Rayleigh channel is considered and the channel noise is equivalent to BER = 0.01.

The developed algorithm was tested for a number of images, two of which are analyzed here. The first image is a 123 × 150 pixel color dental implant image, and the second image is a 508×512 pixel monochrome X-ray bone image, both of which are to be transmitted via TCP/IP. The proposed system follows the diagram in Fig. 2.1 in Chapter 2. Each noisy channel involves a BSC and flat-fading Rayleigh channel with a certain BER. In the simulation, the error bits are generated by randomly inverting a certain percentage of bits in the RS bitstream. To verify the effectiveness of the system,

the image regions are progressively transmitted through four stages, namely, P_1, P_2, P_3, and P_4. During the P_1 stage, the background image is transmitted. P_2 and P_3 are the second and third stages, both for the transmission of the RoI, R1, and R2. P_4 is the fourth stage, mainly to transmit the details of the RoI (and the rest of the image if necessary). In the approach presented here, first, the user (physician) specifies the address of the transmitted medical image in the transmitter within the dialogue-based software. After receiving the low resolution background image, the user identifies the center of the RoI by a mouse and the radius of the RoI by entering a value within the dialogue-based software. Then, the algorithm adjusts the length of the parity codes initially proportional to the proximity to the center of the RoI as C_0, C_0-2, C_0-4 for RoI, R1, and R2, respectively.

Accordingly, the receiver detects and counts the packages in error by estimating the status of the channel. The parity lengths remain the same if the distortion in the reconstructed image is acceptable. Otherwise, the codes will be adjusted automatically. Typically, the ratio of the parity code to the overall code length is larger for the clinically higher priority areas, that is, the areas closer to the center of the RoI as stated in equation (5.1.1). Fig. 5.3 shows the ratios of the parity length and the overall codeword according to the experimental results.

Table 5.1 summaries the average compression ratios for various regions before the channel coding during the four successive transmission stages. The compression ratio is defined as the ratio between the data volume of the coded data and the original data. However, by changing one of the RoI coordinates, or its radius r_a and r_b, data in Tables 5.1 and 5.2 are also changed.

In Fig. 3.7 in Chapter 3, the parity lengths are found by averaging the

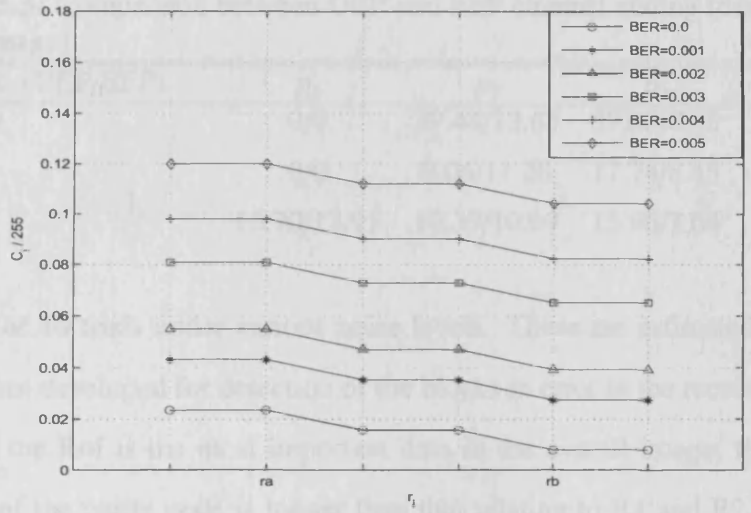

Figure 5.3. The ratios between the lengths of the parity code C_i and overall codeword of 255 symbols in different regions at various fixed noise levels with respect to proximity to the RoI.

Table 5.1. The average compression (bpp) for various regions for the four stages of the progressive image transmission (bone image).

Compression ratios	p_1	p_2	p_3	p_4
Overall image	0.188	0.773	1.08	1.545
RoI	0	2.62	1.86	1.545
R1	0	0.372	0.406	0
R2	0.188	0.219	0.291	0

Table 5.2. The average PSNR (dB) for various regions corresponding to the four progressive image transmission stages (dental implant image).

PSNR	p_1	p_2	p_3	p_4
Overall image	21.02	23.05	27.03	39.79
RoI	0	39.44	39.68	39.79
R1	0	25.08	27.01	0
R2	21.02	21.24	22.11	0

Table 5.3. Comparison between UEP and EEP channel coding (dental implant image).

PSNR, (UEP/EEP)	p_1	p_2	p_3	p_4
RoI	0/0	39.44/13.65	39.68/8.45	39.79/7.4
R1	0/0	9.06/11.28	17.74/8.45	0
R2	16.70/13.91	10.39/10.69	15.96/7.64	0

results of 10 trials under various noise levels. These are estimated by the algorithm developed for detection of the blocks in error in the receiver. The data in the RoI is the most important data in the overall image; thus, the length of the parity code is longer than that relating to R1 and R2. In the proposed system, the codeword length of RS codes is 255, and the number of error bits is generated at random.

Table 5.3 shows the qualities of reconstructed image comparison in UEP with in EEP data protection strategy in same compression ratio. The number of error data being corrected is not always same because the RS corrects a corrupted symbol not a bit and the noise is random signal. However, the data in RoI is error-free based on the experimental results in UEP strategy.

In Table 5.4 shows the compression ratio and PSNR based on various blocksizes in three areas in the EZW, where BS8, BS16, and BS32 express the blocksizes are 8×8, 16×16, and 32×32, respectively. RoI, R1 and R2 are three area with different compression rates adopted in the experiment. According to the results, the compression rate is increased when the blocksize is increased, but the quality is decreased.

Fig. 5.4 shows the PSNRs for the four successive transmission stages under various noise-level conditions. Fig. 5.5(a) shows the background image sent during the P_1 stage. Fig. 5.5(b) is the progressively reconstructed image after stage P_2, in which the RoI, R1, and R2 are reconstructed. At this stage, the center of the RoI is denoted by the user via a mouse click.

Table 5.4. Compression ratio and PSNR based on various blocksizes in three areas in EZW.

area \ (bpp\PSNR)	BS8	BS16	BS32
RoI	4.88/39.79	4.19/39.92	4.00/39.66
R1	2.15/27.92	1.255/27.08	0.934/25.90
R2	0.885/21.01	0.368/19.96	0.218/18.54

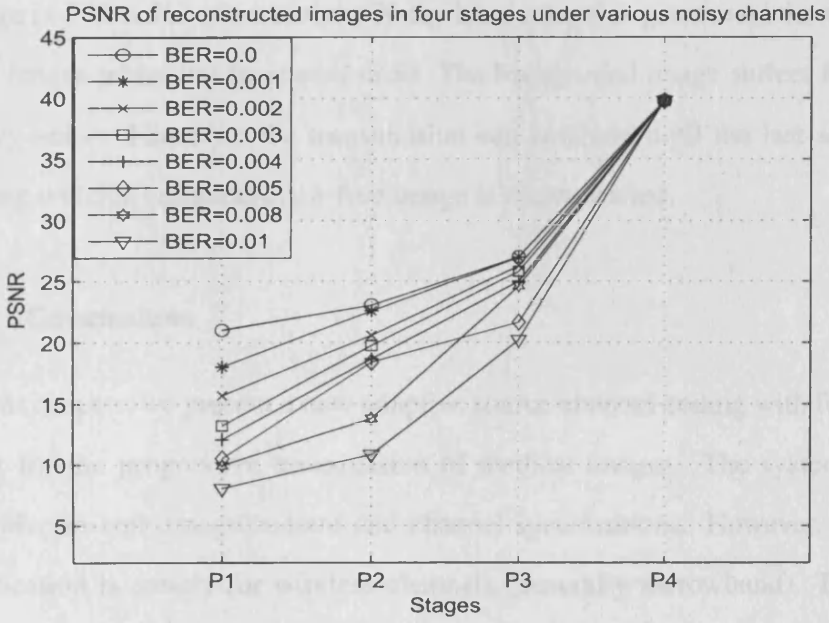

Figure 5.4. PSNR for four successive transmission stages at different BERs under various noise-level conditions.

Fig. 5.5(c) represents the reconstructed image at stage P3 during which the regions RoI, R1, and R2 are reconstructed. The RoI and R1 regions are gradually increased in resolution. Fig. 5.5(d) is the final and complete image after stage P_4. The same procedure can be followed for encoding and transmitting other medical image. However, the coordinates of the center of the RoI as well as the size of the RoI may be adjusted according to the user's requirement. For example, in Fig. 5.6, the RoI is selected in the corner. Figure 5.7 demonstrates that a fixed-size parity code is not suitable for an efficient transmission system. Accordingly, the system has been modified based on the proposed method to allow variable lengths of parity. Fig. 5.8 and Fig. 5.9 show no error in the RoI, indicating that the overall system has been remarkably improved. In Fig. 5.10, another example of a decoded image (a 508×512 monochrome X-ray bone image) is given, and the variable length parity has been examined. The background image suffers from heavy noise. However, the transmission can continue until the last stage during which a complete error-free image is reconstructed.

5.2 Conclusions

In this chapter, we present a new adaptive source-channel coding with feedback for the progressive transmission of medical images. The system is adaptive to both image content and channel specifications. However, this application is merely for wireless channels (generally narrowband). Data error detection capability and correction with automatic adjustment, low image transmission time, and efficient communication are the key features of this proposed system. The length of parity codes can be adjusted automatically based on the location of the image subblocks and the practical characteristics of the communication channel to provide adequate data pro-

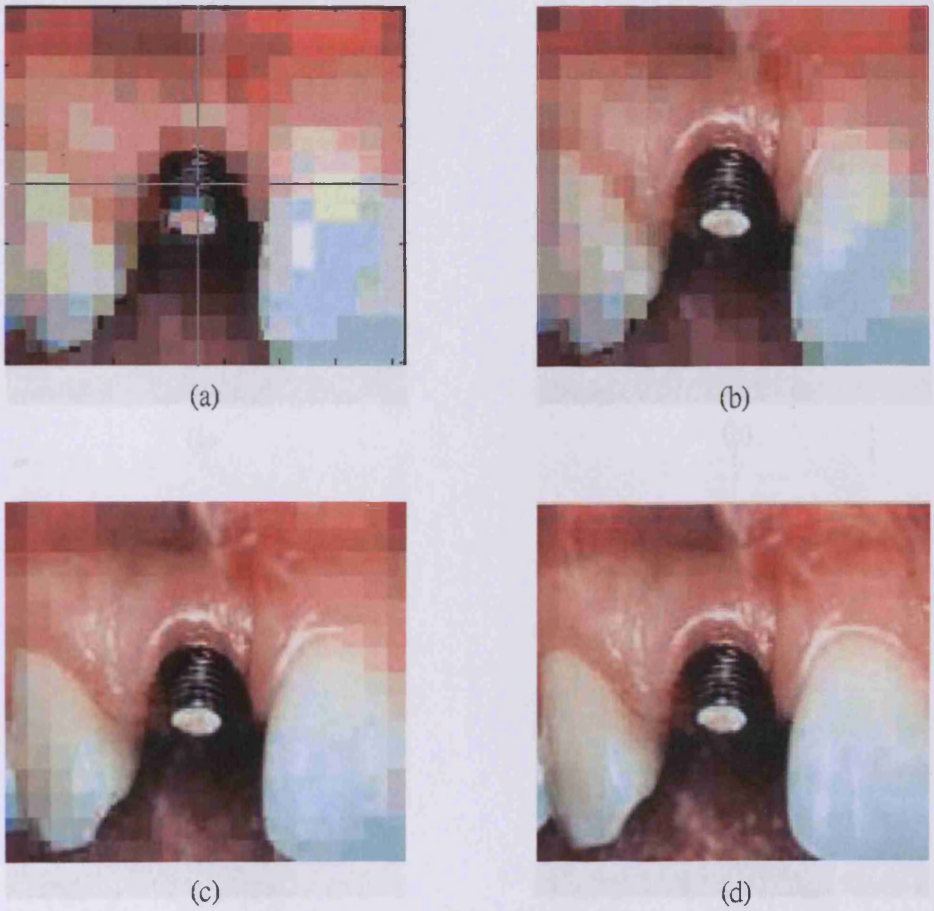

Figure 5.5. The transmitted image over the low noise: (a) the background image at stage P_1 and the location of the RoI in the center of the image, (b) the transmitted image after stage P_2, (c) the transmitted image after stage P_3, and (d) the completely decoded image after stage P_4.

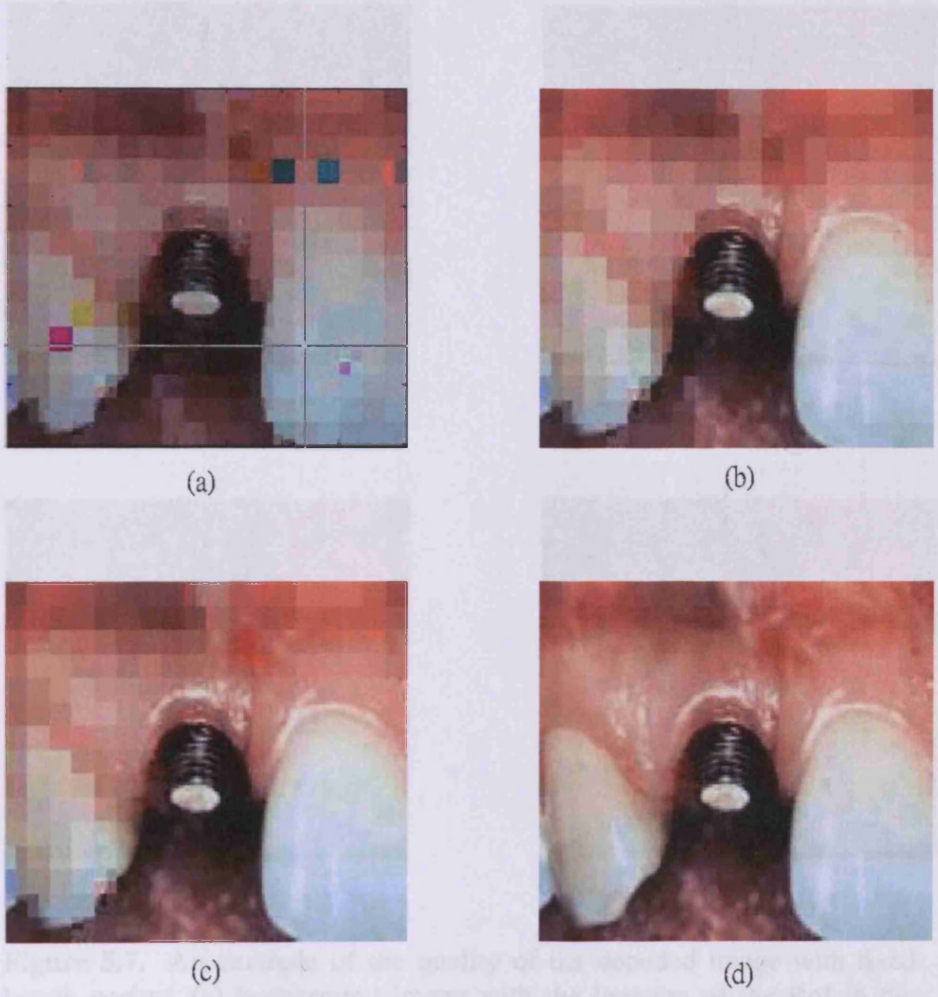

Figure 5.6. Similar results as in Fig. 5.5 when the RoI is selected in the corner of the image.

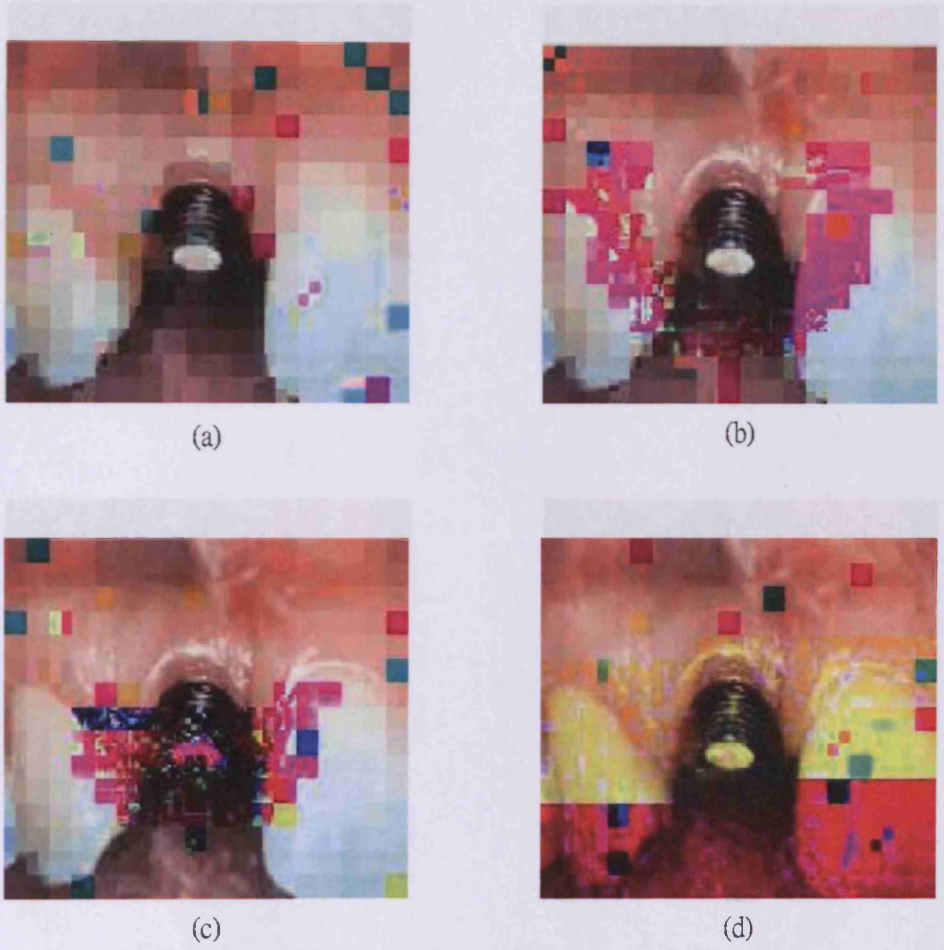

Figure 5.7. An example of the quality of the decoded image with fixed length parity: (a) background image with the location of the RoI in the center, (b) the image reconstructed at stage P2; several subblocks in error in the area of the RoI and some error subblocks in the vicinity of the RoI, (c) the number of subblocks in error increases when the volume of the data in the receiver increases, that is, the resolution of the higher-priority regions increases, and (d) the complete transmitted image.

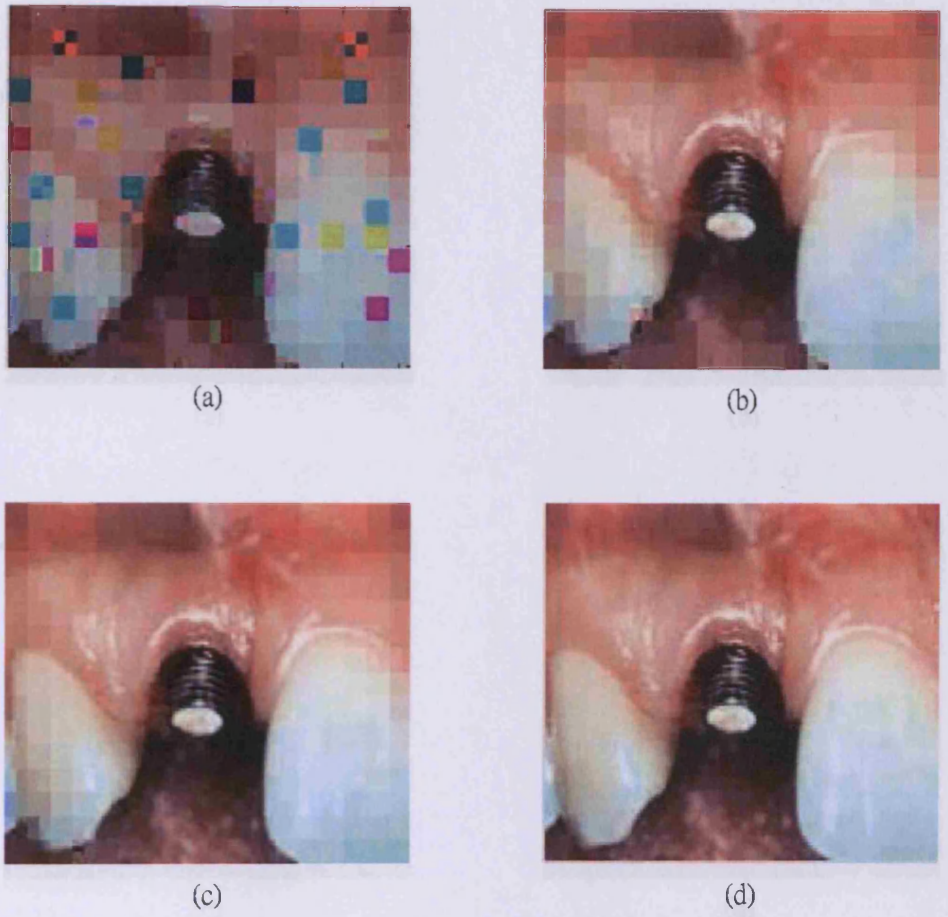

Figure 5.8. The decoded image with variable parity code length over a noisy channel. (a) A background image and the location of the RoI selected in the center of the image reconstructed after stage P_1, (b) the reconstructed image after stage P_2, no error subblocks are found in the reconstructed image because the parity code length are adjusted automatically based on the previous volume of incorrect data in the receiver, (c) the reconstructed image after stage P_3; the lengths of parity bits in stage P_3 are same as in stage P_2 because no incorrect data was found in the reconstructed image after P_2, and (d) the complete transmitted image with no subblocks in error subblocks.

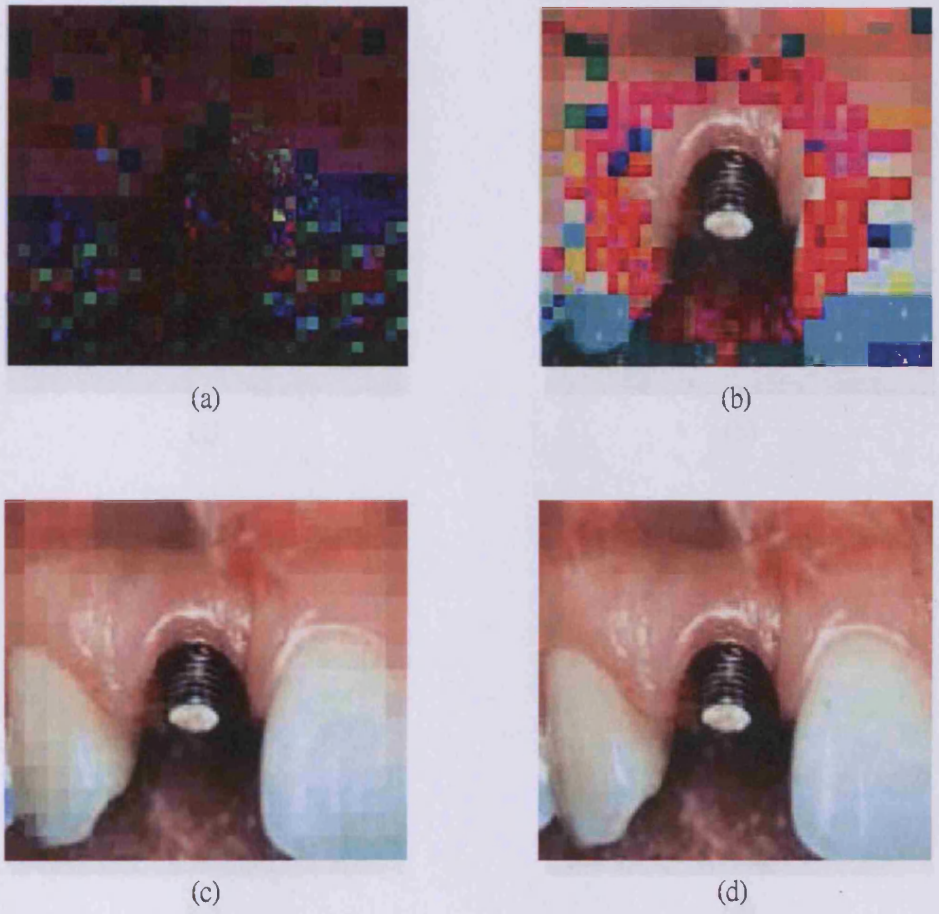

Figure 5.9. A decoded image with variable parity code length over a noisy channel: (a) several error subblocks are detected in stage P_1, (b) several error subblocks are still found in stage P_2, indicating that the feedback message is incorrect or the channel condition is becoming noisier. However, the RoI is still error-free based on the UEP, (c) no error subblock is detected in stage P_3 because the parity length is adjusted again according to the previous channel state, although there can still be some error, and (d) the complete transmitted image with no subblocks in error subblocks.

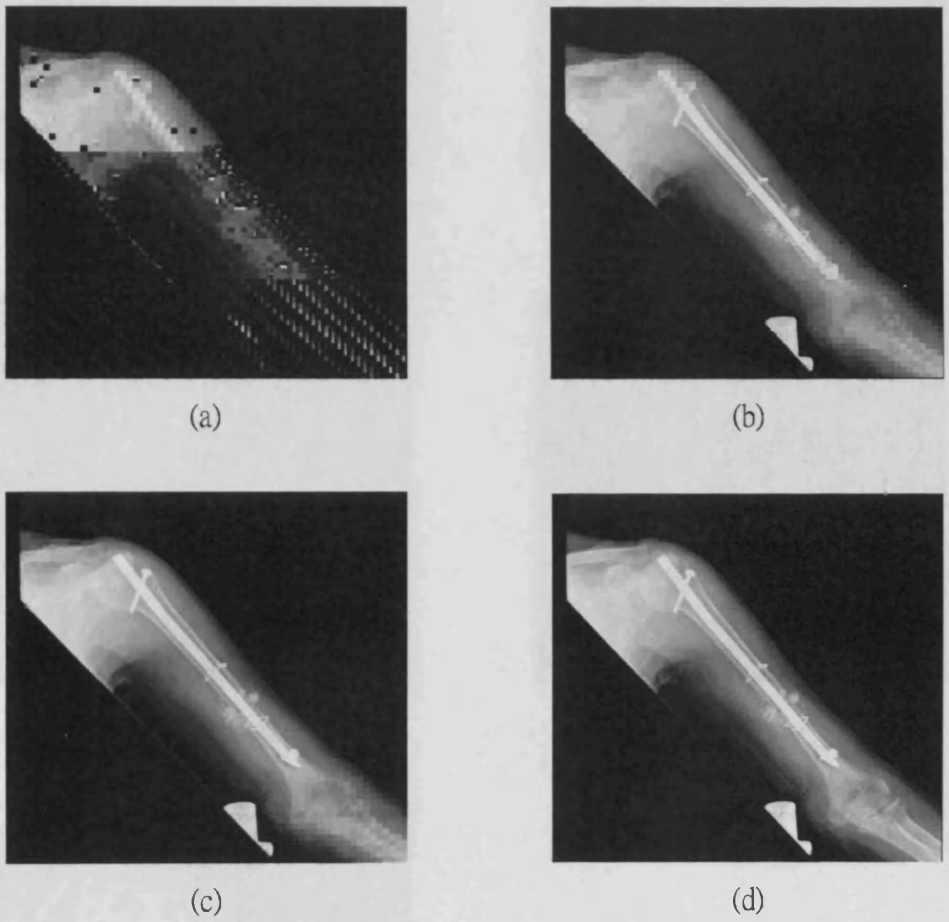

Figure 5.10. A decoded image with variable parity length, which is a 508 × 512 pixel monochrome X-ray bone image: (a) a background image and the location of the RoI selected in the center of the image reconstructed after stage P1; many subblocks are in error in the background image, (b) the reconstructed image after stage P2, no error subblock is found in the reconstructed image, (c) the reconstructed image after stage P3, and (d) the complete transmitted image with no subblocks in error.

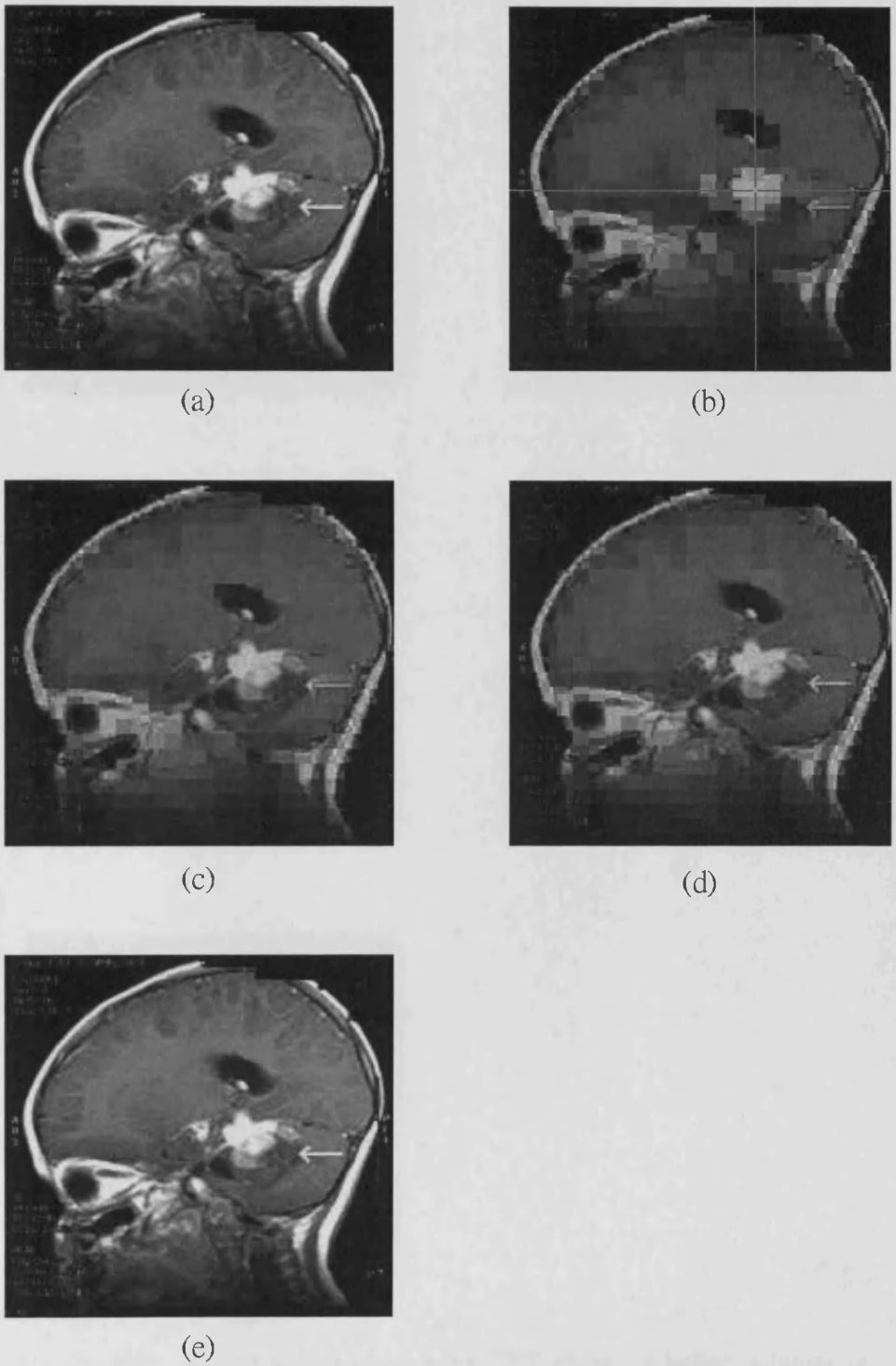

Figure 5.11. A 197 × 200 pixel brain MRI image including a tumor in the sulcus region: (a) the input image, (b) a background image and the location of the RoI selected in the right of the image reconstructed after stage P1, and (c)-(e) are the successive reconstructed images.

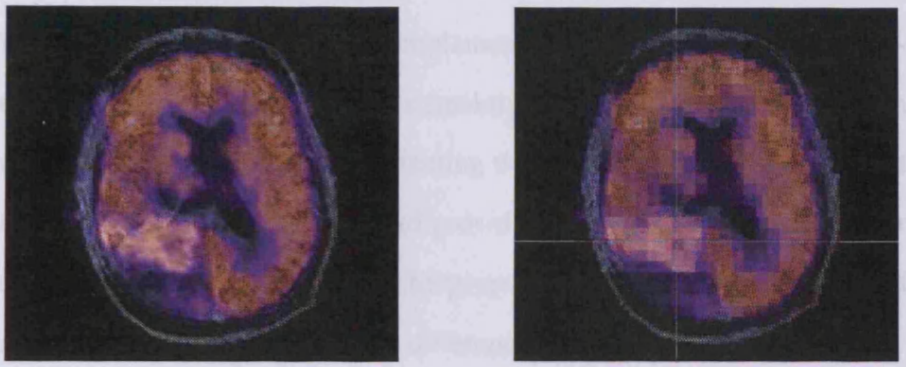

(a) (b)

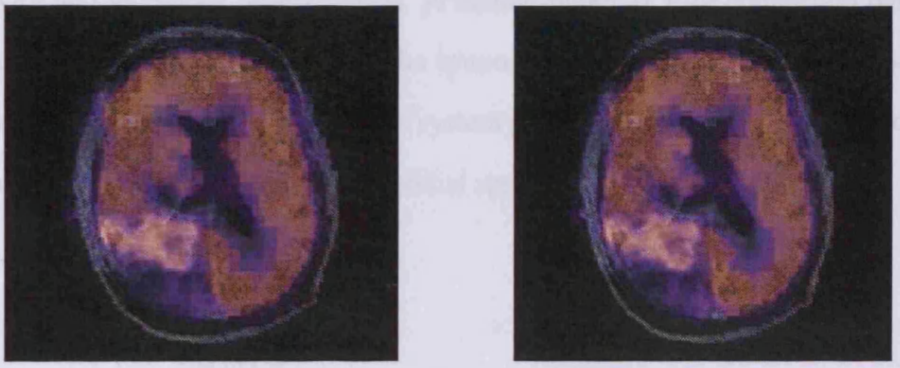

(c) (d)

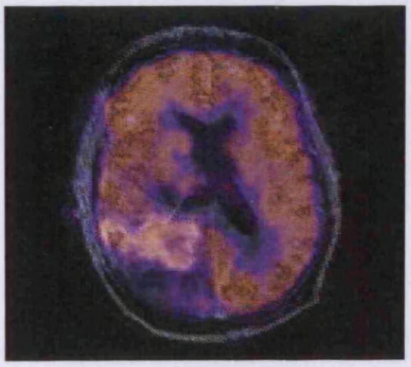

(e)

Figure 5.12. A 256 × 256 pixel brain PET image including a tumor in the left and posterior region: (a) the input image,(b) a background image and the location of the RoI selected in the bottom left corner of the image reconstructed, and (c)-(e) are the successive reconstructed images.

tection. The overall code length for the channel encoder/decoder is fixed. This makes it easy for hardware implementation. A wide range of fluctuations in the channel characteristics (mainly noise level) can be tolerated in the system. The algorithm for detecting the errors in subblocks can detect the header error in the receiver and provide feedback to the transmitter for adjustment of the parity length. The proposed system has also been tested for communication channels with different capacities and noise levels. The presented results verify the effectiveness of the system in terms of both adaptivity and flexibility of interaction. A Matlab-based TCP/IP connection has been established to demonstrate the proposed interactive and adaptive progressive transmission system. This system provides a practical, flexible, and interactive method which suits medical applications.

Chapter 6

HARDWARE IMPLEMENTATION USING SIMULINK TOOLS

In this chapter, we briefly describe the circuit design methods and demonstrate our proposed system circuit design using embedded Matlab function blocks. Based on the information in Fig. 6.1, in the fast-moving market, the product revenue loss is 47% if the product to the market is delayed 6 months. If the delay is 12 months, 90% revenue is lost. Therefore, to simplify the design process, decrease in the design time, and enabling early and rapid verification are very important steps in the circuit design process. Mathworks provides a new tool called Simulink HDL coder, a new feature provided by Matlab within the 2008a version, that allows the engineers to generate automatically bit-true, cycle-accurate, synthesizable VHDL and Verilog codes from the Simulink models and Stateflow diagrams. I therefore, attempt to convert my developed progressive medical image transmission with feedback system into VHDL codes utilizing the Simulink HDL coder, because this design method can increase the circuit design's efficiency, cut down the design cost, and reduce the gap between algorithm development and hardware implementation. The design flow of adopting Simulink HDL coder

directly generates hardware description language (HDL) codes as shown in Fig. 6.2. The major advantage of this approach is to use the same language in both development and implementation of the algorithm.

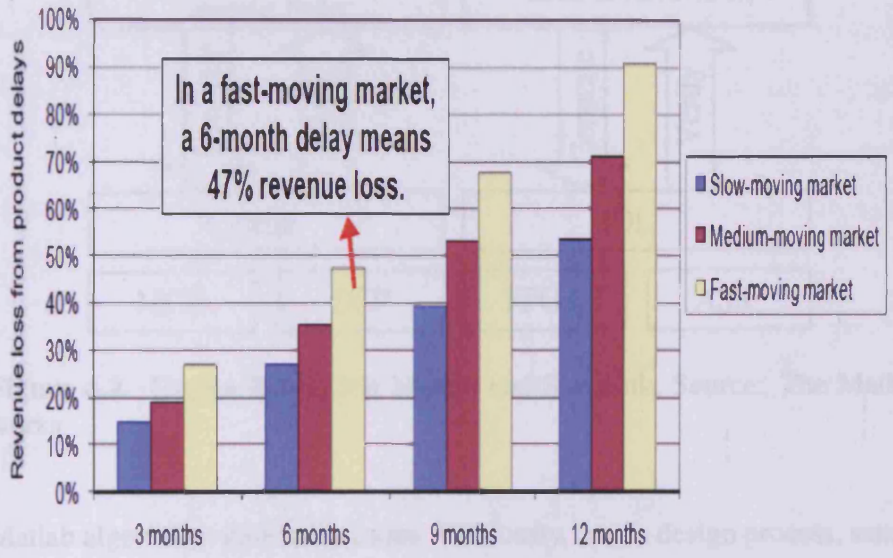

Figure 6.1. Revenue loss because due to product delay, Source: Return on Investment in Simulink for Electronic System Design, IBS study, 2005

For many modern real-time image transmission systems, which require large memories for storage, and a high network speed and bandwidth for transmission activity. Although the software provides greater flexibility of operation, performance is often too slow for high-end multimedia applications. In such instance, conversion of the system from software to hardware is one solution to increase the operational speed. Algorithm developers often create Matlab-based algorithms due to the extensive function libraries in the Matlab and its feasible simulation environment. As the design evolves towards circuit implementation, real-world constraints must be incorporated, which typically requires the designer to manually translate

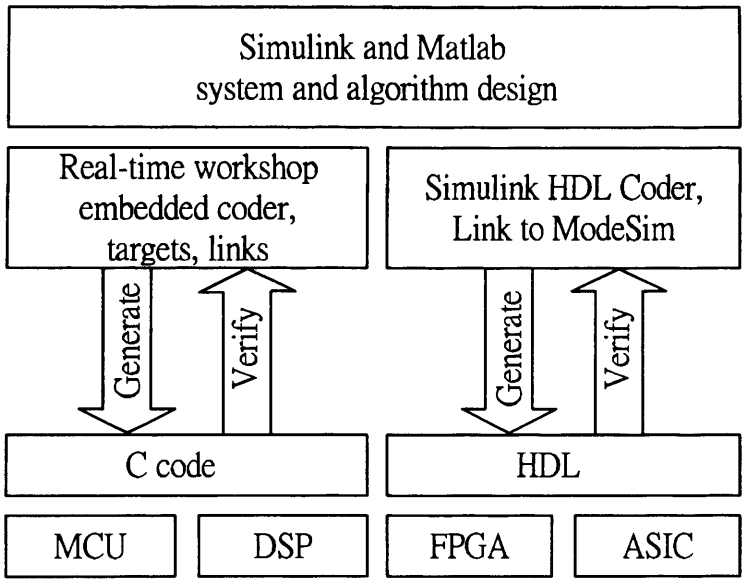

Figure 6.2. Design flow using Matlab and Simulink, Source: The Mathworks

Matlab algorithms into HDL codes. Obviously, in this design process, same algorithm is reduplicated design by two different design languages, Matlab and HDL, at this stage, the designer faces the task of verifying that these copies remain equivalent throughout multiple design stages.

Simulink provides an environment for simulation model-based design for dynamic and embedded systems, interactive graphical models, and a customizable set of block libraries that allow to design, simulate, implement, and test a variety of time-varying systems, including communications, controls, signal processing, video processing, and image processing [119]. The Matlab HDL coder under Simulink can automatically convert a well-defined subset of embedded Matlab codes into HDL codes, such as VHDL and Verilog codes. This technology can reduce the development and verification cost of manual translation from Matlab to HDL. Working within the Embedded Matlab subset, designers can maintain one copy of the developed algorithm and elaborate it directly within Matlab to incorporate hardware

implementation requirements. The advantages of design in the Simulink environment are the design, interactive debugging and visualization capabilities still in Matlab development platform. This approach provides the algorithm developer and the hardware engineer with a common language and shared understanding of the design intent and it can also automatically generate HDL codes from the Embedded Matlab code, eliminating the cost of producing and verifying hand-written HDL codes. However, unlike many Matlab algorithms, the embedded Matlab code for hardware implementation is not an abstract representation of the design. Memory size, input and output should therefore be fixed and are not variable as Matlab. Accordingly, the code developed in Matlab has to comply with the Embedded Matlab requirements.

To generate the VHDL codes of our proposed system, we adopted embedded Matlab function blocks to create a system-level model under Simulink. The Embedded Matlab Function block is specifically designed for the purpose of integrating Matlab codes into a Simulink model. The process starts by defining a top-level Matlab function in the Embedded Matlab Function block. Input variables of the top-level function automatically become either input ports or parameters of the block, and output variables of the function become output ports on the block. Each block becomes a user-defined model after complying with the embedded Matlab function syntax. We can therefore move those user-defined models to build up our required system. To increase our system's operation frequency, a concurrent architecture is adopted in our design.

A few companies have adopted the new design flow to reduce their design life cycle, for example, the latest Digital Video Infrastructure Platform (DVIP) manufactured by Sundance Multiprocessor Technology Ltd

now adopts Simulink HDL Coder to generate HDL for implementation into FPGA [120].

6.1 Introduction to Hardware Design Flow

Image transmission systems are increasing in complexity at an alarming rate, implying that market pressure is also growing. The pressure results in a growing demand for high quality electronic design automation (EDA) tools to aid the designer. For example, Maltab and Simulink are used for algorithm design. VHDL, Verilog, Modelsim [121], Synopsys VCS [122], and Cadence [123] are used for the design and simulation of Register Transfer Level (RTL) circuit. The RTL is a synchronous digital circuit which consists of two kinds of elements, registers and logical gates. Normally, the hardware description languages VHDL and Verilog are the two most widely used in RTL design. VHDL was originally developed for the US Department of Defense's need to document the behavior of the ASICs. Prototype and integrated circuit (IC) are application-specific integrated circuits (ASIC), field-programmable gate arrays (FPGA), and complex programmable logic device (CPLD). A simplified IC design process is shown in Fig. 6.3. Of course, no design necessarily follows the flowchart shown in Fig. 6.3 exactly.

As can be seen in Fig. 6.3, the hardware design process is extremely complex. In each block of this figure, we need to utilize one or more EDA tools to design and verify those circuits. Several IC design manufacturers may be involved in the IC fabrication. Although Matlab platform is used to create the algorithm and generate the HDL code from the Simulink HDL coder, normally the RTL generated in the HDL code has to be verified again by test bench. Generally speaking, the time spent on testing the function is

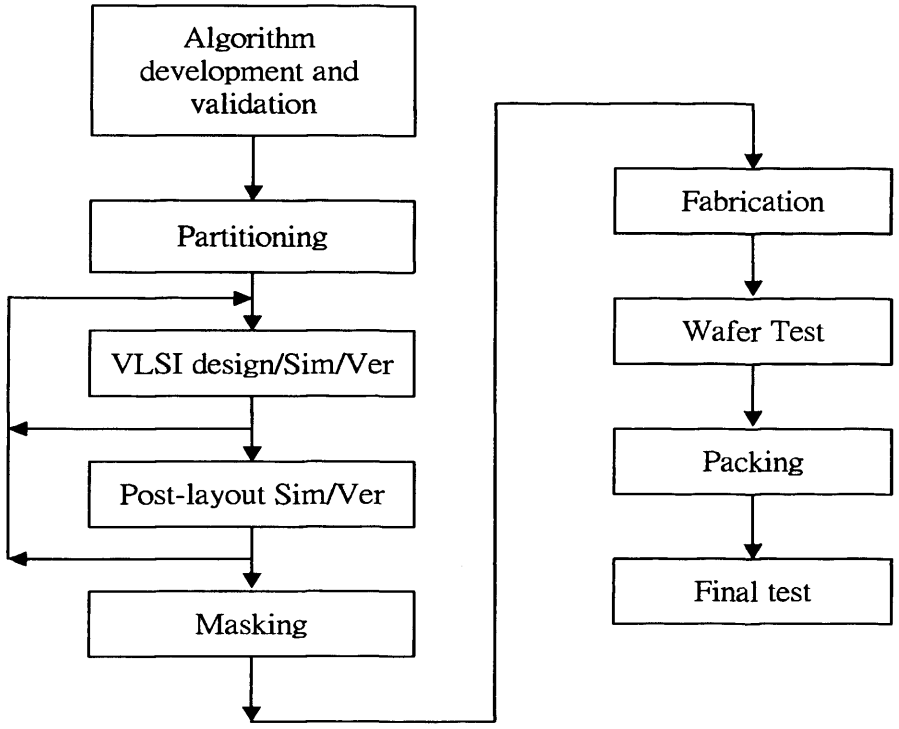

Figure 6.3. A very simplified flowchart of the IC design process

often more than the time required for the algorithm development and hardware design. While the comparison between the embedded Matlab function and VHDL design methods both need to exactly define the input and output pins, Matlab provides more model commands than VHDL. In the embedded Matlab function block, concurrent activity is not available, but concurrent activity can be designed in each component by VHDL. The parallel architecture only exists in the graphical approach in Simulink model. However, the benefit of hardware design using Simulink is that the designers can adopt the models offered by Simulink libraries. Unfortunately, the models provided by Simulink libraries are not suitable for our proposed system. Therefore, we adopted the embedded Matlab function blocks to generate models and then utilized those developed models to achieve the system design.

6.2 The Circuit Diagram

The objective here is to implement the system using FPGA. For the proposed system, the aim is to reduce the circuit complexity and its computational cost. To simplify the design procedure, we adopted the Simulink HDL coder directly in order to transform the embedded Matlab code to the VHDL code. Each block in the Simulink Model is generated from the embedded Matlab function. The circuit architectures are shown in Fig. 6.4 for the transmitter and Fig. 6.5 for the receiver, respectively. The proposed system is designed with parallel architecture to increase the system's operational speed. Therefore, it has three kinds of data for color image input. These are described below:

- The transmitter part (see Fig. 6.4):
  - Haar block: In this block, the input data is segmented into 8×8 subblocks as a tiling technique and then each subblock is transformed by the three-level HWT. The three-level HWT is performed by preset matrices, as in section 2.1.3 of Chapter 2. Performing matrix operations in Matlab makes the whole process faster.
  - Area block: In the original proposed system, three areas are defined in the reconstructed image as in Fig. 2.11. In the block, both the location and radius of the RoI can be assigned by the user after stage P_1. The block output provides the compression level information in each subblock for EZW. Therefore, the resolution in each area is defined by the area block output.
  - EZW block: In this block, each 8×8 subblock is compressed by the EZW based on the information from the Area output.

To achieve the UEP strategy, the compressed symbols generated in those subblocks in the same area are put together for transmission. Therefore, there are three compressed symbol group output based on the design area. In this situation, we can assign different parity lengths to different groups based on the data protection approach. Therefore, dominant and subordinate symbols are defined. Normally, the amount of the subordinate symbols is smaller than that of the dominant symbols. Therefore, the subordinate symbols in the three areas are assigned together to output, namely, SS (see Fig. 6.4), and treated as the most-important data, as in the case of RoI in the channel coding strategy. The DR and DS represent the compressed information in the dominant and subordinate passes, respectively in each subblock after the EZW process. The output *Thr* (threshold) records the initial threshold values in each subblock.

- PL block: This PL block provides variable parity length to the RS encoder based on both feedback information and data protection strategy.
- RS encoder block: This block performs the RS encoder function. The variability of error correction is defined by the PL output. Generally, the data computation time in a component is much more than the data transmission. Therefore, the proposed system is designed in concurrent architecture to increase the operational speed.

- The receiver part (see Fig. 6.5):
  - RS decoder block: The transmitted error data is detected and

corrected here.

- Integration block: The compressed symbols in the dominant pass in the three areas are combined according to the Area component output in the transmitter.
- Reconst block: Inversing EZW, inversing three level HWT, estimating channel state, and reconstructing image algorithms are all implemented in this block. The noise output is the evaluated amount of error caused by the transmission channel.
- Ns block: The noise output in this component is fed back to enable variable channel coding rate in the transmitter.

6.3 Experimental Results

The proposed system is designed using the embedded Matlab function block and the experimental results are shown in Fig. 6.6. We developed the RS(255, k) encoder and decoder in Matlab codes, the parity length is variable. Unfortunately, variable RS codes were hard to implement using the embedded Matlab DHL tool. However, for the rest of the system, a successful implementation of the proposed system is achieved. To my best knowledge, there is no RS model in the Simulink library, therefore the RS coder is not presented in the circuit architecture. Here, the input image is a 123 $\times$ 150 pixels color dental implant image. The proposed progressive scheme was simulated in four stages. The original input image is shown in Fig. 6.6(a). Fig. 6.6(b) shows the reconstructed test image. The result shows that both the developed three level HWT and inverse HWT design are successfully implemented. Here, the decoded image is 120 $\times$ 144, since we adopted 8 $\times$ 8 blocks to tile the image and the remainder was discarded.

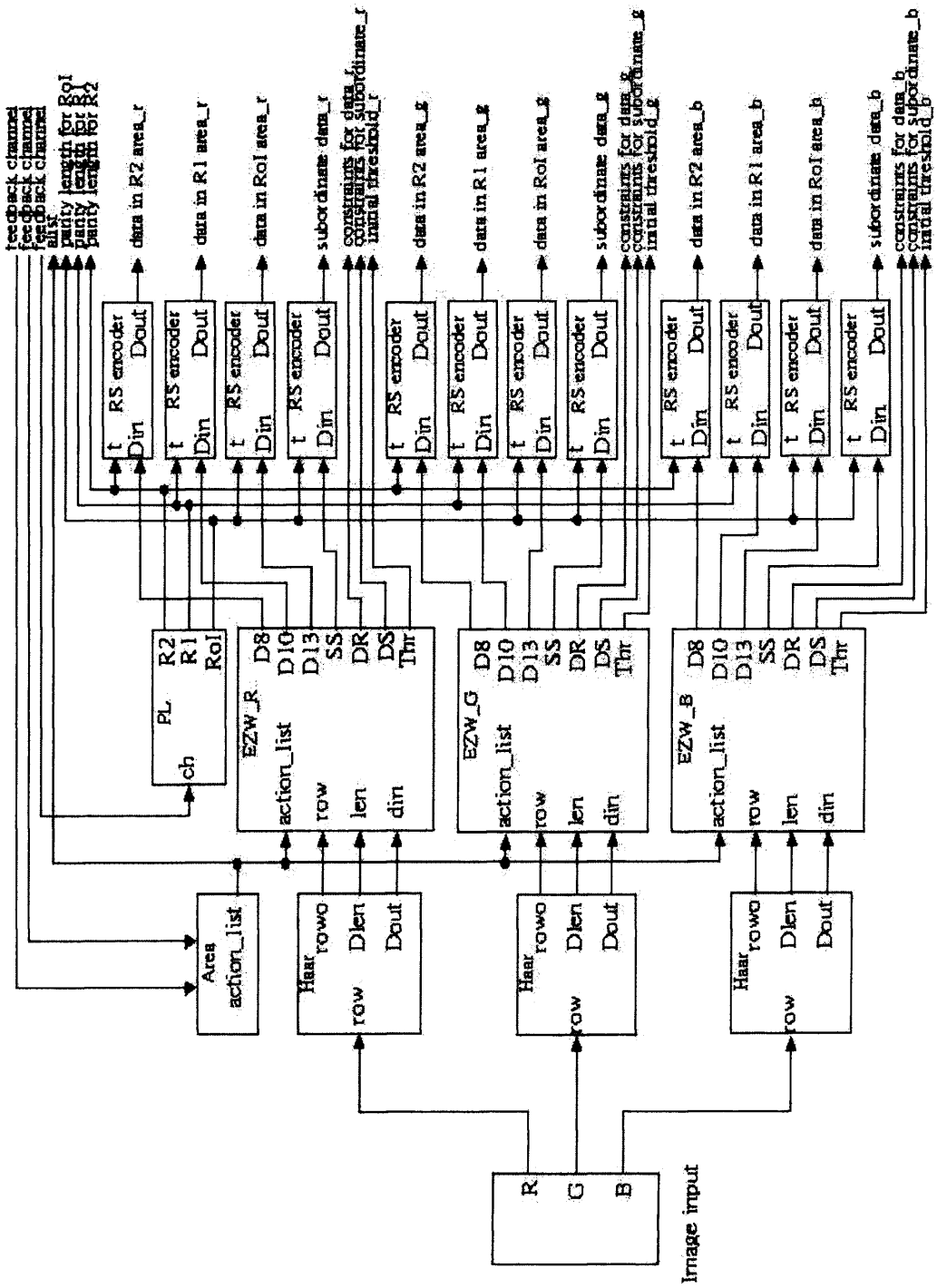

Figure 6.4. Block diagram of the transmitter of the proposed system.

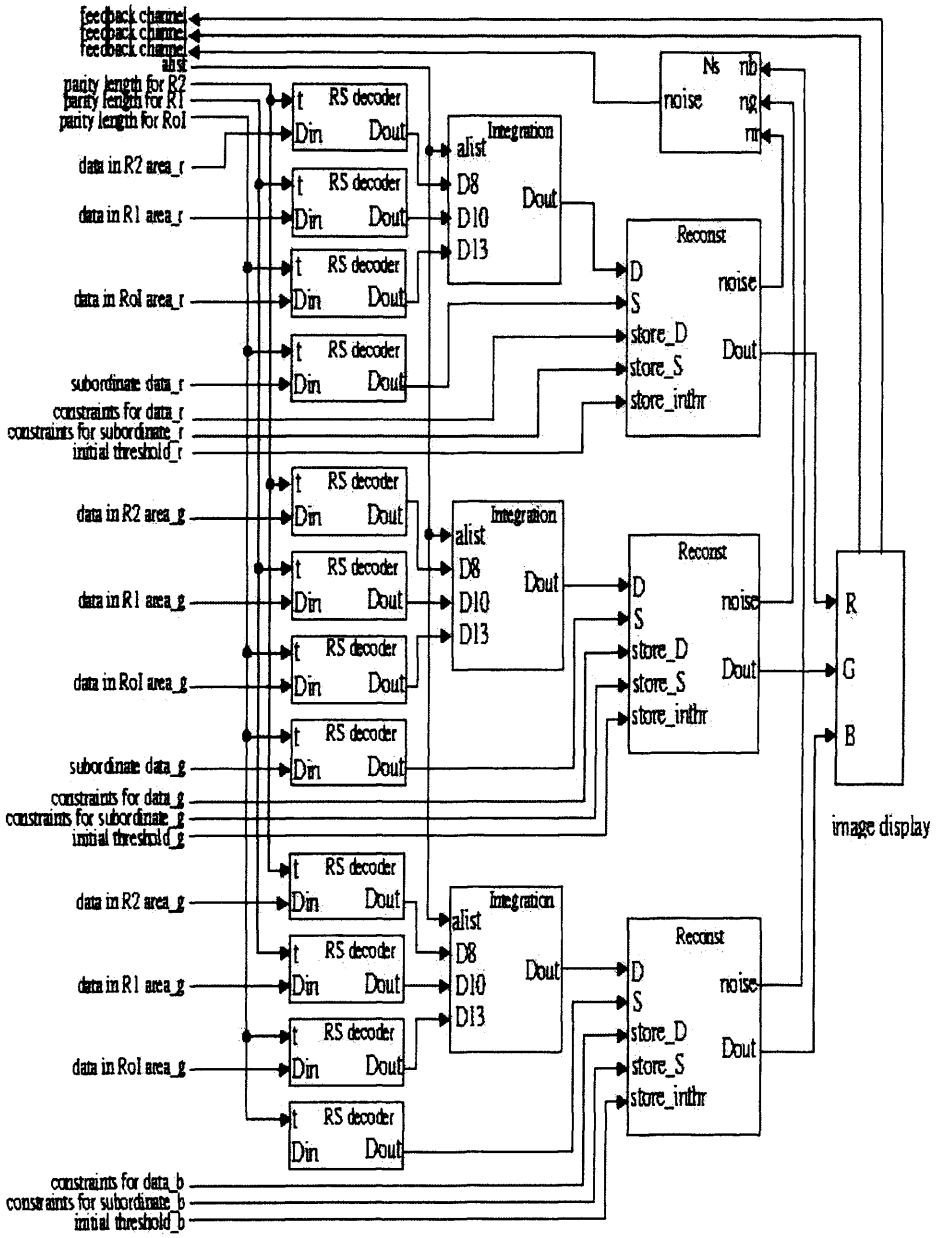

Figure 6.5. Block diagram of the receiver of the proposed system.

In Fig. 6.6(c), the background image after stage P_1 is presented. The user can assign both the radius and center of the RoI in the background image. The assigned information are sent back to the transmitter via the feedback channel. In this simulation, the location of the RoI is set in the center of the image. The reconstructed image in Fig. 6.6(d) is after stage P_2, in the proposed progressive scheme. The quality of the reconstructed image deteriorates with the distance away from the RoI center. Fig. 6.6(e) is the reconstructed image after stage P_3, the clarity of the area has gradually expanded and Fig. 6.6(f) shows the reconstructed image after the final stage, P_4.

6.4 Conclusions

A new hardware design flow is described in this chapter to link the algorithm development and the system-level hardware design using Embedded Matlab code and Simulink models. The method provides the following benefits: 1) algorithm developers can use the Embedded Matlab subset to generate IP for hardware component implementation, 2) designers can also use the Embedded Matlab function block to test their algorithms for real-time data and verify those specifications while keeping the debugging and analysis capabilities of Matlab, 3) the model created by the embedded Matlab function block is a user-defined Simulink model, and 4) HDL codes can be automatically generated from Simulink models for embedded hardware implementation by Simulink HDL coder.

Matlab is widely used for algorithm development, because it provides rich libraries and a powerful simulation environment for designers. In my view, the new design method has two problems: first, more models and libraries have to be added into Simulink to increase the design efficiency,

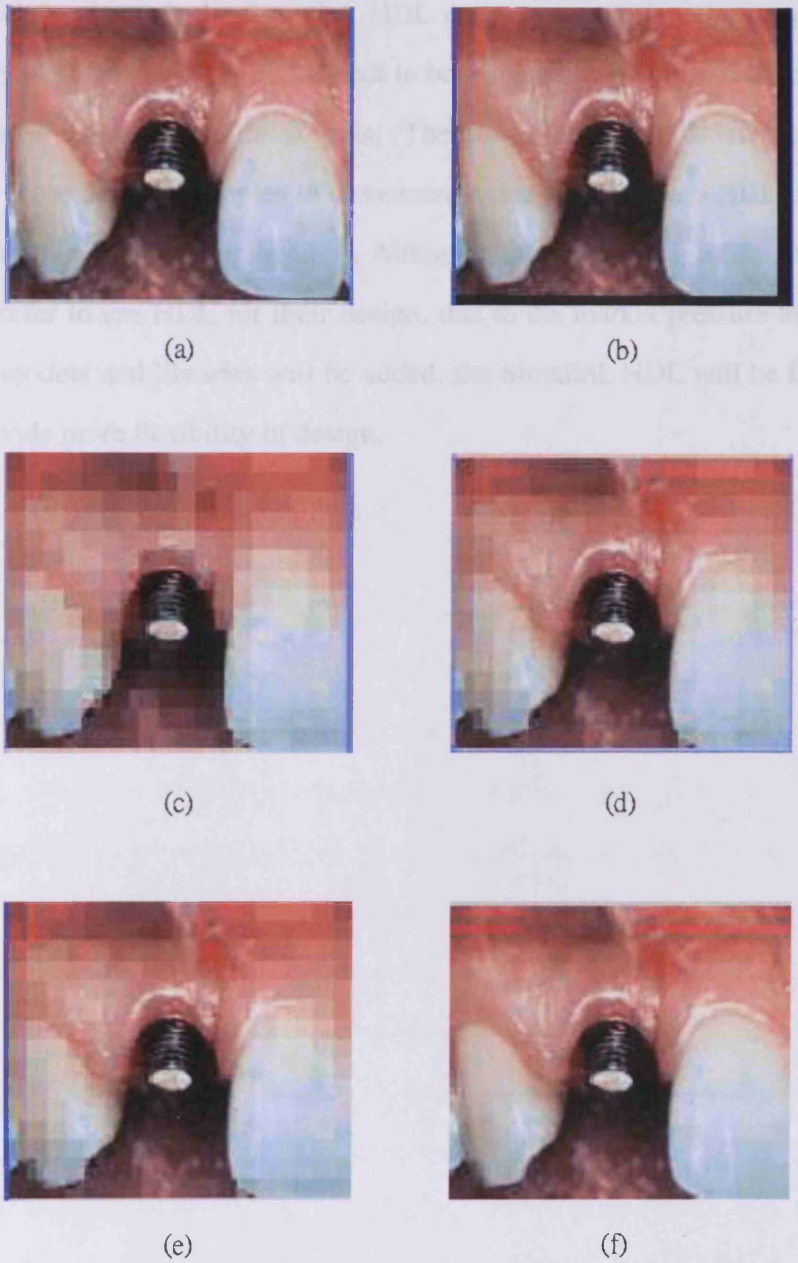

Figure 6.6. Experimental results, (a) input image, (b) the reconstructed image when testing the HWT and inverse HWT, (c) the reconstructed image after stage P_1, (b) the reconstructed image after stage P_2, (e) the reconstructed image after stage P_3, and (f) the reconstructed image after stage P_4, the final stage.

because the models and libraries in Simulink are more limited than those in Matlab. Second, the Simulink HDL coder is a new function, and the quality of generated HDL code needs to be compared with those HDL codes generated using other similar tools. Therefore, the Simulink HDL coder needs more design examples to demonstrate that the generated HDL codes are useful in practical applications. Although, the digital design community still prefer to use HDL for their design, due to the market pressure and as more models and libraries will be added, the Simulink HDL will be likely to provide more flexibility in design.

Chapter 7

SUMMARY, CONCLUSIONS AND FUTURE RESEARCH

7.1 Summary and Conclusions

In this dissertation, a new method for progressive medical image transmission with feedback has been developed. The transmitted data is protected by adaptively generating variable parity length channel codes based on the level of data importance and the channel-related feedback messages. In addition, a simple and efficient method has been developed to estimate the transmission channel state. The feedback system together with consideration of the RoI provide variability of the parity code (while the overall message length is kept fixed) to achieve an efficient progressive transmission system. Also, through a user friendly interaction with the system and using the feedback, both the centre and size of the RoI can be set by the user. Furthermore, for real world applications, the proposed system developed using embedded Matlab functions can be converted by Simulink HDL coder into HDL netlist for FPGA implementation.

Chapter 2 comprehensively reviewed the state-of-the-art in progressive transmission system techniques for medical images, including JSCC, UEP, prioterization of RoI and feedback schemes. The first contribution of the

dissertation is design of an adaptive JSCC with feedback system for progressive transmission and simulated with both BSC and fading channel assumptions. In this system since the level of protection is recursively adapted to the channel state there won't be any failure in transmission and therefore the messages won't need to be re-transmitted.

Many researchers have focussed on the bit-allocation algorithm to achieve an efficient transmission system. Such methods however, are developed based on a pre-defined transmission channel state, not a practical channel state. The simple method proposed in Chapter 3 is used to evaluate the practical transmission channel state. Accordingly, the evaluation of transmission channel state method in Chapter 3 is the second contribution of this dissertation. WT has been used here for source coding. However, other source coding methods can also be used instead. When the channel noise is described in terms of BER, the proposed system can completely recover the data in BERs as high as 0.005, that means at least 11 errors are generated in each transmitted package. In heavier noise however, the proposed method loses its accuracy.

CS is briefly introduced as a new source coding alternative in Chapter 4. The comparison of the results of the HALS-based CS and the EZW shows that the CS has better performance than EZW. Therefore, application of CS as a source coder is highly recommended as a new approach in source coding.

Chapter 5 shows the experimental results of the proposed system. According to those results, the center and radius of RoI can be assigned by the user at any point in the first stage and the quality of decoded images are improved sequentially. The source compression rate is based on the number of times the threshold is halved. However, the compression rate can be fur-

ther improved if the EZW follows another lossless compression algorithms, such as Huffman coding. Also, the code can be easily modified any arbitrary shape RoI.

Such a system enables transmission of large images into portable devices such as note-pads mainly in hospitals in the case of emergency. Accordingly, another contribution in the dissertation is in Chapter 6 where the proposed system is implemented using Simulink HDL coder to convert the Matlab codes into HDL netlist for FPGA implementation. Implementation of the design using Simulink HDL coder is therefore less time consuming. Although variable RS code is successfully implemented in MATLAB, its hardware implementation through Simulink HDL coder is hard to achieve. As far as I know, no RS code with variable parity length has been developed in hardware for practical applications. According to the experimental results in Chapter 6, the new hardware process works successfully.

7.2 Future Work

Medical image transmission is very important in telemedicine. DICOM and PACS standards are used in the hospitals equipped with powerful computational systems. However, doctors out of hospital still have problem in having access to those systems in the case of emergency. An effective and efficient progressive transmission system for delivering the biomedical data is therefore, highly demanded.

The work in this dissertation may be improved mainly to make it more accessible by portable devices. Both source and channel coding components can be improved to accommodate a lower bitrate and more efficient system. The new source coding systems such as CS can be improved and used for this purpose. The channel coding may be modified if a suitable interleaving

is used to keep the data more immune against channel errors. Also, minor modification to the current design enables transmission of signals and bioinformatics data as well as images.

A more realistic channel model can be estimated by developing more complex mathematical tools and implemented for a better feedback system. Consequently, the system tuning and adaptation will be significantly improved.

To make the system fully operational, the overall algorithm should be well integrated within portable devices using an efficient hardware implementation. Therefore, all ports including the variables RS codes should be fully and efficiently transferred into hardware. Finally, the technique should be flexible enough to be integrated within the current communication systems.

BIBLIOGRAPHY

[1] A. Graps, "An introduction to wavelets," *Computational Science and Engineering, IEEE*, vol. 2, pp. 50–61, 1995.

[2] Y. -H. Seo, "EZW example: understanding and application," *Digital Design and Test Lab.*

[3] G. Al-Regib, "Embedded zerotree wavelet encoding (ezw) based on shapiros paper," *Georgia Institute of Technology*, 2000.

[4] J. Chebil, B. Boashash, and M. Deriche, "Combined source channel decoding for image transmission over fading channels," *Proc. 9th APCC*, vol. 1, pp. 297–301, 2003.

[5] J. Romberg and M. Wakin, "Compressed sensing: A tutorial," *IEEE Statistical Signal Processing Workshop, Madison, Wisconsin*, 2007.

[6] "What is telemedicine?," *www.icucare.com/PageFiles/Telemedicine.pdf.*

[7] "Telemedicine," *http://webconferencingcouncil.com/?p=637.*

[8] S. Levy, D. Adam, and Y. Bresler, "Electromagnetic impedance tomography (emit): A new method for impedance imaging," *IEEE Trans. on Medical Imaging*, vol. 21, no. 6, pp. 676–687, 2002.

[9] J. M. Schmitt, "Optical coherence tomography (oct): a review," *IEEE*

Journal of Selected Topics in Quantum Electronics, vol. 5, no. 4, pp. 1205–1215, 1999.

[10] C. E. Shannon, "A mathematical theory of communication," *Bell System Technical Journal*, vol. 27, pp. 379–423, 1948.

[11] S. W. Golomb, "Run-length encodings," *IEEE Trans. on Inform. Theory*, vol. 12, no. 3, pp. 399–401, 1966.

[12] D. A. Huffman, "A method for the construction of minimum-redundancy codes," *Proceedings of the IRE*, vol. 40, no. 9, pp. 1098–1101, 1952.

[13] I. H. Willen, R. M. Neal, and J. G. Cleary, "Arithmatic coding fo data compression," *Communications for the ACM*, vol. 30, no. 6, pp. 520–540, 1987.

[14] N. Ahmed, T. Natarajan, and K. R. Rao, "Discrete cosine transform," *IEEE Trans. Computers*, vol. C-23, no. 1, pp. 90–93, 1987.

[15] A. E. Jacquin, "Fractal image coding: a review," *Proceedings of the IEEE*, vol. 81, no. 10, pp. 1451–1465, 1993.

[16] J. M. Shapiro, "Embedded image coding using zerotree of wavelet coefficients," *IEEE Trans. Sig. Proc.*, vol. 41, no. 12, pp. 3445–3462, 1993.

[17] A. Said and W. A. Pearlman, "A new, fast, and efficient image codec based on set partitioning inhierarchical trees," *IEEE Trans. on Circuits and System for Video Technology*, vol. 6, no. 3, pp. 243–250, 1996.

[18] G. K. Wallace, "The JPEG still picture compression standard," *IEEE Trans. on Consumer Electronics*, vol. 38, no. 1, pp. xviii–xxxiv, 1992.

[19] C. Christopoulos, A. Skodras, and T. Ebrahimi, "The JPEG2000 still image coding system: an overview," *IEEE Trans. on Consumer Electronics*, vol. 46, no. 4, pp. 1103–1127, 2000.

[20] M. Feder and N. Merhav, "Relations between entropy and error probability," *IEEE Trans. on Inform. Theory* , vol. 40, pp. 259–266, Jan. 1994.

[21] R. W. Hamming, "Error detecting and error correcting codes," *Bell System Technical Journal*, vol. 29, pp. 147–160, 1950.

[22] W. W. Peterson and D. T. Brown, "Cyclic codes for error detection," *Proceedings of the IRE*, vol. 49, no. 1, pp. 228–235, 1961.

[23] S. Lin and D. J. Costello, "Error control coding," *Pearson Prentice Hall*, 2004.

[24] J. Hagenauer, "Rate compatible punctured convolutional (RCPC Codes) codes and their applications," *IEEE Trans. Communication*, vol. 36, no. 4, pp. 389–400, 1998.

[25] R. Gallager, "Low-density parity-check codes," *IRE Trans. on Inform. Theory*, vol. 6, no. 1, pp. 21–28, 1962.

[26] C. Berrou and A. Glavieux, "Near optimum error correcting coding and decoding: Turbo-codes," *IEEE Trans. on Communications*, vol. 44, no. 10, pp. 1261–1271, 1996.

[27] K. Sayood, F. Liu, and J. D. Gibson, "A constrained joint source/channel coder design," *IEEE Journal on Selected Areas in Communications*, vol. 12, no. 9, pp. 1584–1593, 1994.

[28] Y. Zhong, F. Alajaji, and L. L. Campbell, "On the joint source–channel

coding error exponent for discrete memoryless systems," *IEEE Trans. on Inform. Theory*, vol. 52, no. 4, pp. 1450–1468, 2006.

[29] A. Gabay, M. Kieffer, and P. Duhamel, "Joint source-channel coding using real BCH codes for robust image transmission," *IEEE Trans. on Image Proc.*, vol. 16, no. 6, pp. 1568–1583, 2007.

[30] M. Srinivasan, and R. Chellappa, "Adaptive source-channel subband video coding for wireless channels," *IEEE Journal on Selected Areas in Communications*, vol. 16, no. 9, pp. 1830–1839, 1998.

[31] Z. Wu, A. Bilgin, and M. W. Marcellin, "Joint source/channel coding for image transmission with JPEG2000 over memoryless channels," *IEEE Trans. on Image Proc.*, vol. 14, no. 8, pp. 1020–1032, 2005.

[32] K. P. Subbalakshmi, and J. Vaisey, "On the joint source-channel decoding of variable-length encoded sources: The additive-Markov case," *IEEE Trans. on Communications*, vol. 51, no. 9, pp. 1420–1425, 2003.

[33] Z. Wu, A. Bilgin, and M. W. Marcellin, "Joint source/channel coding for multiple images," *IEEE Trans. on Communications*, vol. 53, no. 10, pp. 1648–1654, 2005.

[34] M. F. Sabir, H. R. Sheikh, R. W. Heath, Jr., and A. C. Bovik, "A joint source-channel distortion model for JPEG compressed images," *IEEE Trans. on Image Proc.*, vol. 15, no. 6, pp. 1349–1464, 2006.

[35] M. Srinivasan and R. Chellappa, "Joint source-channel subband coding of images," *Proc. ICASSP97*, vol. 4,21-24, pp. 2925–2928, 1997.

[36] D. Taubman, "High performance scalable image compression with EBCOT," *IEEE Trans. Image Proc.*, vol. 9, no. 7, pp. 1158–1170, 2000.

[37] C. Christopoulos, A. Skodras, and T. Ebrahimi, "The JPEG2000 still image coding system: An overview," *IEEE Trans. on Consumer Electronics*, vol. 46, no. 4, pp. 1103–1127, 2000.

[38] P. J. Lee and L. G. Chen, "Error concealment algorithm using interested direction for JPEG 2000 image transmission," *IEEE Trans. on Consumer Electronics*, vol. 49, no. 4, pp. 1396–1402, 2003.

[39] R. S. Dilmaghani, A. Ahmadian, M. Ghavami, and A. H. Aghvami, "Progressive medical image transmission and compression," *IEEE Sig. Proc. Letters*, vol. 11, no. 10, pp. 806–809, 2004.

[40] C. Chapman, S. Sanei, R. Dilmaghani, and F. Said, "Progressive transmission of medical images using embedded zerotree wavelet encoding," *2004 IEEE International Workshop on Biomedical Circuits and Systems*, pp. S3.3–9 S3.3–12, 2004.

[41] V. M. Stankovic, R. Hamzaoui, Y. Charfi, and Z. Xiong, "Real-time unequal error protection algorithms for progressive image transmission," *IEEE Journal on selected areas in communications*, vol. 21, no. 10, pp. 1526–1535, 2003.

[42] J.-S. Chiang, C.-H. Chang, C.-Y. Hsieh, and C.-H. Hsia, "High efficiency EBCOT with parallel coding architecture for JPEG2000," *EURASIP Journal on Applied Sig. Proc.*, vol. 2006, no. DOI 10.1155/ASP/2006/42568, Article ID 42568, Pages 1ąV14, 2006.

[43] G. B. Folland and A. Sitaram, "The uncertainty principle: A mathematical survey," *Journal of Fourier Analysis and Applications*, vol. 3, no. 3, pp. 207–238, 1997.

[44] C. Valens, "A really friendly guide to wavelets," *http://pagesperso-orange.fr/polyvalens/clemens/wavelets/wavelets.html-section2.*

[45] B. B. J. D. Villasenor and J. Liao, "Wavelet filter evaluation for image compression," *IEEE Trans. on Image Proc.*, vol. 4, no. 8, pp. 1053–1060, 1995.

[46] A. Ahmadian, M. A. Oghabian, and R. S. Dilmaghani, "Progressive medical image transmission (PIT) using modified embedded zerotree wavelet (EZW) algorithm," *Iranian Journal of Medical Physics*, vol. 1, no. 1, pp. 1–5, 2003.

[47] S.-C. Tai, C.-C. Sun, and W.-C. Yan, "A 2-D ECG compression method based on wavelet transform and modified SPIHT," *IEEE Trans. on Biomedical Engineering*, vol. 52, no. 6, pp. 999–1008, 2005.

[48] F. W. Wheeler and W. A. Pearlman, "Low-memory packetized SPIHT image compression," *Conference Record of the Thirty-Third Asilomar Conference on Signals, Systems, and Computers*, vol. 2, pp. 1193–1197, 1999.

[49] G. Anastassopoulos and A. Skodras, "JPEG2000 ROI coding in medical imaging applications," *Proceedings of the 2nd IASTED International Conference on Visualisation, Imaging and Image Proc.*, pp. 783–788, 2002.

[50] C. A. Fernandes, L. C. van Spaendonck, and C. Sidney Burrus, "A new framework for complex wavelet transforms," *IEEE Trans. on Sig. Proc.*, vol. 51, no. 7, pp. 1825–1837, 2003.

[51] I. W. Selesnick, R. G. Baraniuk, and N. G. Kingsbury, "The dual-tree complex wavelet transform," *IEEE Sig. Proc. Magazine*, vol. 22, no. 6, pp. 123–151, 2005.

[52] I. Voicu and M. Borda, "Image compression using complex wavelet transform," *The International Conference on Computer as a Tool, EUROCON 2005.*, vol. 2, pp. 919–922, 2005.

[53] P. Piotr and L. Agnieszka, "The haar-wavelet transform in digital image processing: Its status and achievements," *Machine graphics and vision*, vol. 13, no. 1/2, pp. 79–98, 2004.

[54] F. j. Diaz, A. M. Buron, and J. M. Solana, "Haar wavelet based processor scheme for image coding with low circuit complexity," *Computers and Electrical Engineering*, vol. 33, no. 2, pp. 109–126, 2007.

[55] R. Hamzaoui, V. Stankovic, and Z. Xiong, "Optimized error protection of scalable image bit streams," *IEEE Sig. Proc. Magazine*, vol. 22, no. 6, pp. 91–107, 2005.

[56] K. Sayood, H. H. Otu, and N. Demir, "Joint source/channel coding for variable length codes," *IEEE Trans. on Communications*, vol. 48, no. 5, pp. 787–794, 2000.

[57] T. Stockhammer, M. Hannuksela, and T. Wiegand, "H.264/AVC in wireless environments," *IEEE Trans. Circuits System Video Technology*, vol. 13, no. 5, pp. 657–673, 2003.

[58] P. G. Sherwood and K. Zeger, "Progressive image coding on noisy channels," *Data compression conference, DCC97*, pp. 72–81, 1997.

[59] M. Zhao and A. N. Akansu, "Optimization of dynamic UEP schemes for embedded image sources in noisy channels," *International Conference Image Proc.*, vol. 1, pp. 383–386, 2000.

[60] P. C. Cosman, J. K. Rogers, P. G. Sherwood, and K. Zeger, "Combined forward error control and packetized zerotree wavelet encoding for transmission of images over varying channels," *IEEE Trans. on Image Proc.*, vol. 9, no. 6, pp. 982–993, 2000.

[61] J. Rogers and P. Cosman, "Wavelet zerotree image compression with packetization," *IEEE Sig. Proc. Letters*, vol. 5, pp. 105–107, 1998.

[62] V. M. Stankovic, R. Hamzaoui, and X. Zixiang, "Efficient channel code rate selection algorithms for foward error correction of packetized multimedia bitstreams in varying channels," *IEEE Trans. on Multimedia*, vol. 6, no. 2, pp. 240–248, 2004.

[63] P. G. Sherwood and K. Zeger, "Error protection for progessive image transmission over memoryless and fading channels," *IEEE Trans. On Communications*, vol. 46, no. 12, pp. 1555–1559, 1998.

[64] V. M. Stankovic, R. Hamzaoui, and D. Saupe, "Fast algorithm for optimal error protection of embedded wavelet codes," *IEEE workshop Multimedia Sig. Proc.*, pp. 593–598, 2001.

[65] V. Chande and N. Farvardin, "Progressive transmission of images over memoryless noisy channels," *IEEE Trans. on Selected Areas in Communications*, vol. 18, no. 6, pp. 850–860, 2000.

[66] J. Lu, A. Nosratinia, and B. Aazhang, "Progressive source-channel coding of images over bursty error channels," *International Conference on Image Proc., ICIP98*, vol. 2, pp. 127–13, 1998.

[67] Z. Liu, M. Zhao, and Z. Xiong, "Efficient rate allocation for progressive image transmission via unequal error protection over finite-state markov channels," *IEEE Trans. Sig. Proc.*, vol. 53, no. 11, pp. 4430–4338, 2005.

[68] X. Pan, A. H. Bandihashemi, and A. Cuhadar, "Progressive transmission of images over fading channels using rate-compatible," *IEEE Trans. Image Proc.*, vol. 15, no. 15, pp. 3627–3635, 2006.

[69] J. Lu, A. Nosratinia, and B. Aazhang, "Progressive joint source-channel in feedback channels," *Proc. Data Compression Conference*, pp. 140–148, 1999.

[70] V. Chande and N. Farvardin, "Image communication over noisy channels with feedback," *Internation Conference on Image Proc.*, vol. 2, pp. 540–544, 1999.

[71] X. Yu and D. Ma, "Progressive image transmission over memoryless feedback channels using joint source-channel coding strategy," *Workshop on Knowledge Discovery and Data Mining*, pp. 493–498, 2008.

[72] B. A. Banister, B. Belzer, and T. R. Fischer, "Robust image transmission using JPEG2000 and turbo-codes," *IEEE Sig. Proc. Letters*, vol. 9, no. 4, pp. 117–119, 2002.

[73] R. Hamzaoui, V. Stankovic, and Z. Xiong, "Rate-based versus distortion-based optimal joint source-channel coding," *Proceedings Data Compression Conference, DCC 2002*, pp. 63–72, 2002.

[74] Z. Wu, A. Bilgin, and M. W. Marcellin, "Joint source/channel for image transmission with JPEG2000 over memoryless channels," *IEEE Trans. on Image Proc.*, vol. 14, no. 8, pp. 1020–1032, 2005.

[75] L. Pu, M. W. Marcellin, I. Djordjevic, B. Vasic, and A. Bilgin, "Joint source-channel rate allocation in parallel channels," *IEEE Trans. on Image Proc.*, vol. 16, no. 8, pp. 1734–1750, 2007.

[76] C. D. Creusere, "A new method of robust image compression based on the embedded zerotree wavelet algorithm," *IEEE Trans. on Image Proc.*, vol. 6, no. 10, pp. 1436–1442, 1997.

[77] I. S. Reed and G. Solomon, "Polynomial codes over Certain Fields," *Journal of the Society for Industrial and Applied Mathematics*, vol. 8, no. 2, pp. 300–304, 1960.

[78] T. P. C. Chun, and T. Chen, "Adaptive joint source-channel coding using rate shaping," *ICASSP'02*, vol. 2, pp. 1985–1988, 2002.

[79] J. Takahashi, H. Tode, and K. Murakami, "A hybrid FEC method using packet-level convolution and Reed-Solomon codes," *IEICE Trans. Communication*, vol. E89-B, no. 8, pp. 2143–2151, 2006.

[80] R. C. Chang and T. K. Shih, "Innovative decomposition for progressive image transmission," *Asian Journal of Health and Inform. Sciences*, vol. 1, no. 2, pp. 204–227, 2006.

[81] C.-C. Chang, F.-C. Shiue, and T.-S. Chen, "A new scheme of progressive image transmission based on bit-plane method," *Proceedings of Fifth Asia-Pacific Conference on Communications and Fourth Optoelectronics and Communications Conference*, vol. 2, no. 2, pp. 892–895, 1999.

[82] M. Accame and F. Granelli, "Hierarchical progressive image coding controlled by a region based approach," *IEEE Trans. on consumer electronics*, vol. 45, no. 1, pp. 13–20, 1999.

[83] S. Grgic, M. Grgic, and M. Mrak, "Reliability of objective picture quality measures," *Journal of Electrical Engineering*, vol. 55, no. 1-2, pp. 3–10, 2004.

[84] C. C. Chang, T. K. Shih, and I. C. Lin, "An efficient progressive image transmission method based on guessing by neighbors," *The Visual Computer*, pp. 341–353, 2002.

[85] C. N. Doukas, I. Maglogiannis, and G. Kormentzas, "Medical image compression using wavelet transform on mobile devices with RoI coding support," *in Proceedings of the 27th Annual International Conference of the IEEE Engineering in Medicine and Biology Society (EMBC'05)*, vol. 7, pp. 3779–3784, 2005.

[86] Z. Liu, J. Ha, Z. Xiong, Q. Wu, and K. Castleman, "Lossy-to Lossless RoI coding of chromosome images using modified SPIHT and EBCOT," *in Proceedings of IEEE International Symposium on Biomedical Imaging*, pp. 317–320, 2002.

[87] M. Penedo, W. A. Pearlman, P. G. Tahoces, M. Souto, and J. J. Vidal, "Region-based wavelet coding methods for digital mammography," *IEEE Trans. on Medical Imaging*, vol. 22, no. 10, pp. 1288–1296, 2003.

[88] C. Doukas and I. Maglogiannis, "Region of interest coding techniques for medical image compression," *Engineering in Medicine and Biology Magazine, IEEE*, vol. 26, no. 5, pp. 29–35, 2007.

[89] C. Doukas and I. Maglogiannis, "Adaptive transmission of medical image and video using scalable coding and context-aware wireless medical networks," *EURASIP Journal on Wireless Communications and Networking*, vol. 2008, pp. ID 428397, 12 pages, 2008.

[90] T. Kim, S. Choi, R. E. VanDyck, and N. K. Bose, "Classified zerotree wavelet image coding and adaptive packetization for low-bit-rate transport,"

IEEE Trans. on Circuits and System for Video Technology, vol. 11, no. 9, pp. 1022–1034, 2001.

[91] C. S. Pattichis, E. Kyriacou, S. Voskaride, S. Pattichis, R. lstepanian, and C. N. Schizas, "Wireless telemedicine systems: An overview," *IEEE Antenna's and Propagation Magazine*, vol. 44, no. 42, pp. 439–447, 2002.

[92] H. Hourani, "An overview of diversity techniques in wireless communication," *Helsinki University of Technology Communication Lab*, 2004.

[93] P. Dirner and S. Lin, "Measured frequency diversity improvement for digital radio," *IEEE Trans. on communication* , vol. 33, pp. 106–109, Jan. 1985.

[94] R. Schober and L. Lampe, "Differential modulation diversity," *IEEE Trans. on Vehicular Technology* , vol. 51, pp. 1431–1444, Nov. 2002.

[95] P. L. Perini and C. L. Holloway, "Angle and space diversity comparisons in different mobile radio environments," *IEEE Trans. on Antennas and Propagation*, vol. 46, pp. 764–775, June 1998.

[96] A. Nosratinia, J. Lu, and B. Aazhang, "Source-channel rate-allocation for progressive transmission of image," *IEEE Trans. Communications*, vol. 51, no. 2, pp. 186–196, 2003.

[97] E. Gilbert, "Capacity of a burst-noise channel," *Bell System Technical Journal*, vol. 39, pp. 1253–1266, 1960.

[98] H. S. Wang and N. Moayeri, "Finite-state markov channel- a useful model for radio communication channels," *IEEE Trans. on Vehicular Technology*, vol. 44, no. 1, pp. 163–171, 1995.

[99] L. N. Kanal and A. R. K. Sastry, "Models for channels with memory and their applications to error control," *Proceedings of the IEEE*, vol. 66, no. 7, pp. 724–744, 1978.

[100] S. D. Morgera and F. Simard, "Parameter estimation for a burst-noise channel," *ICASSP-91*, vol. 3, pp. 1701–1704, 1991.

[101] D. Donoho, "Compressed sensing," *IEEE Trans. Inform. Theory*, vol. 52, no. 4, pp. 1289–1306, 2006.

[102] E. J. Candes, "Compressive sampling," *in Proc. International Congress of Mathematicians*, vol. 3, pp. 1433–1452, 2006.

[103] B. Han, F. Wu, and D. Wu, "Image representation by compressed sensing," *IEEE International Conference on Image Proc., ICIP*, pp. 1344–1347, 2008.

[104] M. Lustig, D. Donoho, and J. M. Pauly, "Sparse MRI: The application of compressed sensing for rapid mr imaging," *Magnetic Resonance in Medicine*, vol. 58, no. 6, pp. 1182–1195, 2007.

[105] M. Lustig, D. Donoho, J. M. Santos, and J. M. Pauly, "Compressed sensing MRI," *IEEE Sig. Proc. Magazine*, vol. 25, no. 2, pp. 72–82, 2008.

[106] J. Lee, A. Bandyopadhyay, I. F. Baskaya, R. Robucci, and P. Hasler, "Image processing system using a programmable transform imager," *ICASSP*, vol. 5, pp. 101–104, 2005.

[107] R. Robucci, L. K. Chiu, J. Gray, J Romberg, P. Hasler, and D. Anderson, "Compressive sensing on a CMOS separable transform image sensor," *ICASSP*, pp. 5125–5128, 2008.

[108] D. Takhar, J. N. Laska, M. B. Wakin, M. F. Duarte, D. Baron, S. sarvotham, K. F. Kelly, and R. G. Baraniuk, "A new compressive imaging camera architecture using optical-domain compression," *in Proc. SPIE Conference Computational imaging IV*, pp. 43–52, 2006.

[109] J. Romberg, "Imaging via compressive sampling," *IEEE Sig. Proc. Magazine*, vol. 25, no. 2, pp. 14–20, 2008.

[110] E. Candes and M. Wakin, "An introduction to compressive sampling," *IEEE Sig. Proc. Magazine*, vol. 25, no. 4, pp. 21–30, 2008.

[111] E. J. Candes and T. Tao, "Near optimal signal recovery from random projections: Universal encoding strategies?," *IEEE Trans. Inform. Theory*, vol. 52, pp. 5406–5425, 2006.

[112] S. Mallat and Z. Zhang, "Matching pursuits with time-frequency dictionaries," *IEEE Trans. on Sig. Proc.*, vol. 41, no. 12, pp. 3397–3415, 1993.

[113] H. Mohimani, M. Babaie-Zadeh, and C. Jutten, "A fast approach for overcomplete sparse decomposition based on smoothed ℓ_0 norm," *IEEE Trans. on Sig. Proc.*, vol. 57, no. 1, pp. 289–301, 2009.

[114] Y. Rachlin and D. Baron, "The secrecy of compressed sensing measurements," *Communication, Control, and Computing, 46th Annual Allerton Conference*, pp. 813–817, 2008.

[115] E. Candes, J. Romberg, and T. Tao, "Robust uncertainty principles: Exact recovery from highly incomplete fourier information," *IEEE Trans. on Inform. Theory*, vol. 2, no. 52, pp. 489–509, 2006.

[116] R. G. Baraniuk, "Compressive sensing," *IEEE Sig. Proc. Magazine*, vol. 24, no. 4, pp. 118–121, 2007.

[117] A. H. Phan, A. Cichocki, and K. S. Nguyen, "Simple and efficient algorithm for distributed compressed sensing," *Machine Learning for Sig. Proc., MLSP2008*, vol. 16, pp. 61–66, 2008.

[118] I. Daubechies, M. Defrise, and C. De Mol, "An iterative thresholding algorithm for linear inverse problems with a sparsity constraint," *Communications on Pure and Applied Mathematics*, vol. 57, no. 11, pp. 1413–1457, 2004.

[119] "Simulation and Model-Based Design," *The MathWorks*.

[120] "www.electronicspecifier.com/company/Sundance-Multiprocessor-Technology.asp," .

[121] "www.model.com/programs," .

[122] "www.synopsys.com/home.aspx,"

[123] "www.cadence.com/us/pages/default.aspx,"